DLR FB 71-94

DLR FB 71-94

Deutsche Luft- und Raumfahrt

Forschungsbericht 71-94

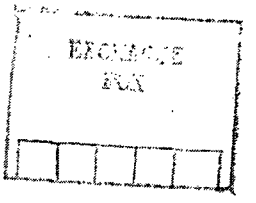

Inertial Navigation System Using Three TDF Gyroscopic Sensors Not Jointly Mounted on a Stable Platform

von

B. Stieler

Deutsche Forschungs- und Versuchsanstalt für Luft- und Raumfahrt

Institut für Flugführung
Braunschweig

1971

DLR FB 71-94

Herausgegeben von der Abteilung Wissenschaftliches Berichtswesen
der Deutschen Forschungs- und Versuchsanstalt für Luft- und Raumfahrt E. V. (DFVLR)
505 Porz-Wahn, Linder Höhe

Preis: DM 21,–

Errata

Page	Line/Eq.	Wrong	Correct
4	5	descirbed	described
5	17	cinstitute	constitute
18	10	vector	vectors
51	10/11	and signal generators	and the different signal generators
55	Eq.(7.7)	ΔL	ΔL^*
61	Eq.(7.23)	$\frac{(I)}{(I)V} = \frac{1}{K} = 7.24 \widehat{\text{sec}}$	$\frac{(I)\varphi}{(I)V} = \frac{1}{K} = 7.24 \frac{\widehat{\text{sec}}}{\text{km/h}}$
72	32	Chapter 5	Chapter 3
82	Eq.(A36)	$\Theta_E(\tau)$	$-\Theta_E(\tau)$
83	Eq.(A40)	$C_{ng}\ \vec{1}^{s}_{g}$	$C_{bn}\ C_{ng}\ \vec{1}^{s}_{g}$
91	Eq.(C7)	L^*	ΔL^*
73	38	dusturbance	disturbance

DEUTSCHE LUFT- UND RAUMFAHRT

FORSCHUNGSBERICHT 71-94

INERTIAL NAVIGATION SYSTEM USING THREE TDF GYROSCOPIC SENSORS NOT JOINTLY MOUNTED ON A STABLE PLATFORM

von

B. Stieler

DEUTSCHE FORSCHUNGS- UND VERSUCHSANSTALT FÜR LUFT- UND RAUMFAHRT E.V.

100 Seiten,
16 Bilder,
6 Tabellen und
15 Literaturstellen

1971

DK 527.62:531.383
53.082.16
629.7.058.82

Inertial Navigation System Using Three TDF Gyroscopic Sensors Not Jointly Mounted On a Stable Platform

Deutsche Forschungs- und Versuchsanstalt für
Luft- und Raumfahrt E.V.

Institut für Flugführung
Abteilung: Kreiselgeräte und
Trägheitsortung

Braunschweig, im Dezember 1971

Institutsdirektor:
Prof. Dr.-Ing. K.H. DOETSCH

Abteilungsleiter:
Dr.-Ing. B. STIELER

Bearbeiter:
Dr.-Ing. B. STIELER

Inertial Navigation System Using Three TDF Gyroscopic Sensors Not Jointly Mounted On a Stable Platform

Summary

An inertial navigation system is descirbed and analyzed based on two two-degree-of-freedom Schuler-gyropendulums and one two-degree-of-freedom azimuth gyro. The three sensors, each base motion isolated about its two input axes, are mounted on a common base, strapped down to the vehicle.

The up and down pointing spin vectors of the two properly tuned gyropendulums track the vertical and indicate physically their velocity with respect to intertial space. The spin vector of the azimuth gyro is pointing northerly parallel to the earth axis.

The system can be made self-aligning on a stationary base. If external measurements for the north direction and the vertical are available, initial disturbance torques can be measured and easily biased out.

The error analysis shows that the system is practicable with today's technology.

Trägheitsnavigationssystem unter Verwendung von drei, nicht auf einer gemeinsamen stabilen Plattform montierten Kreiselsensoren

Übersicht

Ein Trägheitsnavigationssystem, aufbauend auf zwei Schuler-Kreiselpendeln und einem Azimutkreisel mit je zwei Meßfreiheitsgraden, wird beschrieben und analysiert. Die drei Sensoren sind auf einer gemeinsamen Grundplatte montiert, die fest mit dem Fahrzeug verbunden ist. Dabei ist jeder Sensor für sich um seine beiden Eingangsachsen gegenüber der Fahrzeugbewegung isoliert.

Die auf- und abweisenden Drallvektoren der beiden speziell abgestimmten Kreiselpendel zeigen die Fahrzeuggeschwindigkeit gegenüber dem Inertialraum an und ermöglichen es, die Lotrichtung zu ermitteln. Der Drallvektor des Azimutkreisels weist nach Norden, parallel zur Erdachse.

Eine vereinfachte Fehleranalyse ermöglicht, die Ausführbarkeit des Systems zu beurteilen.

Das System ist fähig zur Selbstausrichtung. Wenn externe Referenzen für die Nordrichtung und die Vertikale vorhanden sind, können Anfangsstörmomente gemessen und recht einfach kompensiert werden.

Acknowledgements

This study was accomplished while the author was supported as a Postdoctoral Resident Research Associate by the National Academy of Sciences. During his stay at NASA/Electronics Research Center the author was on a leave of absence from Deutsche Forschungs- und Versuchsanstalt für Luft- und Raumfahrt, Braunschweig, Germany.

Dr. Arthur H. Lipton, the author's Scientific Advisor at NASA/ERC, gave his encouragement for this study, provided the atmosphere in which it could be carried out and gave valuable cirticism. Dr. Shigeo Okubo showed great interest in this study. The author likes to remember the many discussions he had with him. Professor Walter Wrigley, the author's honorable teacher at Massachusetts Institute of Technology, was open to consultation and provided valuable hints. The final analysis was reviewed by Dr. John E. Bortz, (NASA/ERC), Dipl.-Ing. Dietrich Rahlfs and Ing. Egmar Lübeck (both DFVLR), from whom the author received estimable contributions.

The author wishes to express his appreciation to all of them.

TABLE OF CONTENTS

LIST OF FIGURES

LIST OF FIGURES (CONTINUED)

LIST OF TABLES

1. NOTATION

a	m/sec^2	Acceleration of the gyro with respect to an earth fixed point
a^{ig}	m/sec^2	acceleration of the gyro with respect to inertial space
b	m/sec^2	Coriolis and centrifugal acceleration due to horizontal flight over the rotating earth (s. eq. (A21a) to (A23a))
c	m/sec^2	Coriolis acceleration due to vertical velocity over the rotating earth (s. eq. (A21b) to (A23b))
c_x, c_y	$\frac{dyne - cm}{rad/sec}$	damping coefficient of the x, y gimbal bearing (s. Fig. 6.2)
f	m/sec^2	nongravitational specific force which the gyro exerts on its support (s. eq. (A19) to (A24))
$f(t-\tau)$		delayed step function (s. eq. (4.16))
g	m/sec^2	gravity
h	m or km	altitude of the vehicle above the earth's surface
l	rad or deg	longitude angle
m	gm	mass of the pendulosity
$p = \frac{d}{dt}$		operator
r	cm, mm	lever arm of pendulosity
s	1/sec	Laplace operator
t	sec	time
u		abbreviation (s. eq. (B15) and (B16))

v		abbreviation (s. eq. (B15) and (B17))
C		coordinate transformation matrix, e.g. C_{ng} (eq. (A8)) for transformation from the gyro to the navigational frame
F_x, F_y	$\frac{\text{dyne - cm}}{\text{Volt}}$	transfer functions in the gimbal follow-up control (s. Fig. 6.2)
F'	$\frac{\text{Volt}}{\text{Volt}}$	abbrevation for a lead-integral transfer function (s. eq. (6.17))
G	m/sec^2	gravitational field intensity
H	$\frac{\text{gm - cm}^2}{\text{sec}}$	angular momentum of the gyro rotor; in the gyropendulum this is supposed to match the tuning condition (s. eq. (4.10))
H'	$\frac{\text{gm - cm}^2}{\text{sec}}$	angular momentum of gyropendulum for matching the Schuler tuning (s. eq. (3.7a))
H^t	$\frac{\text{gm - cm}^2}{\text{sec}}$	total angular momentum of the gyropendulum (eq. (A1))
I_x, I_y	gm - cm^2	moment of inertia of the x and y gimbal (s. Fig. 6.2)
$K = \frac{1}{\sqrt{gR}}$	$\frac{\text{rad}}{\text{m/sec}}$	gain of the gyropendulum (s. eq. (3.11a,b))
L	rad or deg	latitude angle
M	dyne - cm	torque applied to the gyro
P	km	position
R	m or km	radius of the trajectory with respect to the center of the earth
S		signal generator (s. Fig. 6.2)
T	sec	lead time, integration time (s. eq. (6.17))
$T_o^s = 84.4$ min		Schuler period on the surface of the earth

V	m/sec or km/h	velocity of the vehicle
$(I)\Delta V_N'$	m/sec	abbrevations for computational velocity error terms (s. eq. (C33) to (C35) and (7.13))
$(I)\Delta V_E'$	m/sec	
$(I)\Delta V^{ie'}$	m/sec	
$(I)\Delta V_{iE}'$	m/sec	
$\delta(t-\tau)$	1/sec	impulse function delayed with τ
ϑ	rad or deg	pitch angle, positive, when tail goes down
λ	rad or deg	celestial longitude (s. eq. (A15))
φ	rad or deg	roll angle, positive, when right wing goes down
ψ	rad or deg	yaw angle, positive, when rotation about the downward pointing axis is positive; zero for northerly moving vehicle
ω^d	rad/sec or deg/h	gyro drift
$\omega^{ie} = 7.29 \cdot 10^{-5}$ rad/sec		earth angular rate
ω^{in}	rad/sec	angular rate of the navigational frame with respect to inertial space
$\omega^s = \sqrt{g/R}$	rad/sec	Schuler frequency
$\omega_o^s = 1.235 \cdot 10^{-3}$ rad/sec		Schuler frequency on the surface of the earth
Θ	rad, $\widehat{min}$, $\widehat{sec}$	attitude of the spin vector with respect to a coordinate frame, earmarked in the subscript

For the azimuth gyro:

Θ_E, Θ_D	rad, $\widehat{min}$, $\widehat{sec}$	attitude angles of the spin vector with respect to the equatorial tangent frame; zero when spin axis is pointing northward, parallel to earth axis

Θ_{Eo}^{+}, Θ_{Do}^{+}	rad, $\widehat{min}$, $\widehat{sec}$	initial misalignment angles
Θ_y, Θ_z	rad, $\widehat{min}$, $\widehat{sec}$	attitude angles of the spin vector, measured by gimbal-mounted signal generators
Θ_y', Θ_z'	rad	attitude angles of the spin vector, measured by the pickoffs of an electrostatically supported gyro (ESG)
(I) Θ	$\widehat{min}$	inaccuracy of the signal generators

For the gyropendulum:

Θ_N, Θ_E	rad, $\widehat{min}$, $\widehat{sec}$	attitude angles of the spin vector with respect to the navigational frame; zero, when the spin vector is pointing parallel to the vertical, upward for sensor no. I, downward for sensor no. II
Θ_{No}^{+}, Θ_{Eo}^{+}	rad, $\widehat{min}$, $\widehat{sec}$	initial value for Θ_N and Θ_E
Θ_{No}, Θ_{Eo}	rad, deg, $\widehat{sec}$	angles for the initial static equilibrium of the gyropendulums (s. eq. (4.6), (4.7) and (4.9))
Θ_{N1}, Θ_{E1}	rad, deg, $\widehat{sec}$	angles for the quasi static equilibrium of the gyropendulums (s. eq. (4.4) and (4.5) or (4.24) and (4.25))
Θ_{N2}, Θ_{E2}	rad, deg, $\widehat{sec}$	
$\textcircled{\pi}$		multiplication node (s. Fig. 4.1)
τ	sec	time delay
Ω	1/sec	natural frequency of the gyropendulum including the vertical acceleration p^2h (s. eq. (A27))
Ω^c	1/sec	natural frequency of the gyropendulum excluding the vertical acceleration p^2h (s. eq. (A30))
Ω_o^c	1/sec	initial natural frequency of the gyropendulum for matched initial tuning (H_o)

$\Omega^c\|_{Ho}$	1/sec	natural frequency of the gyropendulum on the moving vehicle for constant angular momentum H_o

Subscripts

a	free azimuth frame
b	body frame
g	gyro frame
h	horizontal
n	navigational frame
t	equatorial tangent frame
v	vertical
x, y, z	gimbal axes (s. Fig. 3.2 and 3.3)
E	east
I	inertial frame
N	north
D	down, orthogonal to east and earth axis
O	initial value, stationary on the ground
1	quasi static equilibrium (s. eq. (4.4) and (4.5))
I	gyropendulum no. I, spin vector pointing up
II	gyropendulum no. II, spin vector pointing down

Superscripts

a	free azimuth frame
b	body frame

c	coning frequency, natural frequency of the gyropendulum disregarding the vertical acceleration p^2h
cm	controlled member, gimbal
cmd	command (torque)
d	disturbance (torque), drift
e	earth
g	gyro frame
i	inertial space
n	navigational frame
qs	quasi static
s	Schuler (frequency, period)
s	spin, in connection with $\vec{1}^s$
T	transpose of a matrix
*	computed or measured values

Symbols

(I)	inaccuracy (preceding the specific term)
(U)	uncertainty (preceding the letter M, i.e. uncertainty torque)
$\vec{1}$	unit vector of the angular momentum
δ	difference of corresponding readouts of gyropendulum no. I and II, s. eq. (8.16)
Δ	difference from stationary values
$\sim$	variable in the Laplace domain
$\vec{\ }$	vector
$\bar{\ }$	mean value

2. INTRODUCTION

Most of the inertial platforms for navigation with respect to the surface of the earth incorporate two or three gyros (two, where two-degree-of-freedom gyros are used; three, where single-degree-of-freedom gyros are used) and two accelerometers as inertial sensors. These platform mounted sensors are interconnected so that the performance of the platform in a dynamic environment is similar to a pendulum with its mass located in the center of the earth and with its lever arm equal to the earth radius. This mathematical pendulum, if it would be practicable, would always indicate the vertical. Schuler [1] has shown that a physical pendulum or a gyropendulum with the same period of T = 84 min as this mathematical pendulum will indicate the vertical if initially aligned with it, even on a moving base. Wrigley [2] introduces for the tuning of an instrument to 84 min the expression "Schuler Tuning".

The history and development of Schuler tuned platforms using gyros and accelerometers are well covered in the literature [3,4,5,6,8]. A different approach to a vertical indicating platform system was carried out by Åström and Hector [9], who use instead of three SDF gyros and two accelerometers, two pendulous SDF gyros (implemented by attaching two SDF gyros to two physical pendulums) and one nonpendulous SDF azimuth gyro mounted on a common stable platform. As the title [9] indicates, the Schuler pendulum is materialized by raising artificially the moment of inertia of the physical pendulum through the application of a command torque proportional to the angular acceleration of the pendulum. The signal proportional to the angular acceleration is generated by the pendulum-mounted SDF gyro with integral feedback. The feedback signal applied to the gyroscope is proportional to the velocity of the instrument with respect to inertial space. This gyropendulum, if Schuler-tuned will indicate the vertical about the input axes. Koenke [10] presents an analysis of this system.

The system described in this study incorporates also three gyroscopic sensors, two gyropendulums and one azimuth gyro and as such bears resemblance to the one developed by Åström and Hector. In contrast to the latter each of the three two-degree-of-freedom gyroscopic sensors is base-motion isolated about its two input axes by means of two gimbals (one gimbal being the gyro case) and a follow-up control. The three gyro-gimbal units are mounted on a common rigid base which is strapped down to the vehicle. The proper tuning of the two gyropendulums when stationary is achieved by a mere center of support and

center of gravity separation which is for a modern gyro (e.g. Autonetics G10) in the order of 0.135 mm. One of the two gyropendulums has its spin vector pointing upward, the other one downward.

Similar to a vertical indicating system where the vertical is physically indicated by the platform, in the system described herein the vertical can be visualized as the mean angle between the spin vectors of the two gyropendulums. As distinguished from other vertical indicating systems, where velocity is generated by an electric integration process, the two gyropendulums indicate physically their velocity with respect to inertial space by the tilt angle of their spin vector from the vertical.

The basic performance of two gyropendulums with their spin vectors pointing up and down was first described by Schuler in 1923 [1] who derived the tuning condition of the sensors for a non-rotating earth. It is shown in this analysis that for a vehicle moving over the rotating earth the tuning condition is affected by the vertical Coriolis and centrifugal acceleration, the vertical component of earth rate and the rate of change of latitude. Thus, the tuning condition becomes a function of ground speed and position and has to be matched by a proper control of the angular momentum of both gyropendulums.

Wrigley [2], in an interpretation of Schuler's paper, mentions the properties of the two sensors as derived by Schuler. Reisch [3], in the description of the development of his first vertical indicating platform during World War II in Germany, mentions Schuler's idea with the two gyropendulums, but rejects their possible use as sensors in an inertial navigation system. In the discussion of Reisch's paper, Fischel points out that they might be used in such a system. In his paper [8] Fischel describes Schuler's idea, but points at the disadvantage that the two gyropendulums indicate only their velocity with respect to inertial space. Indeed, to compute herefrom ground speed, which is of main interest for terrestrial navigation, earth rate has to be known in magnitude and direction. Schuler proposes to measure this vector externally by means of star sighting. In a selfcontained navigation system the direction of earth rate can be stored physically in a gyro, an idea which Stratton [15] also briefly draws attention to, when he discusses the behavior of the Schuler tuned gyropendulum in the spherical gravitational field relative to that of the physical pendulum.

In the navigation system described in this paper the spin vector of the azimuth gyro which stores this direction of earth rate is pointing northerly, parallel to the earth axis. The magnitude of earth rate is updated in a com-

puter.

If the azimuth gyro is gimballed as mentioned above, gimbal lock may occur when latitude plus pitch or roll angle become 90°, i.e., when the vehicle is manoeuvering at high latitudes. This limitation may be circumvented, if necessary, by putting additional gimbals between the gyro and the vehicle or by replacing the gimballed gyro with a non-gimballed electrostatically supported vacuum gyro with direction cosine pattern readout.

With its sensors mounted on a common base strapped down to the vehicle the described system has advantages of a strapdown system (easy mounting and maintainability of the sensors). As against a strapdown system it avoids error sources due to the dynamic input to the sensors and the computational process. Insofar it has advantages of a platform system, too and can be thought of as being a hybrid system.

3. BASIC PERFORMANCE AND IMPLEMENTATION OF THE NAVIGATION SYSTEM

In this chapter we will review Schuler's results [1] with regard to the quasi static performance of two gyropendulums with their spin vectors pointing up or down, respectively. Furthermore, we will see how an inertial navigation system can be implemented, using these gyropendulums and an azimuth gyro as sensors.

Schuler [1] considered only a vehicle moving parallel to the surface of the earth and neglected side effects resulting from Coriolis accelerations and the gyro precession due to the vertical component of earth rate and rate of change of longitude. He derived expressions for the quasi static equilibrium of the gyros when the torque caused by gyro precession due to the horizontal component of earth rate (ω^{ie} cos L) and rate of change of longitude ($\dot{\ell}$cos L) and latitude ($\dot{L}$) is compensated by a pendulous torque mgr Θ (s. [1], eq. (A7), mr = pendulosity of the gyro, Θ = inclination to the vertical, in [1] this is called β). Let us introduce the northerly and easterly velocity instead of $\dot{L}$ and $\dot{\ell}$ cos L

$$V_N = R\ pL \tag{3.1}$$

$$V_E = R \cos L \cdot pl, \tag{3.2}$$

where

$$R = R_o + h \tag{3.3}$$

is the radius of the trajectory with respect to the center of the earth and

$$p = \frac{d}{dt} \tag{3.4}$$

is an operator. From the equilibrium of the two torques we might obtain the following expression for the angles about the north and east axes of the gyropendulum for a vehicle which moves with constant velocity parallel to the surface of the earth

$$\Theta^{qs}_{NI,II} = \mp \frac{H'}{mgr} \frac{V_N}{R} \tag{3.5}$$

$$\Theta^{qs}_{EI,II} = \mp \frac{H'}{mgr} \frac{1}{R} (R\omega^{ie} \cos L + V_E), \tag{3.6}$$

where the subscripts I, II and the signs $\mp$ belong to a gyropendulum with its spin vector pointing up or down, respectively.

Schuler has shown in [1], eq. (A10) that these equations hold even for a horizontally accelerated vehicle under the above mentioned assumptions if the

gyropendulum is tuned to

$$\frac{mgr}{H'} = \sqrt{\frac{g}{R}} = \omega^s \tag{3.7a}$$

which is on the surface of the earth

$$\omega_o^s = 1.235 \cdot 10^{-3} \text{ sec}^{-1} \tag{3.7b}$$

or

$$T_o^s = 84.4 \text{ min.} \tag{3.8}$$

Then we may rewrite eq. (3.5) and (3.6) as

$$\theta_{NI,II}^{qs} = \mp K V_N \tag{3.9}$$

$$\theta_{EI,II}^{qs} = \mp K (R\omega^{ie} \cos L + V_E) = \mp K V_{iE}, \tag{3.10}$$

where V_{iE} is the easterly velocity with respect to inertial space,

$$K = 1/\sqrt{gR} \tag{3.11a}$$

and on the surface of the earth

$$K_o = 1/\sqrt{g_o R_o} = 1.265 \cdot 10^{-4} \frac{\text{rad}}{\text{m/sec}} = 7.24 \frac{\widehat{\text{sec}}}{\text{km/h}}. \tag{3.11b}$$

The eqs. (3.9) and (3.10) show us that the deviation of each spin axis from the vertical takes place in the plane normal to the motion of the vehicle with respect to inertial space. According to this simplified analysis (Chapter 4 represents a more detailed analysis) we obtain for the deviation of a gyropendulum which is stationary at the equator ($V_N = 0$, $V_{iE} = R_o\omega^{ie}$ = 1,675. km/h)

$$\theta_{NI,II}^{qs} = 0 \tag{3.12a}$$

$$\theta_{EI,II}^{qs} = \mp 3.37^\circ. \tag{3.12b}$$

For the implementation of this gyropendulum a sensor may be used similar to the Autonetics G10 two-degree-of-freedom gyro. It is described in [11]; its sketch and some numbers are shown in Fig. 3.1. The rotor is supported by a hydrodynamic spherical gas bearing providing freedom about all three axes. From the gyro data mentioned in Fig. 3.1 and eq. (3.7) it can be derived that

Table 3.1

DATA OF THE G10 TWO-DEGREE-OF-FREEDOM GYROSCOPE

(Taken from [11])

Dimensions

Height:	8.4	cm
Diameter:	8.9	cm
Weight:	907.	gm

Rotor Data

Moment of Inertia:	945.		$gm\text{-}cm^2$
Mass:	135.		gm
Angular Rate:	60.	240.	rps
Angular Momentum:	3.6×10^5	1.44×10^6	$gm\text{-}cm^2/sec$

Drift Data

Compensated Bias rms:	0.1	0.1	deg/h
Random Drift rms:	0.005	0.02	deg/h
Bias Stability rms:	0.3	0.3	deg/h
Temperature Sensitivity:	0.005	0.005	deg/h/F
Drift Due to			
Rotor Mass Unbalance:	0.5	0.5	deg/h/g
Rotor Structural Compliance:	0.4	0.4	deg/h/g
Incompressible Effect of Gas Bearing:	9.6	0.4	$deg/h/g^2$
Compressible Effect of Gas Bearing:	1.6	0.4	$deg/h/g^2$

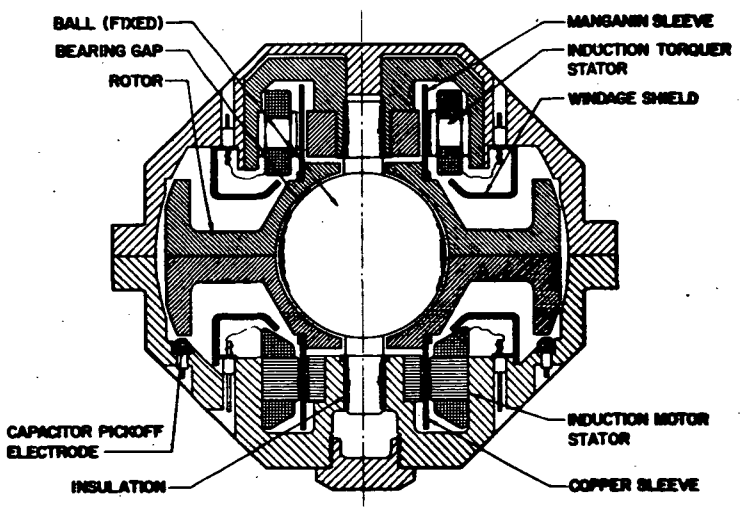

Fig. 3.1 A Gas-Film Supported Free-Rotor Gyro

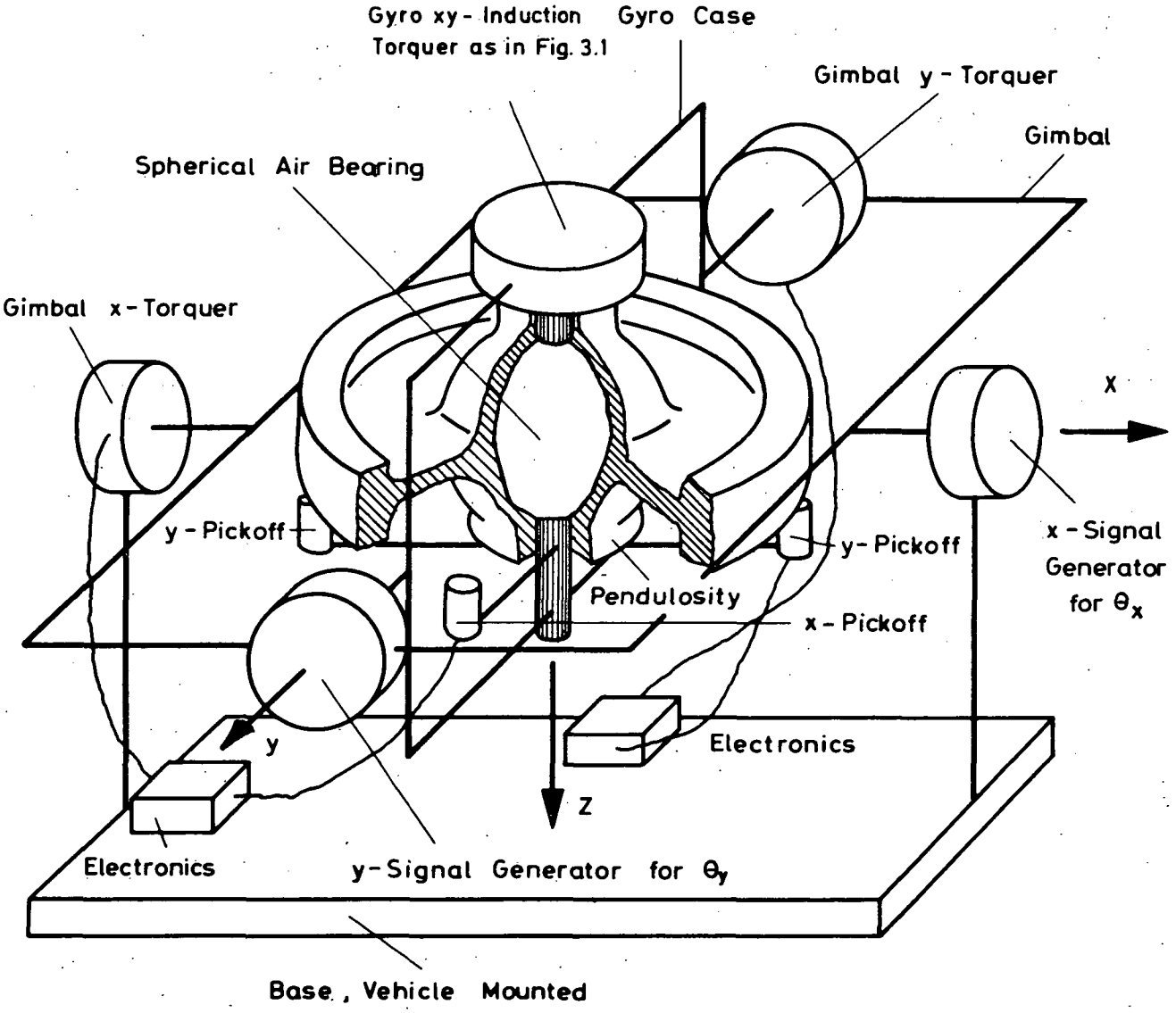

Fig.

Fig. 3.2 Gimballed Gyropendulum

this gyro is Schuler-tuned if the center of gravity is below the center of support by

$$r = \frac{H'}{m\sqrt{gR}} = 0.135 \text{ mm}. \tag{3.13}$$

We will see in the next chapter that the tuning condition is slightly different for a gyro on the moving earth.

The G10 gyro is a null sensor and it must be isolated from the angular motion of the vehicle about the two input axes. This might be accomplished by putting a gimbal between the gyro case and the vehicle which can rotate with respect to the vehicle about the longitudinal axis. The gyro case may rotate with respect to the gimbal about the pitch axis. A sketch of this setup is shown in Fig. 3.2. We see that the gyro case (shown as innermost gimbal) is indeed base-motion isolated about the longitudinal (x-) axis and pitch (y-) axis, but is not isolated from the motion of the vehicle about the yaw (z-) axis. Since this last mentioned angular motion occurs about the gyro's spin axis, it has a negligible effect on the motion of the rotor, especially if the coupling torque due to changes of the relative angular rate between the case and the rotor (i.e. the viscous aerodynamic torque and the motor torque) is small. The relative angular motion between the gyro case and the rotor does affect the readout of the gyro's attitude and the command torques, as will be seen later.

On the axis between the vehicle and the gimbal as well as between the gimbal and the gyro case, two signal generators and two torque generators are mounted. The latter ones are connected to their respective gyro pickoffs via an electronic network in order to null the pickoff signal between the case and the rotor.

The two signal generators read the attitude of the gyropendulum in the body frame. The angles Θ_x about the longitudinal axis (positive when the vehicle moves positively with respect to the gimbal) and Θ_y about the pitch axis (positive, when the gimbal moves positively with respect to the gyro case) are related to the angles Θ_N of the gyropendulum about the north axis and Θ_E about the east axis in the following way (s. eqs. (A45) and (A46) in Appendix A)

$$\Theta_x = \varphi - \Theta_N \cos\psi - \Theta_E \sin\psi \tag{3.14}$$

$$\Theta_y = \vartheta - \Theta_E \cos\psi + \Theta_N \sin\psi, \tag{3.15}$$

where we have assumed that the sequence of rotation between the navigational frame (x pointing north, y pointing east, z pointing down) and the body frame was first about the down axis through the angle ψ (for northerly flying vehicle $\psi = 0$), secondly about the pitch axis through the angle ϑ and thirdly about the longitudinal axis through φ , with φ and ϑ being small angles.

The eqs. (3.14) and (3.15) prove Schuler's results: under the assumptions mentioned above and using eqs. (3.9) and (3.10) the sum of the quasi static readout of both gyropendulumsindicate the vertical

$$(\Theta_{xI} + \Theta_{xII})^{qs}/2 = \varphi \tag{3.16}$$

$$(\Theta_{yI} + \Theta_{yII})^{qs}/2 = \vartheta \tag{3.17}$$

and the difference is proportional to the velocity with respect to space

$$(\Theta_{xI} - \Theta_{xII})^{qs}/2 = \delta\ \Theta_{xI,II}^{qs}/2 = K\ [V_N \cos\psi + V_{iE} \sin\psi\ ] \tag{3.18}$$

$$(\Theta_{yI} - \Theta_{yII})^{qs}/2 = \delta\ \Theta_{yI,II}^{qs}/2 = K\ [V_{iE} \cos\psi - V_N \sin\psi\ ]. \tag{3.19}$$

Solving for V_N and V_E

$$V_N = \frac{1}{2K}\ (\delta\Theta_{xI,II}^{qs} \cos\psi - \delta\ \Theta_{yI,II}^{qs} \sin\psi\ ) \tag{3.20}$$

$$V_E = \frac{1}{2K}\ (\delta\Theta_{yI,II}^{qs} \cos\psi + \delta\Theta_{xI,II}^{qs} \sin\psi\ ) - R\omega^{ie} \cos L, \tag{3.21}$$

where for a known latitude L, the velocity $R\omega^{ie} \cos L$ of a point on the surface of the earth is a known quantity and can be subtracted. The position of the vehicle, i.e. latitude and longitude are easily obtainable from V_N and V_E by an integration (s. eqs. (3.1) and (3.2)). In these equations the azimuth angle ψ is still unknown. The information on the north-direction must be obtained externally based on star sighting, as Schuler proposes it in [1], or it must be stored in a free gyro. In the latter case the resulting navigational system would be self-contained.

For such a self-contained navigational system another, but non-pendulous, G10-gyro may be used for the azimuth reference. The spin vector of this gyro is pointing northerly, parallel to the earth axis. A gimbal between the gyro case and the vehicle provides base motion isolation of the gyro about its input axes, as is shown in Fig. 3.3. From the two output signals of the signal

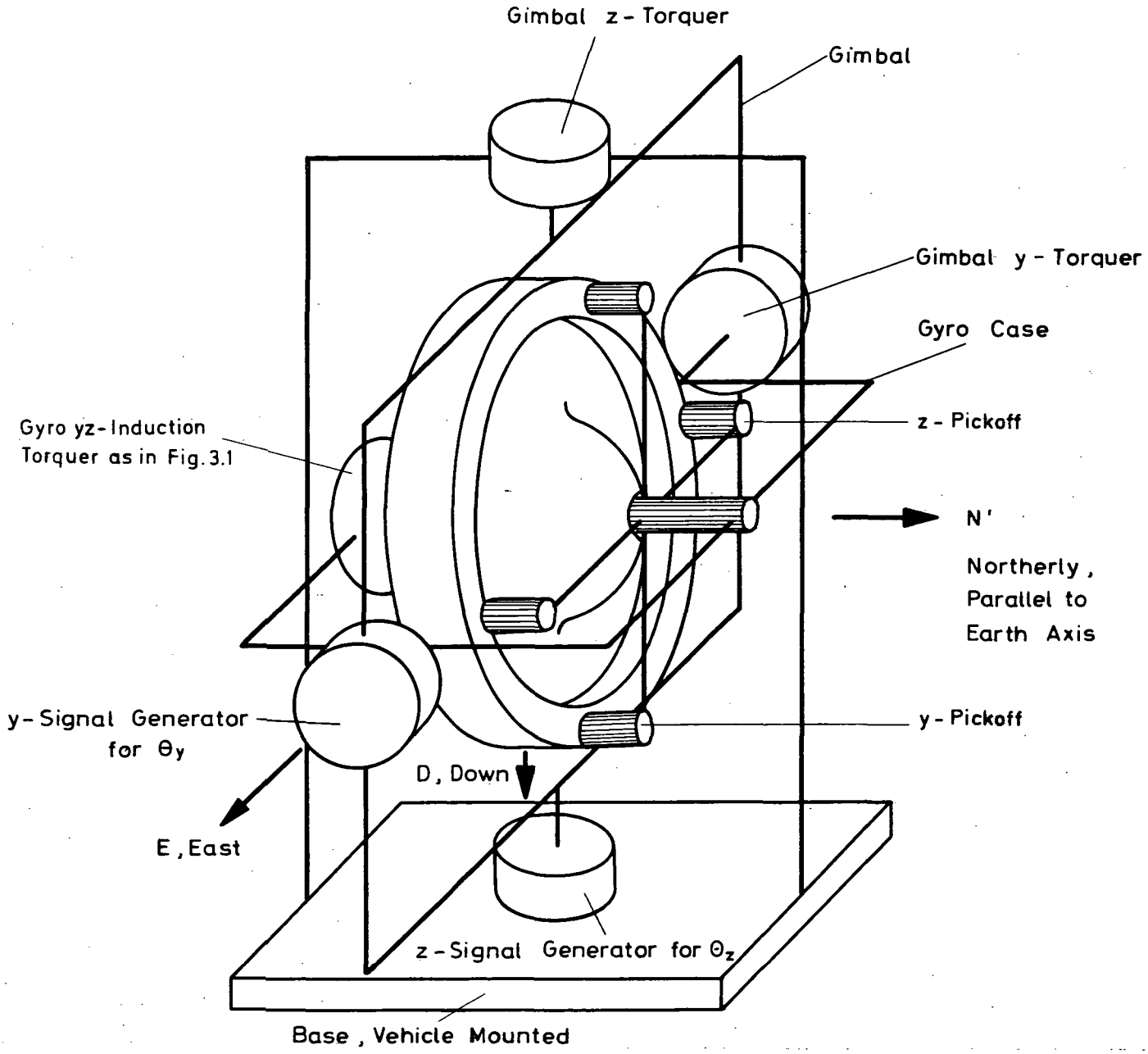

Fig. 3.3 Gimballed Azimuth Gyro

(Signal paths from gyro pickoffs to gimbal torquers not shown here)

generators which are the angles Θ_y (positive, when the gimbal rotates positively with respect to the gyro case) and Θ_z (positive, when the vehicle rotates positively with respect to the gimbal) one might extract (s. Appendix B, eqs. (B18) and (B19)) latitude and azimuth

$$\Theta_y \approx - L + \vartheta \cos\psi + \varphi \sin\psi - \Theta_E \tag{3.22}$$

$$\Theta_z \approx \psi - (\vartheta \sin\psi - \varphi \cos\psi) \tan L + \Theta_D/\cos L \tag{3.23}$$

where Θ_E and Θ_D are error angles due to gyro drift and misalignment. Fig. 3.4 shows the signal flow diagram for this computation.

Since latitude is also a result of the integration of the northerly ground speed obtained from the two gyropendulums (s. eq. (3.20)), one has in eq. (3.22) a redundant information.

Unfortunately, gimbal lock occurs in this kind of azimuth gyro for $\Theta_y = \pm 90^\circ$, when the readout of the z signal generator deteriorates (s. eq. (B13)). At 60° latitude this happens, for instance, when the airplane, making a turn with $\varphi = -30^\circ$, is heading towards east. In Appendix B, Section B3 it is shown that this does not occur, for instance, if an electrostatic gyro (described in [12]) with direction cosine pattern readout is used instead of the gimballed gyro. The readout equations of this kind of gyro are (s. eqs. (B21) and (B22))

$$\Theta'_y \approx 90^0 + L - \vartheta \cos\psi - \varphi \sin\psi + \Theta_E \tag{3.24}$$

$$\Theta'_z = \arccos [- \sin\psi \cos L - (\varphi + \Theta_E \sin\psi) \sin L + \Theta_D \cos\psi] . \tag{3.25}$$

In the following we will assume that a gimballed gyro is used for azimuth reference.

Compared to an azimuth gyro with its spin vector pointing north but parallel to the surface of the earth, in which case Θ_z provides heading information only, eq. (3.23) is more complicated. But with such a gyro a command torque has to be applied to the gyro for compensating the vertical component of earth rate. This causes difficulties insofar as with our proposal the gyro case is not base-motion isolated about the spin axis and the output signal of the gyro yz-torquer would have to change with the motion of the vehicle. With the chosen alignment no command torques have to be applied to the gyro, since the gyro spin axis is supposed to stay inertially fixed.

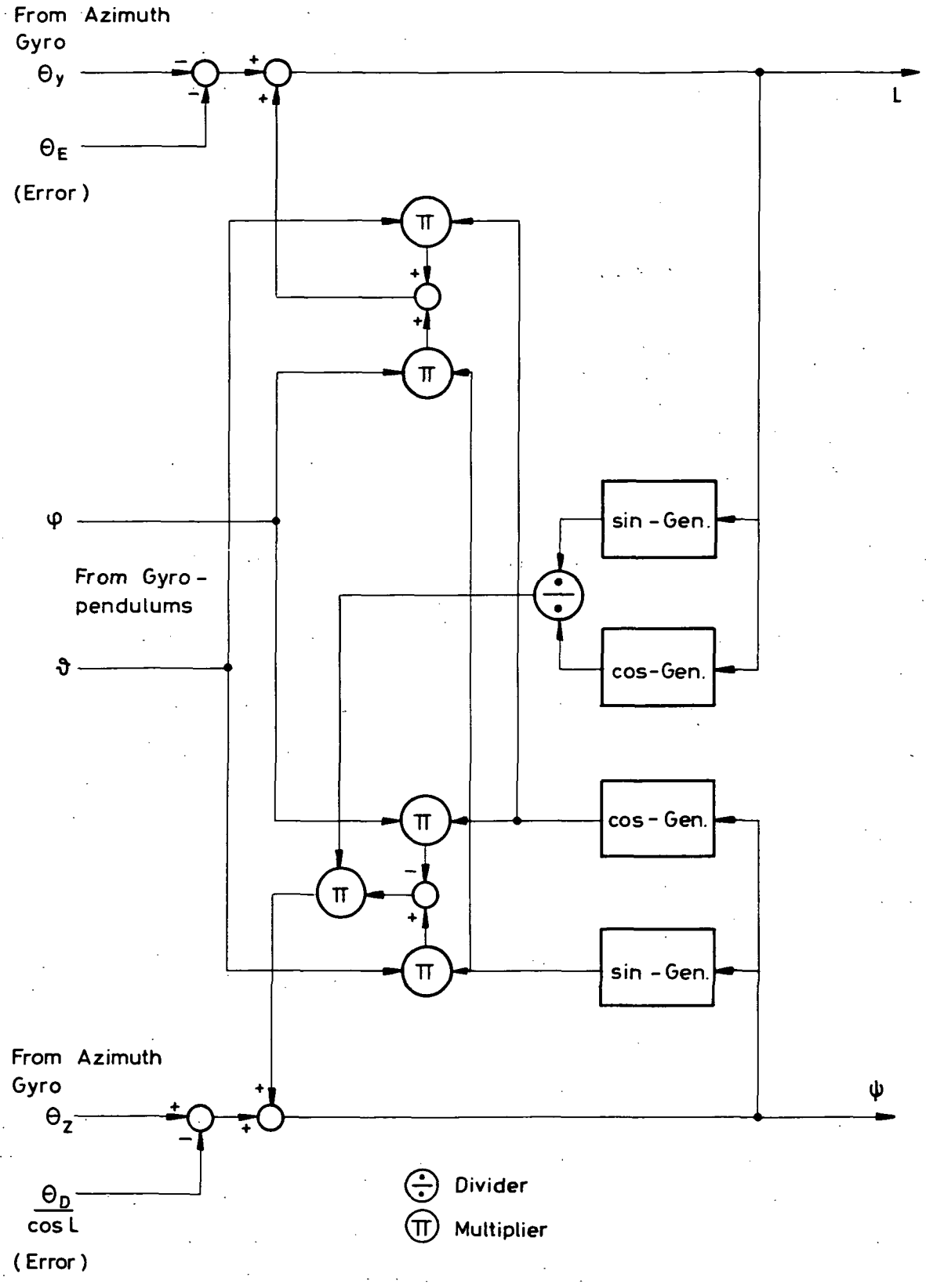

Fig. 3.4 Signal Flow Diagram for the Computation of Azimuth (ψ) and Latitude(L), Based on the Readout of the Azimuth Gyro and Attitude, Derived from the Gyropendulums

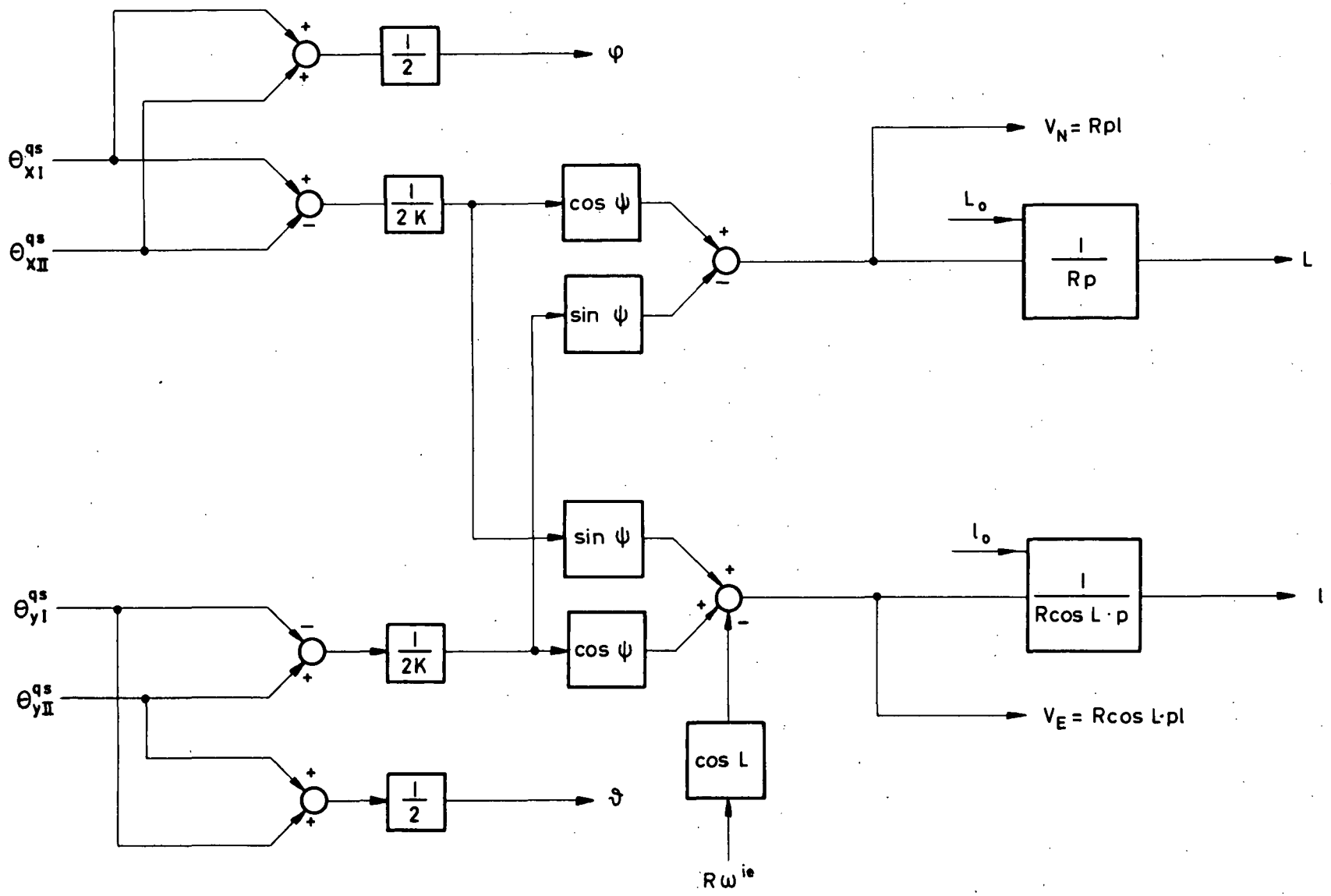

Fig. 3.5 Signal Flow Diagram for the Simplified Computation of Attitude (φ, ϑ), Ground Speed (V_N, V_E) and Position (L, l), Based on the Quasi-Static Readout of 2 Schuler-Tuned Gyropendulums

Fig. 3.5 shows the signal flow of the navigational computation for the vehicle's attitude (φ, ϑ , eqs. (3.16) and (3.17)) with respect to the vertical, the vehicle's north and east velocity (V_N, V_E, eqs. (3.20) and (3.21)) and finally the vehicle's position, namely longitude ℓ and latitude L. The azimuth angle ψ is computed from the azimuth gyro readout according to Fig. 3.4.

4. PERFORMANCE OF THE GYROPENDULUM IN A DYNAMIC ENVIRONMENT UNDER IDEAL TUNING AND COMPENSATION CONDITIONS

In the previous chapter we have seen that one may obtain from the sum and difference of corresponding quasi static readouts of two Schuler tuned gyropendulums with their respective spin vectors pointing up or down and one azimuth gyro, all the information needed for navigation when moving over the earth, namely the vehicle's attitude, azimuth, ground speed and position. In this chapter we will look more thoroughly into the dynamics of the gyropendulums. This allows us to draw certain conclusions on the practicability of a navigational system based on these gyropendulums as inertial sensors. Since all the navigational information, for known azimuth ψ, is already included in the quasi static output signals of the gyropendulums, any superimposed oscillation deteriorates this information and has to be suppressed by means of control loops and proper initial alignment.

Eq. (A26) of Appendix A describes the dynamics of a gyropendulum; Fig. 4.1 is the corresponding signal flow diagram. It shows that any torque about the east axis caused by the torquer (M_E^{cmd}) or a northerly acceleration f_N causes the gyropendulum to tilt about the north axis with respect to inertial space (Θ_N^{ig}). Since the earth is also moving with respect to inertial space and since the motion of the gyropendulum is only affected by the tilt from the vertical, the angle Θ_N^{in} enters the loop at the node 1N. The tilt from the vertical $\Theta_N = \Theta_N^{ig} - \Theta_N^{in}$ causes the gravity and the vertical component of earth rate to generate a torque about the north axis at the node gN, which stimulates the motion about the east axis.

From the left hand side of eq. (A26) we see that in general the spin vector of the gyropendulum describes an undamped motion - actually a coning motion as we will see later - the frequency (s. eq. (A27)) of which

$$\Omega = \frac{mgr}{H}\left(1 + \frac{p^2 h}{g} - \frac{b_v}{g}\right) \pm \left(\omega^{ie} + \frac{V_E}{R\cos L}\right) \sin L \qquad (4.1)$$

depends on the vertical acceleration of the vehicle and the vertical component of earth rate and rate of change of longitude or easterly velocity, respectively. For the same parameters m, r and H of the gyropendulum, the frequency of the instrument with upward pointing spin vector is slightly different from the one with downward pointing spin vector.

The vertical acceleration $p^2 h$ has zero mean indeed for a horizontally flying vehicle, but short time peaks due to vertical gusts might very well

gN gE Pendulous Gyrowheel (North and East Axis) as Torque Summing Member

1N 1E Relative Motion (North and East Axis) between Gyropendulum and Navigational Frame

TT Multiplication Nodes

——— Mechanical Signals —·—·— Magnetic Signals

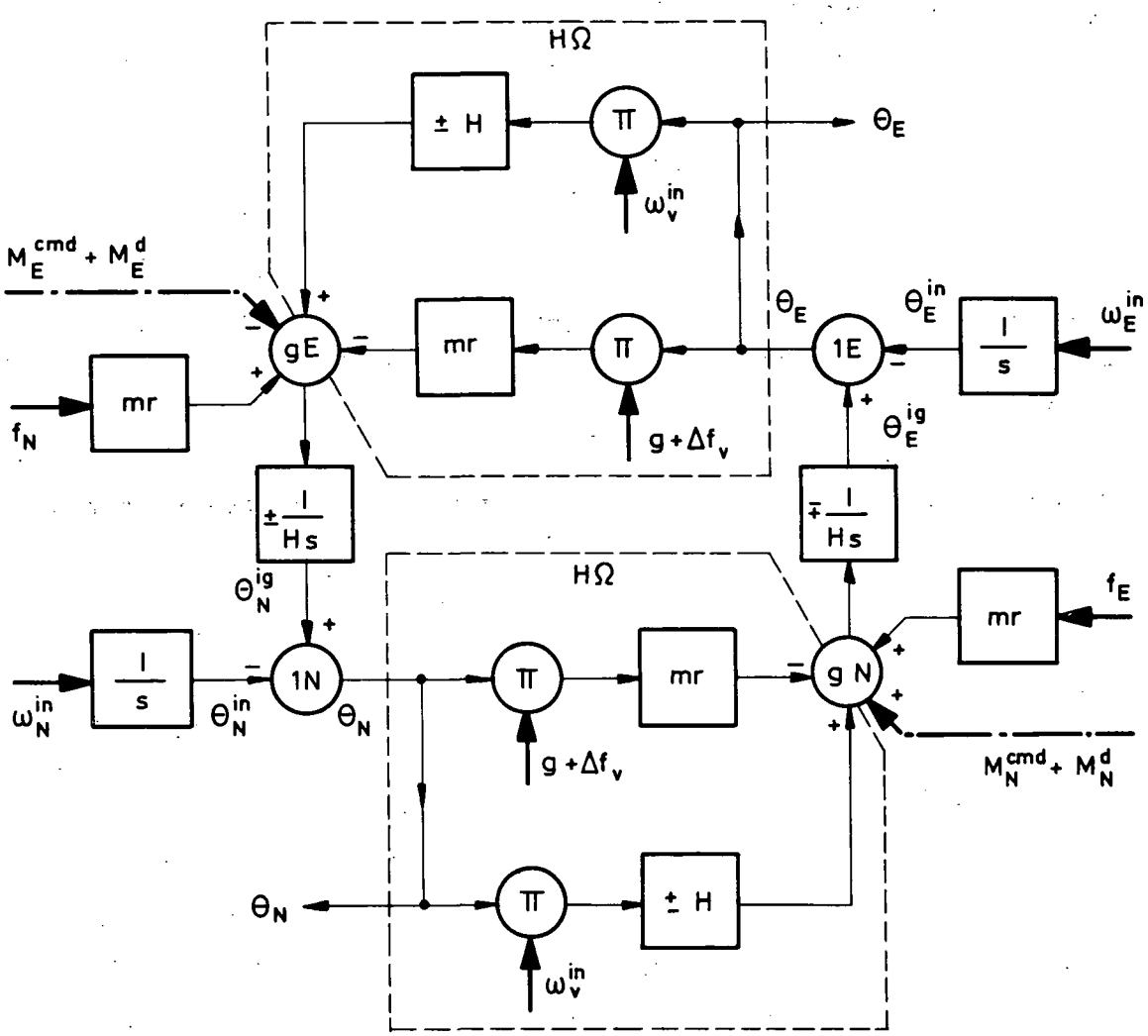

Fig. 4.1 Signal Flow Diagram for a Two-Degree-of-Freedom Gyropendulum with Vertical Spin Axis

exceed 1g. Since these peaks last much less than the period of the gyropendulum, which is in the order of 84 min, we have, in order to estimate its effects upon the motion, approximated the acceleration of one gust by an impulse function occuring at the time τ (s. eq. (A28))

$$\ddot{p}h \approx ph \cdot \delta(t - \tau) . \tag{4.2}$$

Since this form differs from zero only for a short time interval at $t = \tau$, it will be multiplied in eq. (A26) with the constant angles $\Theta_N(\tau)$ or $\Theta_E(\tau)$, respectively. This shows us that the short time vertical acceleration causes an additional forcing function which enters the right hand side of the equation (s. eq. (A36)) while leaving the frequency Ω^c on the left hand side (s. eq. (A30)) given by

$$\Omega^c = \frac{mgr}{H}\left(1 - \frac{b_v}{g}\right) \pm \left(\omega^{ie} + \frac{V_E}{R\cos L}\right) \sin L . \tag{4.3}$$

Based on this slowly varying frequency on the left hand side of eq. (A26), we have extracted the quasi static equilibrium, i.e., the equilibrium between the initial torques on the right hand side (subscript "0") and the slowly varying "spring torques" $H\Omega^c\Theta_{N,E1}$ on the left hand side. This quasi static equilibrium is (s. eqs. (A34) and (A35))

$$\Theta_{N1} = \frac{M_{No}^d}{H\Omega^c} \tag{4.4}$$

$$\Theta_{E1} = \frac{M_{Eo}^d/H \mp \omega^{ie} \cos L}{\Omega^c} . \tag{4.5}$$

These values are essential for the initial alignment of the gyropendulum. Assuming that a command torque is applied to it for damping out the oscillation during initial self alignment mode, it will always settle to this equilibrium which at 45° latitude is for $M_{No}^d = M_{Eo}^d = 0$ and $\Omega_o^c \approx \omega_o^s$

$$\Theta_{No} = 0^o \tag{4.6}$$

$$\Theta_{Eo} \approx \mp 2.39^o . \tag{4.7}$$

If the disturbance torque about the north axis, expressed, like the gyro drift, in degrees per hour, has the following magnitude

$$\frac{M_{No}^{d}}{H} = 1 \text{ MERU} = 0.015 \text{ deg/hr} \tag{4.8}$$

the gyropendulum will settle with an offset angle about the north axis from the vertical of

$$\Theta_{No} \approx 12.2 \widehat{\sec} \ . \tag{4.9}$$

As was pointed out in the previous chapter, the quasi static output signal of the gyropendulum mounted on a moving vehicle contains all necessary navigational information for known azimuth. Any superposed oscillation deteriorates this information. The remaining part of this chapter deals with the requirements to suppress the oscillatory motion by means of control loops and proper initial alignment of the spin axis.

From eq. (A37) to (A39) in Appendix A the following may be concluded: tuning the gyropendulum to

$$\frac{H}{mr\ R} = \Omega^{c} \tag{4.10}$$

causes in eq. (A38) and (A39) the parenthesis of the first term on the right hand side to cancel with the determinant Δ and the second term to become zero. Physically this means that the gyropendulum will indicate the north and east velocity V_N and V_{iE} without time lag and oscillation and that it becomes insensitive to the horizontal accelerations $p\Delta V \hat{=} s\Delta\tilde{V}$. Since we have not specified in Appendix A the transient of ΔV_N and ΔV_{iE} except for continuity ($\Delta V_{No}^{+} = \Delta V_{iEo}^{+} = 0$), this result holds for any continuous motion of the vehicle.

The tuning condition (4.10) can be easily derived from the signal flow diagram in Fig. 4.1, keeping in mind that, caused by the earth's geometry, any northerly acceleration, for instance, is coupled with an angular rotation about the east axis ($f_N = sV_N = Rs\omega_E^{in}$). Proper tuning requires that the signal flow, originating in f_N for instance, is not circulating in the closed loop but ends in the point 1E. This means that the northerly accelerated gyropendulum tilts about the north axis ($\Theta_N = mr\ f_N/sH = V_N\ mr/H$) but tracks the vertical about the east axis ($\Theta_E = 0$ or $\Theta_E^{ig} = \Theta_E^{in}$) .

Before we continue in the derivation of the performance equations of the gyropendulum, let us first have a look at the Coriolis and centrifugal acceleration for three types of aircraft: a private plane or helicopter, a sub-

sonic jet and a supersonic transport, flying at different speeds in northerly, north-easterly and easterly directions. For these aircraft, equations (A21a) to (A23a) have been evaluated. As we see from Table 4.1 these accelerations are very small, the largest value being $b_N = b_V = 1.5 \cdot 10^{-2} g$ for the SST flying at 2,500 km/h in an easterly direction. But it can be easily shown that already the horizontal Coriolis acceleration of the private plane or helicopter has a serious effect on inertial navigation. In order to prove this physically, let us look at a normal pendulum subject to a constant horizontal Coriolis acceleration b_h in the gravitational field. The ratio b_h/g is the value of the steady state angle which the pendulum indicates with respect to the vertical. The same is true of the gyropendulum and since 1 $\widehat{\text{sec}}$ tilt angle of the gyropendulum corresponds to 0.14 km/h ground speed, (s. eq. (3.11)) the indicated ground speed error caused by the horizontal Coriolis acceleration is

$$\Delta V = 2.9 \cdot 10^4 \, b_h/g \text{ km/h} \quad . \tag{4.11}$$

Table 4.1 Coriolis and Centrifugal Acceleration for Three Types of Aircraft Flying Horizontally at 45° Latitude

No.	Flight Direction	Components of Coriolis and Centrifugal Acceleration	Aircraft: Private Plane, Helicopter	Aircraft: Subsonic Jet	Aircraft: Supersonic Transport
			V = 250 km/h h = 1 km	V = 900 km/h h = 10 km	V = 2,500 km/h h = 20 km
1	North ($V_N=V$, $V_E=0$)	b_N/g	0	0	0
2		b_E/g	$3.65 \cdot 10^{-4}$	$1.32 \cdot 10^{-3}$	$3.65 \cdot 10^{-3}$
3		b_V/g	$7.70 \cdot 10^{-5}$	$1.00 \cdot 10^{-4}$	$7.70 \cdot 10^{-3}$
4	North-East ($V_N=V_E=V/\sqrt{2}$)	b_N/g	$5.50 \cdot 10^{-4}$	$2.35 \cdot 10^{-3}$	$9.10 \cdot 10^{-3}$
5		b_E/g	$2.98 \cdot 10^{-4}$	$1.43 \cdot 10^{-3}$	$6.45 \cdot 10^{-3}$
6		b_V/g	$5.90 \cdot 10^{-4}$	$2.86 \cdot 10^{-3}$	$1.19 \cdot 10^{-2}$
7	East ($V_N=0$, $V_E=V$)	$b_N/g = b_V/g$	$8.15 \cdot 10^{-4}$	$3.62 \cdot 10^{-3}$	$1.50 \cdot 10^{-2}$
8		b_E/g	0	0	0

From Table 4.1 we see that for a private plane flying easterly, this error amounts to $\Delta V = 23$ km/h! Hence these error terms have to be very well taken care of.

In order to judge the usability of the gyropendulum as an inertial sensor we will now derive from eq. (A38) and (A39) the performance equations under the following assumptions which have to be matched in the real world:

a) the torques caused by the Coriolis and centrifugal accelerations of a horizontally flying vehicle are properly compensated, i.e.

$$M_N^{cmd} = -mr\, b_E \tag{4.12}$$

$$M_E^{cmd} = mr\, b_N, \tag{4.13}$$

b) the gyropendulum is properly tuned according to eq. (4.10),

c) the disturbance torques acting on the gyropendulum do not change from their static values, i.e. $\Delta M_N^d = \Delta M_E^d = 0$.

With these assumptions we obtain for the displacement angles of the gyropendulum about the north and east axis from their quasi static equilibrium in eq. (4.4) and (4.5) in the time domain:

$$\begin{aligned}\Delta\Theta_N = {} & \mp \frac{mr}{H}\Delta V_N + \Delta\Theta_{No}^{+}\cos\Omega^c t \mp \Delta\Theta_{Eo}^{+}\sin\Omega^c t \\ & + \frac{mr}{H}\,ph\, f(t-\tau)\left[\frac{V_{iE}}{R\Omega^c} - \left(\frac{V_{iE}}{R\Omega^c} \pm \Theta_E(\tau)\right)\cos\left(\Omega^c(t-\tau)\right)\right. \\ & \left. \mp\left(\frac{V_N}{R\Omega^c} \pm \Theta_N(\tau)\right)\sin\left(\Omega^c(t-\tau)\right)\right]\end{aligned} \tag{4.14}$$

$$\begin{aligned}\Delta\Theta_E = {} & \mp \frac{mr}{H}\Delta V_{iE} + \Delta\Theta_{Eo}^{+}\cos\Omega^c t \pm \Delta\Theta_{No}^{+}\sin\Omega^c t \\ & - \frac{mr}{H}\,ph\, f(t-\tau)\left[\frac{V_N}{R\Omega^c} - \left(\frac{V_N}{R\Omega^c} \pm \Theta_N(\tau)\right)\cos\left(\Omega^c(t-\tau)\right)\right. \\ & \left. \pm\left(\frac{V_{iE}}{R\Omega^c} \pm \Theta_E(\tau)\right)\sin\left(\Omega^c(t-\tau)\right)\right]\end{aligned} \tag{4.15}$$

where

$$f(t-\tau) = \begin{cases} 0 \text{ for } \tau > t \\ 1 \text{ for } \tau \leq t\ . \end{cases} \tag{4.16}$$

When the gyropendulum, mounted on a stationary vehicle ($\Delta V_N = \Delta V_{iE} = ph = 0$), is initially aligned with the vertical, i.e. $\Delta\Theta_{No}^{+} = -\Theta_{No}$ and $\Delta\Theta_{Eo}^{+} = -\Theta_{Eo}$

(s. eq. (4.9) and (4.7)), it oscillates in a coning motion about Θ_{No} and Θ_{Eo} as shown in Fig. 4.2.

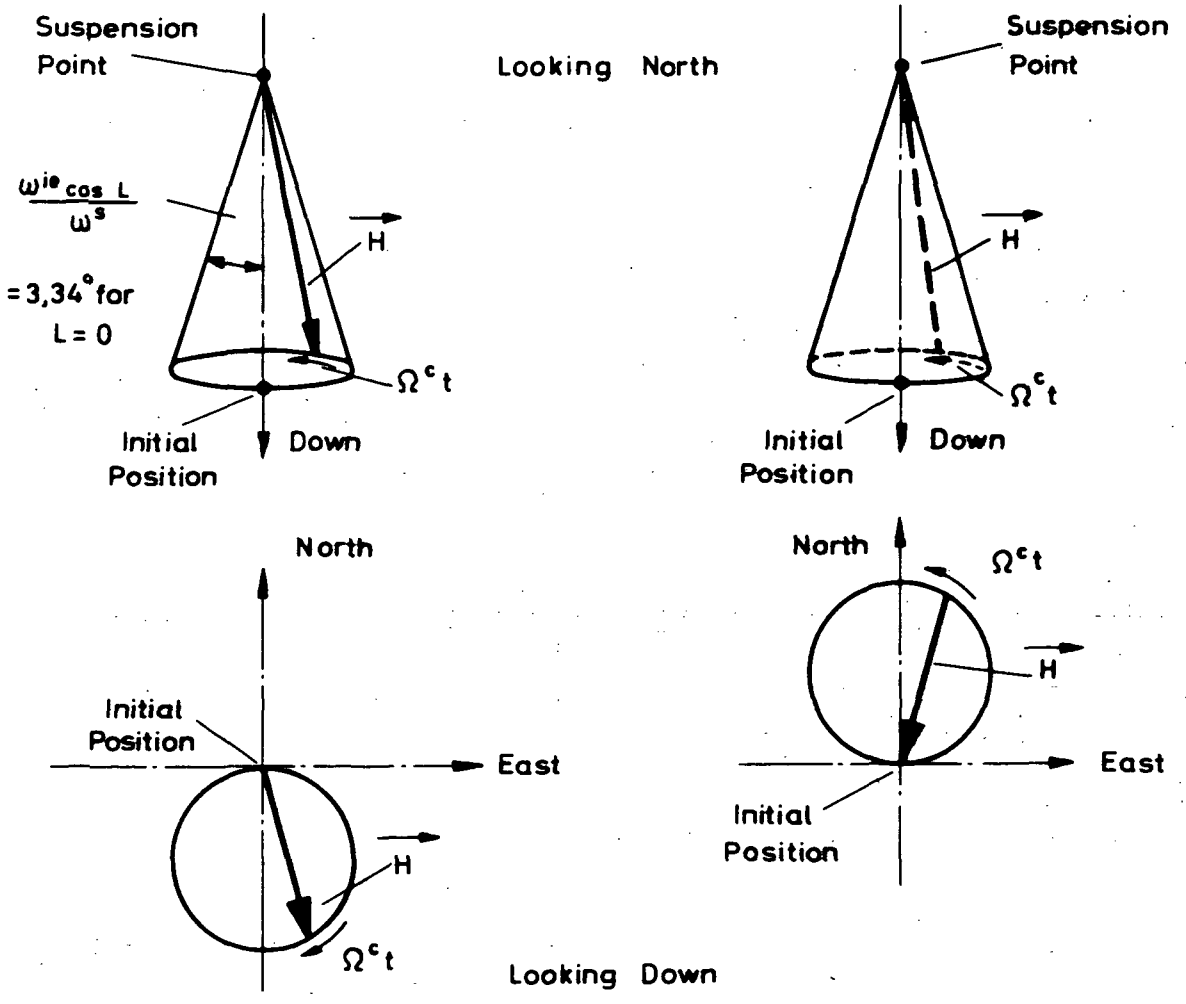

Fig. 4.2 **Coning Motion of a Gyropendulum with Spin Vector Pointing Up or Down, Respectively**

Let us now turn our attention to the angles $\Theta_N(\tau)$ and $\Theta_E(\tau)$ on the right hand side of eq. (4.14) and (4.15). The coefficient of these two angles is at the time $t \geq \tau$ for ph = 1 m/sec

$$\frac{mr}{H} ph = \frac{ph}{R\Omega^c} \approx \frac{ph}{R\omega_o^s} \approx 1.3 \cdot 10^{-4}, \tag{4.17}$$

having kept in mind eq. (4.10). This may be neglected compared with 1 on the left hand side of eq. (4.14) and (4.15) even for higher vertical velocities.

Thus we can neglect $\Theta_N(\tau)$ and $\Theta_E(\tau)$ on the right hand side as compared with the left hand side, and for $t = \tau$ we obtain for a perfectly aligned gyropendulum neglecting the gyro drift in eq. (4.4) and (4.5):

$$\Theta_N(\tau) \approx \mp\left(\frac{mr}{H}\Delta V_N\right)(\tau) = \mp\left(\frac{V_N}{R\Omega^c}\right)(\tau) \tag{4.18}$$

$$\Theta_E(\tau) \approx \mp\left(\frac{\omega^{ie}\cos L_o}{\Omega^c} + \frac{mr}{H}\Delta V_{iE}\right)(\tau) = \mp\left(\frac{V_{iE}}{R\Omega^c}\right)(\tau). \tag{4.19}$$

Introducing these into the right hand side of eq. (4.14) and (4.15) we see that the vertical acceleration p^2h, which we have assumed to be an impulse function at the time τ, does not stimulate an oscillation, provided that ground speed remains constant during ascent or descent. It can be easily shown that oscillations due to changes in ground speed are negligible (s. eq. (C23) of Appendix C).

For the total angle of the gyropendulum about the north and east axes we may write

$$\begin{aligned}\Theta_N &= \Theta_{N1} + \Delta\Theta_N \\ &= \mp\frac{mr}{H}V_N + \frac{M^d_{No}}{H\Omega^c} + \frac{mr}{H}\frac{V_{iE}}{R\Omega^c}\,ph\,f(t-\tau) + \Delta\Theta^+_{No}\cos\Omega^c t \mp \Delta\Theta^+_{Eo}\sin\Omega^c t\end{aligned} \tag{4.20}$$

$$\begin{aligned}\Theta_E &= \Theta_{E1} + \Delta\Theta_E \\ &= \mp\frac{mr}{H}V_{iE} + \frac{M^d_{Eo}}{H\Omega^c} - \frac{mr}{H}\frac{V_N}{R\Omega^c}\,ph\,f(t-\tau) + \Delta\Theta^+_{Eo}\cos\Omega^c t \pm \Delta\Theta^+_{No}\sin\Omega^c t.\end{aligned} \tag{4.21}$$

The result that the vertical acceleration does not stimulate an oscillation but yields only an angle displacement proportional to the product $V_{iE}\,ph$ or $V_N\,ph$ respectively, is really surprising and we have to find a physical explanation for it making use of the signal flow diagram in Fig. 4.1. Assuming that we have a perfect and accurately aligned gyropendulum ($M^d = 0, \Delta\Theta^+_o = 0$) and that the vehicle is flying eastward, we have prior to the vertical acceleration $\Theta_N = 0$, $\Theta_E = \mp\frac{mr}{H}V_{iE}$. When the vertical acceleration $p^2h \hat{=} s^2h$ occurs there will be an additional torque with the magnitude $-mrs^2h\,\Theta_E$ at the torque summing member marked gE in Fig. 4.1. This torque is integrated in the gyropendulum by $\pm 1/sH$, resulting in an offset angle $\Delta\Theta_N$ about the north axis. The torque $-H\Omega^c\Delta\Theta_N$ caused by this offset angle arrives at the torque summing

member gN in Fig. 4.1. After the vertical acceleration, the vehicle has a vertical velocity sh which causes an easterly Coriolis acceleration sh V_{iE}/R resulting also in a torque at the torque summing member gN. If both torques cancel each other, the signal generated by the vertical acceleration will not circulate in the loop and hence will not stimulate an oscillation. The mathematical condition for this is

$$(-\,mr\,s^2h\,\Theta_E)\;(\pm\,1/Hs)\;(-\,H\Omega^c) \stackrel{!}{=} -\,mr\,sh\,V_{iE}/R \qquad \text{or}$$

$$\Theta_E \stackrel{!}{=} \mp\,V_{iE}/(R\Omega^c) = \mp\,\frac{mr}{H}\,V_{iE}$$ which coincides with the assumption stated above.

After this consideration of the signal flow the offset angle $\Delta\Theta_N$ has also become understandable. It is the result of the integrated torque caused by the vehicle acceleration and we find

$$\Delta\Theta_N\,(ph) \mathrel{\hat{=}} \pm\,\frac{mr\,s^2h}{sH}\;\;\Theta_E \mathrel{\hat{=}} \frac{mr}{H}\,\frac{V_{iE}}{R\Omega^c}\;\;ph \qquad (4.22)$$

which proves the results in eq. (4.20).

Since the velocity is computed from the difference of corresponding readouts of both gyropendulums with their spin vectors pointing up and down, this offset due to vertical velocity does not affect directly the velocity computation. It does affect the attitude computation which is derived from the sum of corresponding readouts and via the circumference of the azimuth computation it does also affect the velocity computation (s. eqs. (3.23), (3.20) and (3.21)). But its effect on attitude is not too weighty. For an easterly flying SST (V_E = 2,500 km/h, V_{iE} = 3,685 km/h at L = 45°), the offset angle about the north or pitch axis respectively for ph = 1 m/sec and with $1/(R\Omega^c) = mr/H \approx K$ (s. eqs. (4.10) and (4.26)) is

$$\frac{\Delta\Theta_N(ph)}{ph} \mathrel{\hat{=}} \frac{\Delta\vartheta(ph)}{ph} \approx K^2\,V_{iE} = 3.4\,\frac{\widehat{sec}}{m/sec}\;. \qquad (4.23)$$

It will be shown in Chapter 7.2 that its effect on the velocity computation is not too significant either. Furthermore, to achieve higher accuracy, this offset angle can be easily biased out by defining as the new quasi static equilibrium

$$\Theta_{N2} = \Theta_{N1} + \Delta\Theta_N \text{ (ph)}$$

$$= \frac{M^d_{No}}{H\Omega^c} + \frac{mr}{H}\frac{V_{iE}}{R\Omega^c} \text{ ph} \qquad (4.24)$$

$$\Theta_{E2} = \Theta_{E1} + \Delta\Theta_E \text{ (ph)}$$

$$= \frac{M^d_{Eo}/H \mp \omega^{ie} \cos L_o}{\Omega^c} - \frac{mr}{H}\frac{V_N}{R\Omega^c} \text{ ph} \qquad (4.25)$$

(Θ_{N1}, Θ_{E1}, s. eq. (4.4), (4.5)). In an airplane, for instance, a signal for the vertical velocity ph is readily available and the compensation can be easily accomplished.

In the following mathematical derivation we will neglect the effect of vertical velocity on attitude and velocity and leave the proof for the validity of this assumption to Chapter 7.2.

Eqs. (4.20) and (4.21) show us that under the previously mentioned assumptions a to c (compensation for the Coriolis acceleration in horizontal flight, constant disturbance torques, perfect tuning) the gyropendulum when initially perfectly settled to its equilibrium ($\Delta\Theta^+_{No} = \Delta\Theta^+_{Eo} = 0$) indicates indeed the velocity of the vehicle with respect to space as stated by Schuler [1] (s. eqs. (3.9) and (3.10)), with only the gains seeming to be different. In order to examine this, we solve eqs. (4.3) and (4.10) for mr/H, introduce this into eqs. (4.20) and (4.21) and calculate the difference and the sum of corresponding angles of the two gyropendulums. As we recollect, this is needed for velocity and attitude computation. Keeping in mind that the vertical Coriolis acceleration is a small quantity (s. Table 4.1) we find from eqs. (4.3), (4.10) and (3.11)

$$\frac{mr}{H} \approx K\left[\left(1 + \frac{b_v}{2g}\right) \mp \frac{1}{2\omega^s}\left(\omega^{ie} + \frac{V_E}{R\cos L}\right)\sin L\right], \qquad (4.26)$$

where we have neglected in the square root of K (s. eq. (3.11)) $\left[\left(\omega^{ie} + \frac{V_E}{R\cos L}\right)(\sin/2g)\right]^2$ compared with $1/gR$. For $V_E = 0$ and $L = 45^o$ this term is 10^4 times smaller.

The angles of the gyropendulum's spin vector about the north and east axes from the quasi static equilibrium in eq. (4.4) and (4.5) are thus

$$\Delta\Theta_N = \Theta_N - \Theta_{N1} = \mp K\left[\left(1 + \frac{b_v}{2g}\right) \mp \frac{1}{2\omega^s}\left(\omega^{ie} + \frac{V_E}{R\cos L}\right)\sin L\right]\Delta V_N + \Delta\Theta^+_{No}\cos\Omega^c t \mp \Delta\Theta^+_{Eo}\sin\Omega^c t \qquad (4.27)$$

$$\Delta\Theta_E = \Theta_E - \Theta_{E1} = \mp K\left[\left(1 + \frac{b_v}{2g}\right) \mp \frac{1}{2\omega^s}\left(\omega^{ie} + \frac{V_E}{R\cos L}\right)\sin L\right]\Delta V_{iE} + \Delta\Theta^+_{Eo}\cos\Omega^c t \mp \Delta\Theta^+_{No}\sin\Omega^c t\,. \qquad (4.28)$$

Similar to these equations, it is convenient for the following evaluations to have the quasi-static equilibrium of eqs. (4.4) and (4.5) biased out from the readout angles Θ_x and Θ_y. This may be done according to eqs. (A45) and (A46) in the following way:

$$\Delta\Theta_x = \Theta_x + \Theta_{N1}\cos\psi + \Theta_{E1}\sin\psi = \varphi - \Delta\Theta_N\cos\psi - \Delta\Theta_E\sin\psi \qquad (4.29)$$

$$\Delta\Theta_y = \Theta_y + \Theta_{E1}\cos\psi - \Theta_{N1}\sin\psi = \vartheta - \Delta\Theta_E\cos\psi + \Delta\Theta_N\sin\psi\,. \qquad (4.30)$$

The navigational computation is based on the difference and sum of these readout angles of the two gyropendulums. The computer assumes the unknown misalignment angles $\Delta\Theta^+_{No}$ and $\Delta\Theta^+_{Eo}$ from the quasi-static equilibrium to be zero and relies on the following basic equations:

$$(\Delta\Theta_{xI} - \Delta\Theta_{xII})/2 = K\,(1 + b_v/2g)(\Delta V^*_N\cos\psi + \Delta V^*_{iE}\sin\psi) \qquad (4.31)$$

$$(\Delta\Theta_{yI} - \Delta\Theta_{yII})/2 = K\,(1 + b_v/2g)(\Delta V^*_{iE}\cos\psi - \Delta V^*_N\sin\psi) \qquad (4.32)$$

$$(\Delta\Theta_{xI} + \Delta\Theta_{xII})/2 = \varphi^* - \frac{K^2}{2}V_{iE}\tan L\,(\Delta V^*_N\cos\psi + \Delta V^*_{iE}\sin\psi) \qquad (4.33)$$

$$(\Delta\Theta_{yI} + \Delta\Theta_{yII})/2 = \vartheta^* - \frac{K^2}{2}V_{iE}\tan L\,(\Delta V^*_{iE}\cos\psi - \Delta V^*_N\sin\psi), \qquad (4.34)$$

where the asterisk denotes a computed value as against the true value.

The eqs. (4.31) and (4.32) show us that the gain relating the velocity with respect to inertial space and the readout differences is modified from the gain in eq. (3.11) by the vertical Coriolis and centrifugal acceleration and we may write:

$$K' = K\,(1 + b_v/2g)\,. \qquad (4.35)$$

Now we solve eqs. (4.31) to (4.34) for the vehicle's velocity and attitude and find for the computation carried out in the computer:

$$\Delta V_N^* = V_N^* = \frac{1}{2K'} \left[(\Delta\Theta_{xI} - \Delta\Theta_{xII}) \cos\psi - (\Delta\Theta_{yI} - \Delta\Theta_{yII}) \sin\psi \right] \tag{4.36}$$

$$\Delta V_{iE}^* = V_E^* + R\omega^{ie} (\cos L^* - \cos L_o) =$$

$$\frac{1}{2K'} \left[(\Delta\Theta_{yI} - \Delta\Theta_{yII}) \cos\psi + (\Delta\Theta_{xI} - \Delta\Theta_{xII}) \sin\psi \right] \tag{4.37}$$

$$\varphi^* = \frac{(\Delta\Theta_{xI} + \Delta\Theta_{xII})}{2} + \frac{(\Delta\Theta_{xI} - \Delta\Theta_{xII})}{2} \frac{K^2 V_{iE} \tan L}{2K'} \tag{4.38}$$

$$\vartheta^* = \frac{(\Delta\Theta_{yI} + \Delta\Theta_{yII})}{2} + \frac{(\Delta\Theta_{yI} - \Delta\Theta_{yII})}{2} \frac{K^2 V_{iE} \tan L}{2K'} \; . \tag{4.39}$$

Fig. 4.3 shows the signal flow diagram for the navigational computation of the vehicle's attitude (φ, ϑ), ground speed (V_N, V_E) and position (ℓ, L). The inputs of this diagram are the output signals of the gyropendulums ($\Theta_{xI,II}$, $\Theta_{yI,II}$), the azimuth angle ψ derived from the output signal of the azimuth gyro, the altitude derived from the altimeter for updating R and finally the quasi static equilibrium angles $\Theta_{N1I,II}$ and $\Theta_{E1I,II}$ of the two gyropendulums. For continuously updated earth rate component and continuously updated disturbance torques based on the model M^d = f (acceleration, temperature, etc) which is derived from laboratory tests, the latter angles are known quantities. If the disturbance torques are unknown, they can initially be measured when the vertical and true north are measured externally. We will consider the alignment problem in Chapter 8.

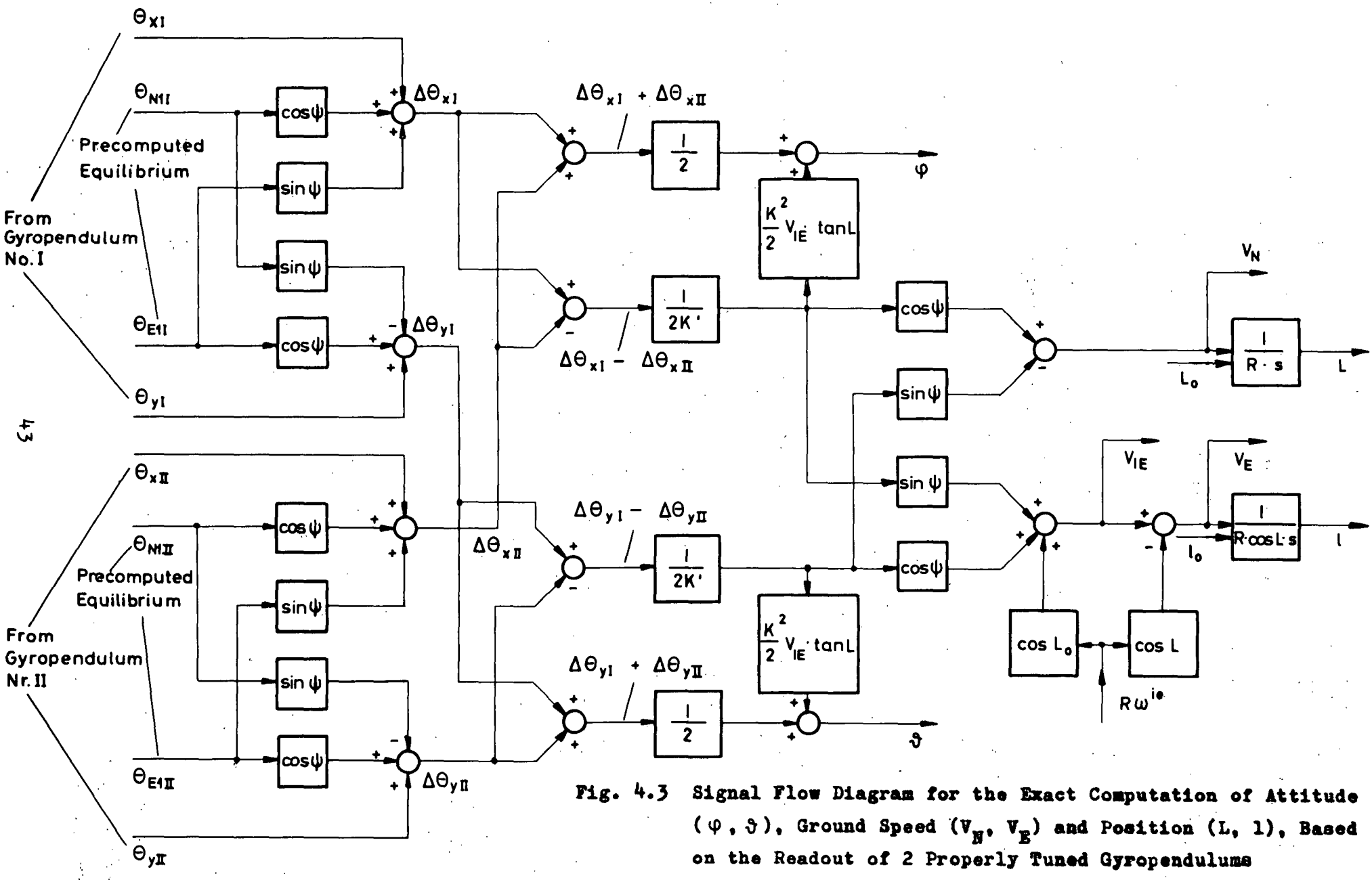

Fig. 4.3 Signal Flow Diagram for the Exact Computation of Attitude (φ, ϑ), Ground Speed (V_N, V_E) and Position (L, l), Based on the Readout of 2 Properly Tuned Gyropendulums

5. PERFORMANCE OF THE AZIMUTH GYRO

Chapter 3 has shown us that a self-contained navigational system may be implemented using two TDF gyropendulums and one TDF azimuth gyro. We have looked into the ideal performance of the gyropendulums in Chapter 4 and will now examine the performance of the azimuth gyro whose spin vector points northerly parallel to the earth axis.

The basic equations for this gyro in the so called "equatorial tangent coordinate frame" (s. Fig. B1; subscript "t"; x or N' pointing north, parallel to the earth axis, y or E pointing east, z or D pointing down, orthogonal to x and y) are derived in Appendix B.

From the determinant Δ in eq. (B6)

$$\Delta = s^2 + (\omega^{it})^2 \tag{5.1}$$

where the frequency is from eq. (B2)

$$\omega^{it} = \omega^{ie} + V_E/(R \cos L) \tag{5.2}$$

we conclude that this gyro describes an undamped 24 hr mode in a stationary vehicle. This is quite obvious if we consider that this non-pendulous gyro ideally keeps its attitude with respect to space, i.e. if the spin vector does not point exactly northward, it will describe a circular motion around true north with a 24 hr period. This oscillation of the displacement angles Θ_E and Θ_D about the east and down axis may be derived from eqs. (B4) and (B5) as

$$\Theta_E = \frac{\omega_D^d}{\omega^{it}} + \left(\Theta_{Eo}^+ - \frac{\omega_D^d}{\omega^{it}}\right) \cos \omega^{it} t + \left(\Theta_{Do}^+ + \frac{\omega_E^d}{\omega^{it}}\right) \sin \omega^{it} t \tag{5.3}$$

$$\Theta_D = -\frac{\omega_E^d}{\omega^{it}} + \left(\Theta_{Do}^+ + \frac{\omega_E^d}{\omega^{it}}\right) \cos \omega^{it} t - \left(\Theta_{Eo}^+ - \frac{\omega_D^d}{\omega^{it}}\right) \sin \omega^{it} t \; . \tag{5.4}$$

The errors caused by initial misalignment need no further comment. The ones caused by the drift terms oscillate about the static equilibrium when the uncertainty torque $H\omega^d$ is compensated by the gyroscopic torque $\Theta H\omega^{it}$ which

is the component of earth rate experienced by the input axis when the corresponding spin vector is misaligned. It is interesting to note that this error angle due to constant gyro drift is greater for a westerly ($V_E < 0$) than for an easterly flying vehicle.

Compared to an azimuth gyro with its spin vector pointing north but parallel to the surface of the earth, the chosen orientation seems to be more advantageous because the angular rate along the spin axis with respect to inertial space, which balances the gyro drift, is the maximum possible thus minimizing in eqs. (5.3) and (5.4) the error angles ω_E^d/ω^{it} and ω_D^d/ω^{it}. But if we consider the nature of the output signal of the z signal generator mounted on the gimbal (s. Fig. 3.3 and eq. (B19))

$$\Theta_z \approx \psi - (\vartheta \sin\psi - \varphi \cos\psi) \tan L + \frac{\Theta_D}{\cos L} \tag{5.5}$$

we see that the effect of the error angle Θ_D or gyro drift, respectively, on the azimuth computation increases with growing latitude like in a conventional platform system (s. [13], eq. (2.45)).

The output signal Θ_y of the y signal generators may be used for redundant measurement of latitude (s. eq. (B18))

$$\Theta_y \approx -L + \vartheta \cos\psi + \varphi \sin\psi - \Theta_E \tag{5.6}$$

where ϑ and φ are derived from the two gyropendulums.

6. DESIGN CONSIDERATIONS OF THE CONTROL LOOPS FOR THE GYROPENDULUM AND THE AZIMUTH GYRO

Chapter 4 has shown us that the gyropendulum must be tuned in order to indicate the ground speed without time lag or oscillation (s. eq. (4.10)). Since this tuning condition changes with ground speed and latitude, a loop has to be designed for the control of the angular momentum.

For the gyropendulum and the azimuth gyro, a gimbal servo system has to be designed. Finally command torques have to be applied to the gyropendulum in order to compensate the torques due to the Coriolis and centrifugal accelerations in the horizontal flight (s. eqs. (4.12) and (4.13)). We will treat these control loops in this chapter.

6.1 Tuning-Control of the Gyropendulum

The tuning condition (4.10), which is a function of ground speed and latitude, has to be matched by the proper control of the angular momentum. In order to appreciate the urgency of the tuning control, let us first examine how strongly the frequency Ω^c depends on the flight condition if the angular momentum is kept constant at that magnitude H_o which provided tuning of the gyropendulum on a stationary basis. From eq. (4.26) we find for H_o

$$H_o = \frac{mg_o r}{\omega_o^s \mp \frac{1}{2}\omega^{ie}\sin L_o} = \frac{H_o'}{1 \mp \frac{\omega^{ie}\sin L_o}{2\omega_o^s}}, \tag{6.1}$$

where H_o' is

$$H_o' = \frac{mg_o r}{\omega_o^s} = mr\sqrt{g_o R_o}\,. \tag{6.2}$$

So according to eq. (3.7a) H_o' achieves the Schuler tuning of the gyropendulum on the ground which corresponds to the exact tuning condition for nonrotating earth.

With eqs. (6.1) and (4.3) we find for the coning frequency Ω_o^c on the ground

$$\Omega_o^c \approx \omega_o^s \mp \frac{1}{2}\omega^{ie}\sin L_o\,. \tag{6.3}$$

Assuming that the actual frequency for constant angular momentum H_o is

$$\Omega^c\Big|_{H_o} = \Omega^c_o + \Delta\Omega^c\Big|_{H_o} \tag{6.4}$$

furthermore making the following assumptions for R and g

$$R = R_o + h \tag{6.5}$$

$$g = \frac{g_o}{(1 + h/R_o)^2} \quad , \tag{6.6}$$

we find from eq. (4.3) for the change in frequency for constant angular momentum

$$\frac{\Delta\Omega^c\Big|_{Ho}}{\omega^s_o} \approx -\frac{2h}{R_o} - \frac{b_v}{g}$$

$$\pm \frac{1}{\omega^s_o}\left[(\omega^{ie}\cos L_o + \frac{V_E}{R\cos^2 L_o})\,\Delta L + \frac{V_E}{R}\tan L_o\right], \tag{6.7}$$

where we have made use of the approximations $\sin L \approx \sin L_o + \Delta L \cos L_o$ and $\tan L \approx \tan L_o + \Delta L/\cos^2 L_o$.

Table 6.1 shows us that this change in frequency exceeds 11 % for the easterly flying SST.

The change of angular momentum with changing flight condition for matched tuning can be easily derived from eq. (4.26). With

$$H = H_o + \Delta H \tag{6.8}$$

and $1/H \approx (1 - \Delta H/H_o)/H_o$ we obtain for this change in angular momentum expressed in terms of the frequency change for constant angular momentum

$$\frac{\Delta H}{H_o} \approx \frac{1}{2}\frac{\Delta\Omega^c\Big|_{H_o}}{\omega^s_o} + \frac{1}{2}\frac{h}{R_o} \quad . \tag{6.9}$$

The second term on the right hand side ($h/2R_o$) takes into account that according to eqs. (4.3) and (4.10) the tuning condition not only depends on gravity as does the frequency for constant H_o but also on the radius R of the flight path with respect to the center of the earth.

Table 6.1 Percentage Change of Coning Frequency $\Delta\Omega^c\big|_{H_o}$ of the Moving Gyropendulum for Constant Angular Momentum with Respect to Frequency $\Omega_o^c \approx \omega_o^s$ of the Stationary Gyropendulum

No.	Frequency Change	Aircraft		
		Private Plane, Helicopter	Subsonic Jet	Supersonic Transport
		V = 250 km/h h = 1 km	V = 900 km/h h = 10 km	V = 2,500 km/h h = 20 km
1	$\Delta\Omega^c(h)/\omega_o^s$	- 0.03	- 0.31	- 0.63
2	$\Delta\Omega^c(b_v)/\omega_o^s$	- 0.08	- 0.36	- 1.50
3	$\Delta\Omega^c(\Delta L)/\omega_o^s$ $(V_E = 0)$	$\pm$ 0.37	$\pm$ 0.37	$\pm$ 0.37
4	$\Delta\Omega^c(\Delta L)/\omega_o^s$ $(V_E = V)$	$\pm$ 0.52	$\pm$ 0.92	$\pm$ 1.91
5	$\Delta\Omega^c(V_E)/\omega_o^s$ $(\Delta L = 0)$	$\pm$ 0.88	$\pm$ 3.15	$\pm$ 8.75
6	Total: $\Delta\Omega^c/\omega_o^s$	- 0.11 $\pm$ 1.40	- 0.67 $\pm$ 3.52	- 2.13 $\pm$ 9.12

According to [11], in the G10 gyro the rotor speed is optically measured and can be controlled by means of supply voltage control. The functional diagram of the gyropendulum in Fig. 6.1 shows this control input.

At the end of this consideration let discuss the change of the coning frequency for matched tuning in terms of the already known frequency change for constant angular momentum H_o. We write eq. (4.10) in the following form

$$\Omega^c = \Omega_o^c + \Delta\Omega^c = \frac{H_o + \Delta H}{mr\, R_o(1+h/R_o)} \tag{6.10}$$

from which we may derive the approximation

$$\frac{\Delta\Omega^c}{\Omega_o^c} \approx \frac{\Delta H}{H_o} - \frac{h}{R_o} \approx \frac{\Delta\Omega^c\big|_{H_o}}{2\omega_o^s} - \frac{h}{2R_o}\,. \tag{6.11}$$

Except for the altitude term, the magnitude of this frequency change is half the amount of the values listed in Table 6.1.

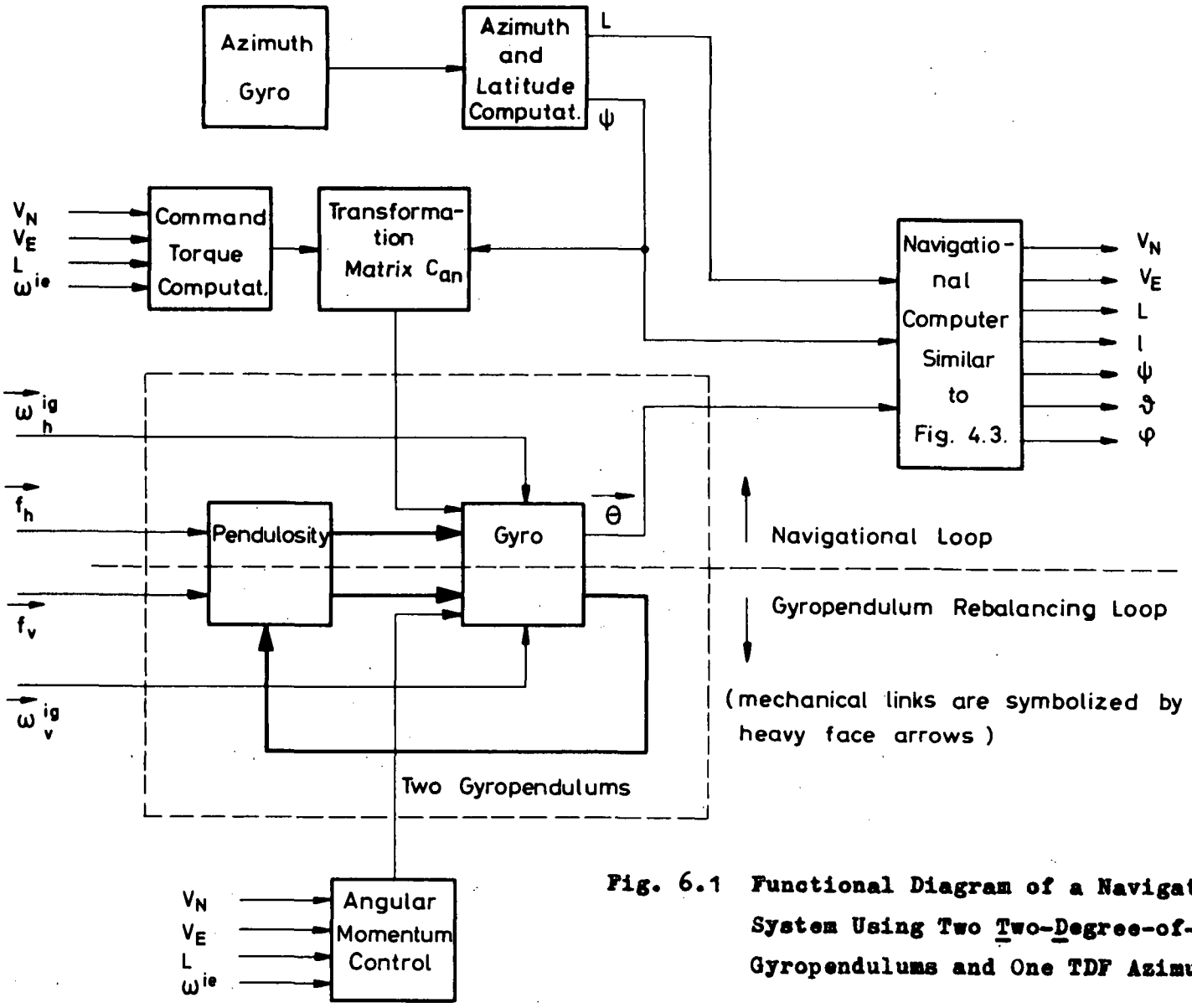

Fig. 6.1 Functional Diagram of a Navigational System Using Two Two-Degree-of-Freedom Gyropendulums and One TDF Azimuth Gyro

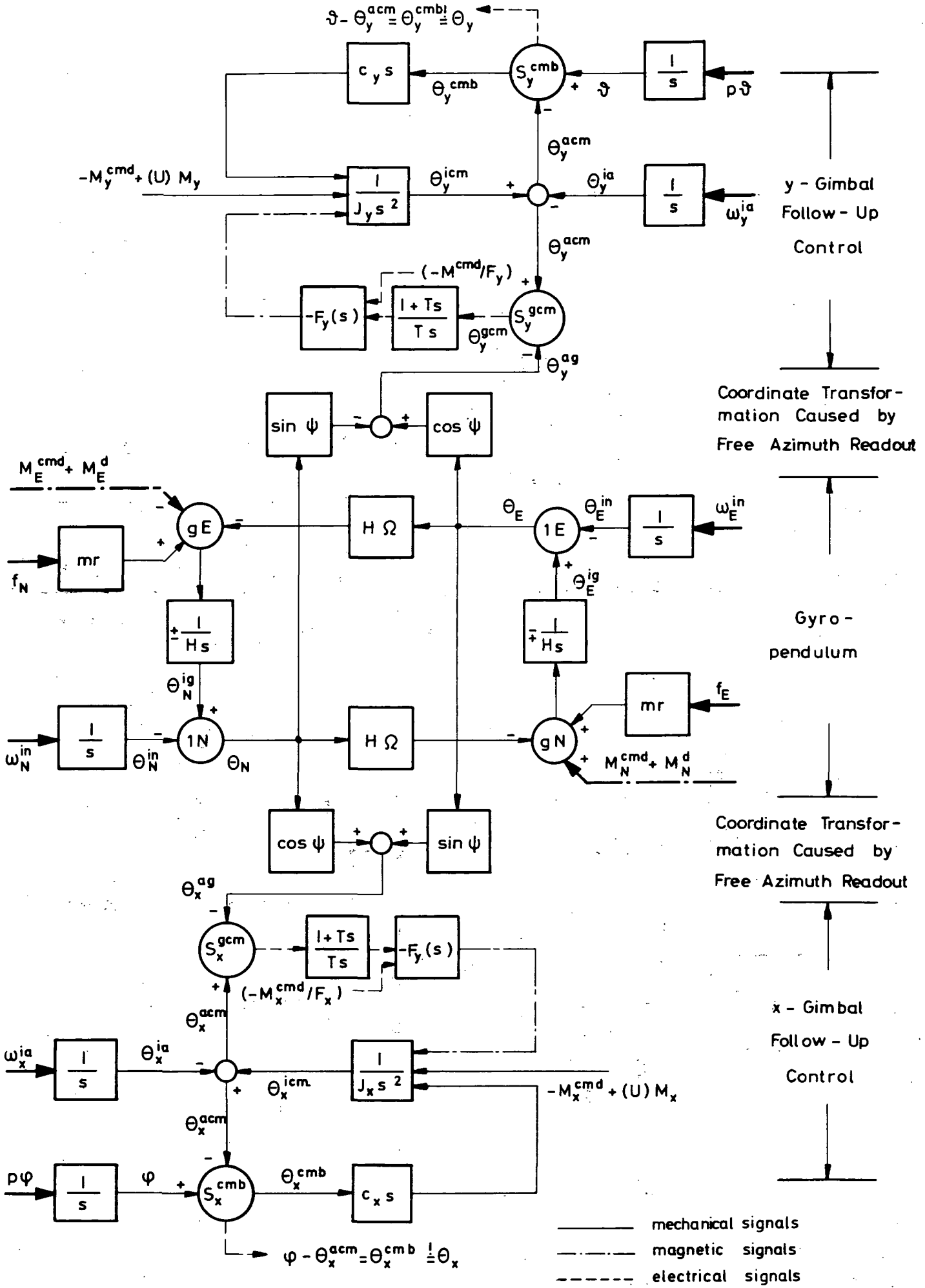

Fig. 6.2 Signal Flow Diagram for the Gimballed Gyropendulum

6.2 Gimbal Control and Command Torques

The principle of gimbal control for the gyropendulum was outlined in Chapter 3 and Fig. 3.2. The output signals of the x and y pickoffs in the gyro case are fed via an electronic network to the x and y torquers of the gimbals.

The signal flow diagram of the gyropendulum including the gimbal follow-up control is shown in Fig. 6.2. The central part of this diagram describes the signal flow in the sensor and is the same as in Fig. 4.1. In order to understand the kinematics of the different pickoffs namely $S^{gcm}_{x,y}$ between the gyro (rotor, "g") and the controlled member (inner gimbal or gyro case, "cm") and signal generators $S^{cmb}_{x,y}$ between the inner and outer gimbal or outer gimbal and vehicle ("b"), respectively in the gimbal follow-up control, let us first have a look at the coordinate frames and the angles between them. (We omit in the following the subscripts x and y, since the signal flow is identical for both loops). Fig. 6.3 shows one representative axis from each of the

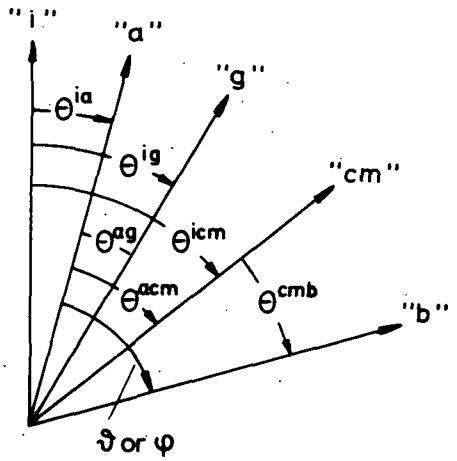

Fig. 6.3 Angles between Coordinate Frames

5 frames involved, namely the inertial frame ("i"), the free azimuth frame ("a", this frame moves with the vehicle about the vertical z axis with the angle ψ, but stays horizontal about the x and y axis), the body frame ("b"), the gimbal frame ("cm" according to "controlled member"), and the gyropendulum frame ("g"). For the gimbal follow-up control we direct our attention first to the angle Θ^{gcm}, i.e., the output signal of the gyro pickoff S^{gcm}. This angle shall be driven to zero by the control loop, because from

$$\Theta^{gcm} = \Theta^{acm} - \Theta^{ag} \tag{6.12}$$

we conclude that then $\Theta^{acm} = \Theta^{ag}$, i.e., the gimbal follows the gyropendulum exactly. What are these angles Θ^{acm} and Θ^{ag}?

The most convenient reference frame for measuring the attitude of the gyropendulum is the navigational frame, where the readout angles are Θ_N and Θ_E. Since the pickoffs of the gyropendulum move with the vehicle about the vertical axis, we take the free azimuth frame as a reference frame for describing the attitude of the gyropendulum. The angles in this frame are

$$\Theta_x^{ag} = \Theta_N \cos\psi + \Theta_E \sin\psi \tag{6.13}$$

$$\Theta_y^{ag} = \Theta_E \cos\psi - \Theta_N \sin\psi \tag{6.14}$$

which may be derived from eqs. (A45) and (A46) for $\vartheta = \varphi = 0$. Remember the free azimuth frame and the body frame coincide when the vehicle flies horizontally.

Let us now have a look at the gimbal attitude Θ^{acm} with respect to the free azimuth frame. Any torque acting on the gimbal causes it to rotate through Θ^{icm} with respect to inertial space. Since the free azimuth frame is moving with respect to inertial space too, only the difference

$$\Theta^{acm} = \Theta^{icm} - \Theta^{ia} \tag{6.15}$$

effects the readout equation (6.12) of the gyro pickoff S^{gcm}.

The gimbal attitude Θ^{acm} with respect to the free azimuth frame is read out by the gimbal signal generator S^{cmb} whose output is the angle Θ^{cmb}. But since the vehicle moves relative to the free azimuth frame through the attitude angles φ and ϑ, the readout angle is equal to the difference of the vehicle's attitude and the gimbal attitude from the free azimuth frame. We have seen eq. (6.12) that for $\Theta^{gcm} = 0$, the gimbal attitude Θ^{acm} is equal to the gyropendulum's attitude Θ^{ag} specified in eqs. (6.13) and (6.14). So in this case, the angle Θ^{cmb} is truly the angle we seek and which we have derived in eqs. (A45) and (A46).

The output Θ^{gcm} enters the electronic network and torque generator (s. Fig. 3.2 or in Fig. 6.2 the boxes $[(1 + Ts)/Ts] \cdot F(s)$) as an electrical signal (----) and is transformed into a magnetic signal (— · —). The transfer function for the output of a y-gimbal signal generator say S_y^{cmb}, is

$$\Theta_y = \frac{1}{I_y s^2 + c_y s + F_y F'} \left[\Theta_y^{ag} F_y F' - \vartheta (I_y s^2 + F_y F') \right.$$

$$\left. - \Theta_y^{ia} I_y s^2 + M_y \right], \qquad (6.16)$$

where

$$F' = \frac{1 + Ts}{Ts} . \qquad (6.17)$$

For nearly frictionless gimbal bearings ($c_y \to 0$) this simplifies to

$$\Theta_y \approx - \vartheta + \frac{1}{I_y s^2 + F_y F'} \left[\Theta_y^{ag} F_y F' - \Theta^{ia} I_y s^2 + M_y \right]. \qquad (6.18)$$

For low frequencies ($s \to 0$), the output of the gimbal signal generators S^{cmb} is the desired one $\Theta_y \approx - \vartheta + \Theta^{ag}$, especially since according to eq. (6.17) F' then behaves like an integrator. For high frequencies F' approaches unity and F_y can be designed to obtain a damped network by putting a proper lead into it.

The performance of the network can be improved if the box F is biased with the negative command torque ($- M^{cmd}/F$). This torque is a known quantity (s. eqs. (4.12), (4.13), (A49) and (A50)). Then changes in the disturbance torque M_y^d only cause short term errors.

The design philosophy of gimbal follow-up control is very similar to that of the control loop for a servo test table for testing gyroscopes. The latter is treated in more detail by Lübeck and the author in [14], Appendix 7, and it worked satisfactorily, even in the presence of high uncertainty torques.

We omit the discussion of the follow-up control of the azimuth gyro which is very similar to that of the gyropendulum.

7. SIMPLIFIED ERROR ANALYSIS

The requirements for accurate operation of a self-contained inertial navigational system using two gyropendulums and one azimuth gyro as sensors have been found in Chapters 4 and 5. The following errors in the operation of the gyropendulum limit the accuracy of the system:

a) tuning errors in eq. (4.10),
b) initial alignment errors (I) Θ^{+}_{No} and (I) Θ^{+}_{Eo} from the equilibrium in eqs. (4.4) and (4.5),
c) errors in the compensation of the biases due to disturbance torques (I) M^{d}_{No} and (I) M^{d}_{Eo} and to horizontal earth rate (I)(ω^{ie} cos L_o/Ω^c) (s. eqs. (4.4), (4.5), (4.29), (4.30) and Fig. 4.3),
d) errors in the command torques (I) M^{cmd}_{N} and (I) M^{cmd}_{E} for compensating Coriolis and centrifugal accelerations due to horizontal velocity (s. eqs. (4.12) and (4.13)),
e) errors due to the change of the disturbance torques ΔM^{d}_{N} and ΔM^{d}_{E} and
f) readout errors (I) Θ_x and (I) Θ_y.

The system's accuracy is similarly affected by the following errors in the operation of the azimuth gyro:

g) alignment errors (I)Θ^{+}_{Eo} and (I)Θ^{+}_{Do} ,
h) gyro drift ω^{d}_{E} and ω^{d}_{D} and
i) readout errors (I)Θ_y and (I)Θ_z.

For the three types of aircraft, the private plane or helicopter, the subsonic jet and the supersonic transport we will derive in this chapter the magnitude of each error source that causes an indicated velocity error of 1 km/h. Thereby we will first assume that it is possible to measure the attitude of the gyropendulum in the navigational frame where attitude and azimuth angles are zero. Attitude errors and the effect of an erroneous azimuth information will be considered in a separate section. In a final section we will consider briefly the frequencies of the error oscillations.

7.1 Computational Velocity Errors of a Gyropendulum with Signal Generators Aligned with the Navigational Frame

The derivation of the corresponding error equations can be found in Appendix C. The inaccuracy terms which are the differences between the computed or measured terms (denoted with an asterisk) and the accurate ones, are indicated by a preceding (I), e.g.

$$(I)M_N^{cmd} = M_N^{cmd*} + mr\, b_e \tag{7.1}$$

$$(I)M_E^{cmd} = M_E^{cmd*} - mr\, b_N \tag{7.2}$$

(s. eqs. (C1) and (C2)). The initial alignment inaccuracies according to eqs. (C3) and (C4) are

$$(I)\Theta_{No}^{+} = \Theta_{No}^{+} - \Theta_{No} = \Theta_{No}^{+} - M_{No}^{d}/(H\Omega_o^c) \tag{7.3}$$

$$(I)\Theta_{Eo}^{+} = \Theta_{Eo}^{+} - \Theta_{Eo} = \Theta_{E}^{+} - (M_{Eo}^{d}/H \mp \omega^{ie}\cos L_o)/\Omega_o^c\ . \tag{7.4}$$

These values can be easily introduced into eqs. (A38) and (A39). It is more difficult to show the effect of an erroneous angular momentum H^* which influences the tuning condition and the coning frequency. The computed tuning condition is based upon the equation (C5)

$$H^*/(mr\, R^*) = \Omega^{c*} \tag{7.5}$$

the evaluation of which may be undertaken in similar fashion to the derivation of eqs. (6.1) to (6.9) resulting in (s. eq. (C6))

$$H^* = H_o + \Delta H = H_o\left(1 + \frac{\Delta\Omega^c\big|_{H_o}}{2\omega_o^s} + \frac{h^*}{2R_o}\right). \tag{7.6}$$

This can be solved numerically when we assume that the initial angular momentum is accurately known from laboratory tests. The altitude h^* is a measured quantity and also $\Omega^{c*}\big|_{H_o}$ is based on measured information. According to eq. (C7) it is

$$\frac{\Delta\Omega^{c*}\big|_{H_o}}{\omega_o^s} \approx -\frac{2h^*}{R_o} - \frac{b_v^*}{g_o} \pm \frac{1}{\omega_o^s}\left[\left(\omega^{ie}\cos L_o + \frac{V_E^*}{R^*\cos^2 L_o}\right)\Delta L + \frac{V_E^*}{R^*}\tan L_o\right]. \tag{7.7}$$

The inaccuracy within this equation which affects the computation of the angular momentum is, according to eq. (C9)

$$\frac{(I)\Omega^c\big|_{H_o}}{\omega_o^s} \approx -\frac{2(I)h}{R_o} - \frac{(I)b_v}{g_o} \pm \frac{1}{\omega_o^s}\left[\left(\omega^{ie}\cos L_o + \frac{V_E^*}{R_o\cos^2 L_o}\right)(I)L + \frac{(I)V_E}{R_o}\tan L_o\right]. \tag{7.8}$$

The error in the computed angular momentum according to eq. (C12) is

$$(I)\,H = H^* - H \approx \frac{H_o}{2}\left[\frac{(I)\Omega^c\big|_{H_o}}{\omega_o^s} + \frac{(I)h}{R_o}\right]. \tag{7.9}$$

The actual coning frequency $\Omega^c(H^*)$ of the gyropendulum depends on the one hand upon the accurate values of the flight condition (h, b_v, L, V_E etc.) and on the other upon the computed angular momentum H^*. Its relationship to the theoretical frequency Ω^c and the computed frequency Ω^{c*} is found in eq. (C13) and (C16) to be

$$\Omega^c(H^*) \approx \Omega^c - \omega_o^s\,(I)H/H_o \tag{7.10a}$$

$$\approx \Omega^{c*} - \omega_o^s\left[\frac{2(I)H}{H_o} - \frac{(I)h}{R_o}\right] \tag{7.10b}$$

where Ω^{c*} can be computed similarly to eq. (6.11).

Based upon these errors, the error of the indicated attitude of the gyropendulum could be obtained from eq. (A34) plus (A38) and (A35) plus (A39). The result can be seen from eq. (C21) plus (C24) and (C23) plus (C25). In the signal flow from the indicated attitude of the spin vectors of the two gyropendulums to the computed ground speed some additional errors might creep in which should be mentioned briefly with reference to Fig. 4.3. (Remember, for readout in the navigational frame: $\psi = \vartheta = \varphi = 0$.)

First, there is the readout inaccuracy of the signal generators, which we denote as $(I)\Theta_N$ and $(I)\Theta_E$. The second error source is the bias error (s. eq. (C28) and (C29)) due to the difference between the computed and true values for the quasi static equilibrium Θ_{N1}, and Θ_{E1} of the gyropendulums defined in eq. (4.4) and (4.5). The third and final error might occur in the computation of the easterly ground speed V_E from the easterly velocity V_{iE} with respect to inertial space. This error is due to erroneous altitude and latitude information (s. eq. (C41)).

In eq. (C32) to (C35) we have introduced some abbreviations which have the physical meaning of dynamic velocity error for perfect initial alignment

$$(I)\Delta V'_N = 2\,\frac{(I)H}{H_o}\,\Delta V_N \mp \frac{R_o}{H_o}\,((I)M_N^{cmd} + \Delta M_N^d) \tag{7.11}$$

$$(I)\Delta V'_E = 2\,\frac{(I)H}{H_o}\,\Delta V_E \mp \frac{R_o}{H_o}\,((I)M_E^{cmd} + \Delta M_E^d) \tag{7.12}$$

$$(I)\Delta V'_{iE} = 2\,\frac{(I)H}{H_o}\,\Delta V_{iE} \mp \frac{R_o}{H_o}\,((I)M_E^{cmd} + \Delta M_E^d) \tag{7.13}$$

where the last equation is the sum of eq. (C34) and (C35).

With these abbreviations we find in eq. (C36) and (C42) the following computational velocity errors for the north and east component based on the output signal of either gyropendulum whose signal generators are aligned with the navigational frame:

$$\begin{aligned}(I)V_N \approx\ & (I)\,V'_N \mp R_o\,\omega_o^s\,(I)\Theta_N \pm R_o\,(I)M_{No}^d/H_o \\ & - \left[(I)\Delta V'_N \pm R_o\,\omega_o^s\,(I)\Theta_{No}^+\right]\cos\Omega^c(H^*)\,t \\ & \mp \left[(I)\Delta V'_{iE} \pm R_o\,\omega_o^s\,(I)\Theta_{Eo}^+\right]\sin\Omega^c(H^*)\,t\end{aligned} \tag{7.14}$$

$$\begin{aligned}(I)V_E \approx\ & (I)\Delta V'_E + R^*\omega^{ie}\left[\cos L_o\left(\frac{2(I)H}{H_o} - \frac{(I)h}{R_o}\right) + (I)L\sin L_o\right] \\ & \mp R_o\,\omega_o^s\,(I)\Theta_E \pm R_o\,(I)\,M_{Eo}^d/H_o \\ & - \left[(I)\Delta V'_{iE} \pm R_o\,\omega_o^s\,(I)\Theta_{Eo}^+\right]\cos\Omega^c(H^*)\,t \\ & \mp \left[(I)\Delta V'_N \pm R_o\,\omega_o^s\,(I)\Theta_{No}^+\right]\sin\Omega^c(H^*)\,t\ .\end{aligned} \tag{7.15}$$

In the proposed navigational system ground speed is computed from the difference of the output signals of the two gyropendulums with their spin vectors pointing up and down. The computational velocity error has in reality on the right hand side of eq. (7.14) and (7.15), the mean error terms of both sensors. This dependence of the velocity error upon the mean inaccuracies has

especially a favorable effect upon (I)H (s. eq. (7.8) and (7.9)). But we have to keep in mind that the coning frequency $\Omega^c(H^x)$ is not exactly the same for both gyropendulums (s. eq. (4.3) and Table 6.1) and oscillations with opposite signs will not always cancel each other in the velocity computation. This might confirm us to neglect this favorable effect in the following.

From eq. (7.11) to (7.15) it can be seen that the inaccuracies may be summarized into 5 types of error sources which we will evaluate in the following in order to find the magnitude of each error source which yields a computational velocity error of (I)V = 1 km/h.

The first type of error source is the initial spin vector alignment and readout error (I)Θ which amounts to:

$$\frac{(I)\Theta}{(I)V} \approx \frac{1}{R_o \omega_o^s} = 7.24 \frac{\widehat{sec}}{km/h} . \tag{7.16}$$

The second type of error source is the latitude error (I)L in eq. (7.15) which amounts to:

$$\frac{(I)L}{(I)V} \approx \frac{1}{R_o \omega^{ie} \sin L_o} \approx 0.0048 \frac{deg}{km/h} \tag{7.17}$$

at L ≈ 45°. This corresponds to a position error of:

$$\frac{(I)P}{(I)V} \approx 0.54 \frac{km}{km/h} . \tag{7.18}$$

The third type of error source is the altitude error (I)h which at L = 45° is the same as the position error

$$\frac{(I)h}{(I)V} \approx \frac{1}{\omega^{ie} \cos L_o} = 0.54 \frac{km}{km/h} . \tag{7.19}$$

The fourth type of error source is the change of the disturbance torques ΔM^d or the inaccuracy in the compensation of the initial disturbance torque $(I)M_o^d$ and it includes also the inaccuracy of the command torques $(I)M^{cmd}$

$$\frac{\Delta M^d/H}{(I)V} = \frac{(I)M_o^d/H}{(I)V} = \frac{(I)M^{cmd}/H}{(I)V} \approx \frac{1}{R_o} = 0.009 \frac{deg/h}{km/h} . \tag{7.20}$$

As to the inaccuracy (I) M^{cmd} of the command torque, it is of interest how this is related to the inaccuracy in the computation of the Coriolis and

centrifugal acceleration b_h in horizontal flight, whose torque is to be compensated by the command torque. We find

$$\frac{(I)b_h/b_h}{(I)V} = \frac{1}{b_h}\frac{H}{mr}\frac{(I)M^{cmd}/H}{(I)V} \approx \frac{\omega_o^s}{b_h} \quad . \tag{7.21}$$

The small figures in Table 7.1a show us that the system is rather sensitive to the inaccuracy in the computation and compensation of the Coriolis and centrifugal acceleration. Remember, the larger these numbers the more careless one might be in the compensation of this effect.

Table 7.1a Error Terms, Affecting the Operation of the Gyropendulum and Causing Each a Computational Ground Speed Error of 1 km/h

No.	Error Term	Dim.	Aircraft		
			Private Plane, Helicopter	Subsonic Jet	Supersonic Transport
			V = 250 km/h h = 1 km	V = 900 km/h h = 10 km	V = 2,500 km/h h = 20 km
1	$(I)\Theta$	$\widehat{sec}$	7.24	7.24	7.24
2	$(I)L$	deg.	0.0048	0.0048	0.0048
3	$(I)P$ $(I)h$	km	0.54	0.54	0.54
4	$\Delta M^d/H$ $(I)M_o^d/H_o'$ $(I)M^{cmd}/H$	$\frac{deg}{h}$	0.009	0.009	0.009
5	$(I)b_h/b_h$	%	4.3	0.98	0.24
6	$(I)H/H$	%	0.035	0.024	0.014

The fifth type of error source is the inaccuracy of the angular momentum $(I)H$ or rotor speed control. Its effect is largest for an easterly flying vehicle (first term of eq. (7.12) plus second term of eq. (7.15))

$$\frac{(I)H/H_o}{(I)V} \approx \frac{1}{2\,(R\omega^{ie}\cos L + V_E)} = \frac{1}{2V_{iE}} \tag{7.22}$$

which is evaluated in Table 7.1a along with the other types of errors.

In Table 7.1b those error terms are evaluated which according to eq. (7.8) and (7.9) make up the computational inaccuracy of the angular momentum control (I)H. The numerical values are derived by equating each term of eq. (7.8) and (7.9) with the value 2 (I)H/H_o listed in Table 7.1a. So each of the inaccuracies in Table 7.1b contributes a computational velocity error of 1 km/h via the angular momentum control.

Table 7.1b Error Terms, Affecting the Gyropendulum's Rotor Speed Control and Causing Each a Computational Ground Speed Error of 1 km/h

No.	Error Term	Dim.	Aircraft		
			Private Plane, Helicopter	Subsonic Jet	Supersonic Transport
			V = 250 km/h h = 1 km (I)H/H=0.035%[1)]	V = 900 km/h h = 10 km (I)H/H=0.024%[1)]	V = 2,500 km/h h = 20 km (I)H/H=0.014%[1)]
1	-(I)h	km	4.460	3.060	1.786
2	$-(I)b_v/b_v$	%	86.0	13.3	1.87
3	$\pm(I)L$	deg	0.67	0.26	0.07
4	$\pm(I)P$	km	75.	29.	7.8
5	$\pm(I)V_E$	km/h	16.6	11.4	6.4

[1)] s. Table 7.1a

The values listed in Table 7.1a require indeed today's high performance technology; they are achievable, however. Fortunately the requirements for the angular momentum control are less severe.

7.2 Attitude Errors and Requirements for the Azimuth Gyro

The computational velocity errors in Section 7.1 were derived under the assumption that the signal generators of the gyropendulums are always aligned with the navigational frame, so errors due to inaccurate attitude and azimuth information were not yet included. The attitude computation is based upon the

output signals of the two gyropendulums and hence coupled with the velocity computation and its errors. From eq. (3.11) we conclude that a velocity error of (I)V = 1 km/h corresponds to an attitude error of

$$\frac{(I)\vartheta}{(I)V} = \frac{(I)}{(I)V} = \frac{1}{K} = 7.24 \widehat{\text{sec}} \tag{7.23}$$

which is not too weighty. All the velocity error contributors listed in Table 7.1a and b can hence be easily converted into attitude error contributors. In eqs. (4.22) and (4.23) it was shown that the vertical velocity ph causes an additional attitude error which for the easterly flying SST amounts to $\Delta\vartheta(ph) = 3.4 \widehat{\text{sec}}$ per ph = 1 m/sec. This is negligible for attitude control purposes.

The requirements for azimuth accuracy can be derived from a physical insight into the system. We have seen in Chapter 3 that the gyropendulum tilts from the vertical in the plane normal to the motion of the vehicle. According to eqs. (3.9) to (3.11) the angle is proportional to the velocity of the vehicle with respect to space, i.e., it is largest for an easterly moving vehicle. Since the readout takes place in the body frame, one has to know true north (the angle ψ) in order to evaluate this information for navigational purposes (s. eqs. (3.20) and (3.21)). If ψ is not accurately known

$$(I)\psi = \psi^* - \psi, \tag{7.24}$$

the system evaluates this error as a velocity in the orthogonal direction, i.e., for the easterly moving vehicle as a northerly component

$$(I)V_N \approx V_{iE}\,(I)\psi\,. \tag{7.25}$$

Requiring that this error shall not exceed 1 km/h, we find the admissible inaccuracy for $(I)\psi$, which is evaluated in Table 7.1c for the three types of airplanes. Eqs. (5.4) and (5.5) show us that the values $(I)\psi$ are also applicable to the requirements for initial alignment and readout accuracy $(I)\Theta$ of the azimuth gyro, the requirements for the drift rate and the compensation accuracy for the attitude angles $(I)\vartheta$ and $(I)\varphi$.

As to the effect of gyro drift on the computational velocity error, we know from eq. (5.4) that this drift causes an effect about the z - (down) axis of $\Theta_D = \omega^d/\omega^{it}$ where $\omega^{it} = \omega^{ie} + V_E/(R\cos L)$ (s. eq. (5.2)) and via Θ_D causes an azimuth error of

$$(I)\psi = \Theta_D/\cos L = R\omega^d/V_{iE} \tag{7.26}$$

Table 7.1c Error Terms, Affecting the Operation of the Azimuth Gyro and Causing Each a Computational Ground Speed Error of 1 km/h

No.	Error Term	Dim.	Aircraft		
			Private Plane, Helicopter V = 250 km/h h = 1 km	Subsonic Jet V = 900 km/h h = 10 km	Supersonic Transport V = 2.500 km/h h = 20 km
1	(I) ψ (I) Θ	$\widehat{\text{min}}$	2.40	1.65	0.94
2	ω^d	$\frac{\text{deg}}{\text{h}}$	0.009	0.009	0.009

(V_{iE} s. eq. (A14)). So we obtain for the azimuth gyro drift that causes (I)V = 1 km/h computational velocity error

$$\frac{\omega^d}{(I)V} = \frac{V_{iE}}{R}\frac{(I)\psi}{(I)V} = \frac{1}{R} = 0.009\ \frac{\text{deg/h}}{\text{km/h}}\ . \qquad (7.27)$$

This error is identical with the one found in eq. (7.20) for the gyropendulums in terms of $(I)M^d/H$.

As to the computation accuracy requirements for the attitude angles $(I)\vartheta$ and $(I)\varphi$, we have seen in eq. (7.23) that they meet those in Table 7.1c. In Chapter 4 it had been assumed that the attitude errors caused by the vertical velocity have a negligible effect on the azimuth and velocity computation. This remains still to be proved. This attitude error is largest for an easterly moving vehicle (s. eqs. (4.20) and (4.21), third term on the right side) when $\Delta\Theta_N(ph)$ according to eq. (4.22) corresponds to a pitch error $\Delta\vartheta(ph)$. The resulting azimuth error is (s. eq. (3.23))

$$\Delta\psi(ph) = \Delta\vartheta(ph)\ \tan L\ . \qquad (7.28)$$

Using eqs. (7.25), (7.28) and (4.23) we find for the resulting velocity error

$$\frac{\Delta V(ph)}{ph} = \frac{\Delta V(ph)}{\Delta\psi(ph)}\cdot\frac{\Delta\psi(ph)}{\Delta\vartheta(ph)}\cdot\frac{\Delta\vartheta(ph)}{ph} \approx (KV_{iE})^2\ \tan L = 0.006\ \frac{\text{km/h}}{\text{m/sec}} \qquad (7.29)$$

for the easterly flying SST at $L = 45^\circ$. The position offset after a climb to a certain altitude h is

$$\frac{\Delta P(ph)}{h} = (KV_{iE})^2 \tan L = 1.675 \cdot 10^{-2} \frac{m}{m} \qquad (7.30)$$

for the same airplane. It is in general a negligible error. If not, it can be easily biased out as shown in eqs. (4.24) and (4.25).

7.3 Frequencies of the Error Oscillation

Britting has shown in [13], Chapter 2.4 that a vertical indicating system if stationary with respect to the earth, for instance, carries out an error oscillation with a 24 hour period and a Foucault modulated Schuler frequency (s. [13], eq. (2.31)).

In the navigational system in question, the 24-hour error oscillation is generated by the azimuth gyro as shown in Chapter 5. An equation corresponding to the Foucault modulated Schuler frequency in the bracket of [13], eq. (2.31) might be derived, if the difference and the sum of the gyropendulum's readouts are calculated in the Laplace domain. The common denominator of the combined readouts is

$$(s^2 + \Omega_I^{c2})\,(s^2 + \Omega_{II}^{c\,2}) =$$

$$s^4 + 2\,s^2\,(\omega^{s2} + \omega^{ie2} \sin^2 L) + (\omega^{s2} - \omega^{ie2} \sin^2 L)^2. \qquad (7.31)$$

This proves that also in the dynamics of the navigational system in question, no major differences are to be expected as compared with the conventional vertical indicating system.

8. INITIAL ALIGNMENT CONSIDERATION

In this chapter two initial alignment procedures shall be briefly outlined and a simplified error analysis presented. These two procedures are:

a) The alignment based on external measurements for attitude and azimuth of the stationary vehicle. This allows us to draw conclusions on the actual stationary disturbance torques acting on the gyropendulum and to bias them out.

b) The self-alignment, where based upon the initial state of the two gyropendulums and its precomputed values including the disturbance torques, the attitude and azimuth of the vehicle are defined.

In these two alignment procedures, the azimuth gyro is not actively involved because it is not a north-seeking sensor. Once the direction of the earth axis is found, either on the basis of external measurements (item a) or self-alignment (item b), the azimuth gyro is slewed into this direction, which is then stored within the gyro.

The basic equations for the analysis of the initial alignment are the equations of the accurate initial static equilibrium about the north and east axis (s. eqs. (4.4) to (4.9))

$$\Theta_{NoI,II} = \frac{M^d_{NoI,II}}{(H\Omega^c_o)_{I,II}} \approx \frac{M^d_{NoI,II}}{H'_o\,\omega^s_o} \tag{8.1}$$

$$\Theta_{EoI,II} = \frac{M_{EoI,II}/H_{I,II} \mp \omega^{ie}\cos L_o}{\Omega^c_{oI,II}}$$

$$\approx \frac{M^d_{EoI,II}}{H'_o\,\omega^s_o} \mp \frac{\omega^{ie}\cos L_o}{\Omega^c_{oI,II}}\,, \tag{8.2}$$

where (from eq. (6.3))

$$\Omega^c_{oI,II} \approx \omega^s_o \mp \frac{1}{2}\omega^{ie}\sin L_o\,. \tag{8.3}$$

They are also the equations of the actual readout angles of the x and y signal generators

$$\Theta^*_{xoI,II} = (I)\Theta_{xI,II} + \varphi_o - \Theta^+_{NoI,II}\cos\psi_o - \Theta^+_{EoI,II}\sin\psi_o \tag{8.4}$$

$$\Theta^{*}_{yoI,II} = {}^{(I)}\Theta_{yI,II} + \vartheta_o - \Theta^{+}_{EoI,II} \cos\psi_o + \Theta^{+}_{NoI,II} \sin\psi_o . \qquad (8.5)$$

The asterisk denotes that these actual readout angles differ from the accurate ones in eqs. (A45) and (A46) by the readout inaccuracies $^{(I)}\Theta_x$ and $^{(I)}\Theta_y$ (which may also include errors due to vibration of the vehicle) and the true tilt angles Θ^{+}_{No} and Θ^{+}_{Eo} of the spin axis with respect to the vertical. These true tilt angles again differ according to eqs. (C3) and (C4) from the true equilibrium in eqs. (8.1),(8.2) by the inaccuracy terms $^{(I)}\Theta^{+}_{No}$ and $^{(I)}\Theta^{+}_{Eo}$.

8.1 Initial Alignment Based on External Measurements

If sensors for measuring the vertical (e.g. a tiltmeter for measuring φ_o and ϑ_o) and the north direction (e.g. gyrocompass for measuring ψ_o) are available, one might compute from the actual readout angles in eqs. (8.4) and (8.5) the static equilibrium Θ_{No} and Θ_{Eo} for both gyropendulums. The signal flow for this computation is shown in Fig. 8.1. Once Θ_{No} and Θ_{Eo} are known, they may be used directly as input signals Θ_{N1}, and Θ_{E1} (s. eqs. (4.4) and (4.5)) in the signal flow diagram for the navigational computation (s. Fig. 4.3) thus compensating automatically for the constant disturbance torques (s. eqs. (8.1)) and (8.2)). The model which we use for the readout angles is similar to eqs. (A45) and (A46)

$$\Theta^{*}_{xoI,II} = \varphi^{*}_o - \Theta^{*}_{NoI,II} \cos\psi^{*}_o - \Theta^{*}_{EoI,II} \sin\psi^{*}_o \qquad (8.6)$$

$$\Theta^{*}_{yoI,II} = \vartheta^{*}_o - \Theta^{*}_{EoI,II} \cos\psi^{*}_o + \Theta^{*}_{NoI,II} \sin\psi^{*}_o , \qquad (8.7)$$

where φ^{*}_o , ϑ^{*}_o and ψ^{*}_o are the external measurements, differing from the accurate ones by the sensor inaccuracies, e.g.

$$^{(I)}\varphi_o = \varphi^{*}_o - \varphi_o \quad \text{etc.} \qquad (8.8)$$

Θ_{No} and Θ_{Eo} are the equilibrium angles which we want to compute; they are erroneous by, e.g.

$$^{(I)}\Theta_{No} = \Theta^{*}_{No} - \Theta_{No} . \qquad (8.9)$$

Equating eqs. (8.6) and (8.7) with (8.4) and (8.5), we find for the error of this computation

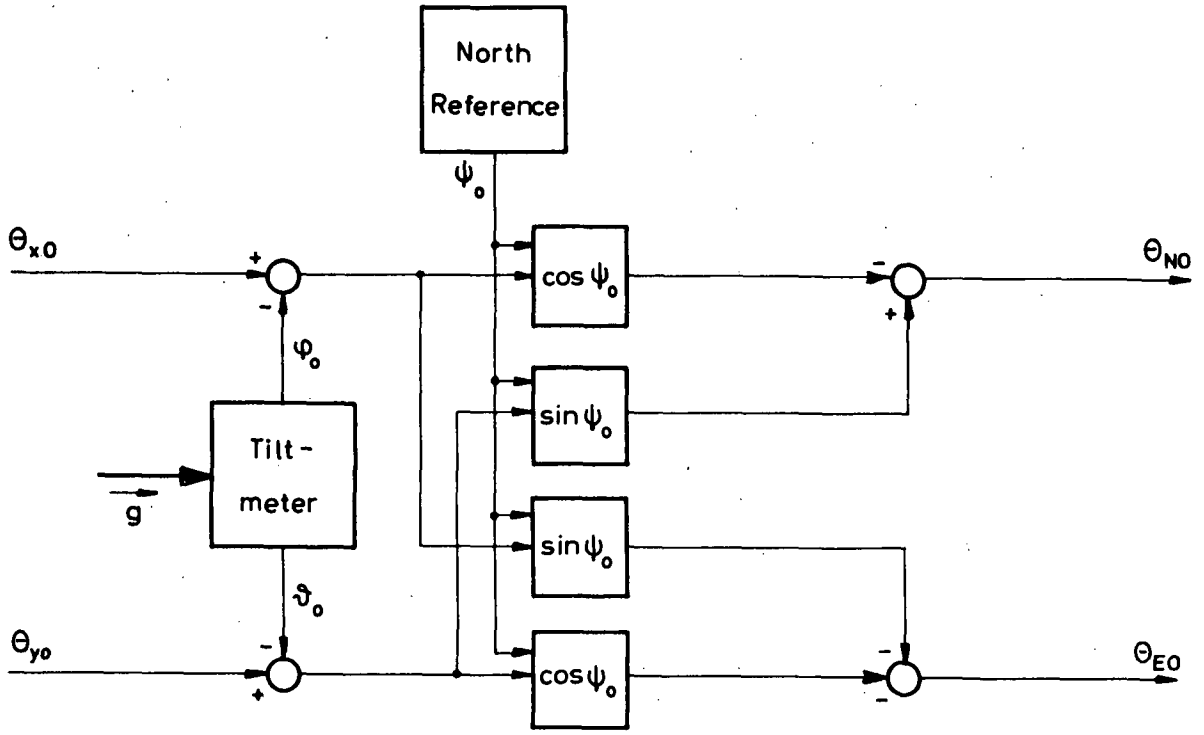

Fig. 8.1 Signal Flow Diagram for Measuring Θ_{NO} and Θ_{EO} of a Gyropendulum During Initial Alignment Based on External Measurements

$$ {}^{(I)}\Theta_{NoI,II} \approx {}^{(I)}\Theta^{+}_{NoI,II} - \left[{}^{(I)}\Theta_{xI,II} - {}^{(I)}\varphi_o \right] \cos\psi_o $$

$$ + \left[{}^{(I)}\Theta_{yI,II} - {}^{(I)}\vartheta_o \right] \sin\psi_o - {}^{(I)}\psi_o \, \Theta_{EoI,II} \qquad (8.10) $$

$$ {}^{(I)}\Theta_{EoI,II} \approx {}^{(I)}\Theta^{+}_{EoI,II} - \left[{}^{(I)}\Theta_{yI,II} - {}^{(I)}\vartheta_o \right] \cos\psi_o $$

$$ - \left[{}^{(I)}\Theta_{xI,II} - {}^{(I)}\varphi_o \right] \sin\psi_o \, . \qquad (8.11) $$

In eq. (4.9) we have found that a disturbance torque expressed in 1 MERU = 0.015 deg/h causes the gyropendulum to settle with a displacement angle of 12.2 $\widehat{\text{sec}}$ from the theoretical equilibrium. With respect to eqs. (8.10) and (8.11) we may reverse this statement. If we allow each term in these equations only to be smaller than 12.2 $\widehat{\text{sec}}$, then each term contributes an uncertainty of less than 1 MERU in the final computation and compensation of the constant initial disturbance torque. Briefly:

Initial misalignment of spin axis	${}^{(I)}\Theta^{+}_{No}$, ${}^{(I)}\Theta^{+}_{Eo}$
Readout inaccuracy	${}^{(I)}\Theta_{x}$, ${}^{(I)}\Theta_{y}$
Tiltmeter inaccuracy	${}^{(I)}\vartheta_o$, ${}^{(I)}\varphi_o$

$$ \left.\begin{array}{l} \\ \\ \\ \\ \\ \end{array}\right\} \stackrel{!}{\leq} 12.2 \ \widehat{\text{sec}} \text{ per MERU } \frac{{}^{(I)}M^{d}}{H} \, . \qquad (8.12) $$

With $\Theta_{Eo} \approx 2.4^{\circ}$ we find from eq. (8.10) for the equivalent accuracy requirement of the gyrocompass

$$ {}^{(I)}\psi_o \stackrel{!}{\leq} 4.9 \ \widehat{\text{min}} \text{ per MERU } \frac{{}^{(I)}M^{d}}{H} \, . \qquad (8.13) $$

Compared to the inaccuracy for initial misalignment and readout of 7.24 $\widehat{\text{sec}}$ contributing a velocity error of 1 km/h (s. Table 7.1a), the requirement of eq. (8.12) is less stringent. The achievable accuracy of sensors for measuring the vertical and the north direction is better than required for eq. (8.12) and (8.13).

8.2 Self Alignment

This initial alignment procedure makes direct use of the signal flow in Fig. 4.3, where the input signals for a stationary vehicle are the actual readout angles $\Theta_{xoI,II}$ and $\Theta_{yoI,II}$ of the two gyropendulum's signal generators (s. eqs. (8.4) and (8.5)) and the precomputed values for the equilibrium $\Theta^*_{NoI,II}$ and $\Theta^*_{EoI,II}$ (s. eqs. (8.1) and (8.2)). For a stationary vehicle these angles correspond to the angles $\Theta_{N1I,II}$ and $\Theta_{E1I,II}$ mentioned in Fig. 4.3.

For perfect values of $\Theta_{xoI,II}$, $\Theta_{yoI,II}$ and $\Theta_{NoI,II}$, $\Theta_{EoI,II}$ and perfectly known azimuth ψ, the indicated initial velocity of the stationary vehicle must be zero, i.e., in Fig. 4.3 the differences $\Delta\Theta_{xI} - \Delta\Theta_{xII}$ and $\Delta\Theta_{yI} - \Delta\Theta_{yII}$ must vanish. This condition may be used for the self-alignment procedure. Based on the inputs mentioned above, the azimuth ψ^*_o entering on the left hand side of Fig. 4.3 first column of $\sin\psi$ and $\cos\psi$ boxes is modified until the differences $\Delta\Theta_{xI} - \Delta\Theta_{xII}$ and $\Delta\Theta_{yI} - \Delta\Theta_{yII}$ vanish.

The angles $\Delta\Theta^*_{xoI,II}$ and $\Delta\Theta^*_{yoI,II}$ which in this chapter replace the angles $\Delta\Theta_{xI,II}$ and $\Delta\Theta_{yI,II}$ are according to eqs. (4.29) and (4.30)

$$\begin{aligned}\Delta\Theta^*_{xoI,II} &= \Theta^*_{xoI,II} + \Theta^*_{NoI,II}\cos\psi^*_o + \Theta^*_{EoI,II}\sin\psi^*_o \\ &\approx {}^{(I)}\Theta_{xI,II} + \varphi_o - \left[{}^{(I)}\Theta^+_{NoI,II} - {}^{(I)}\Theta_{NoI,II}\right]\cos\psi_o \\ &\quad - \left[{}^{(I)}\Theta^+_{EoI,II} - {}^{(I)}\Theta_{EoI,II}\right]\sin\psi_o + {}^{(I)}\psi_o\,\Theta_{EoI,II}\cos\psi_o \qquad (8.14)\end{aligned}$$

$$\begin{aligned}\Delta\Theta^*_{yoI,II} &= \Theta^*_{yoI,II} + \Theta^*_{EoI,II}\cos\psi^*_o - \Theta^*_{NoI,II}\sin\psi^*_o \\ &\approx {}^{(I)}\Theta_{yoI,II} + \vartheta_o - \left[{}^{(I)}\Theta^+_{EoI,II} - {}^{(I)}\Theta_{EoI,II}\right]\cos\psi_o \\ &\quad + \left[{}^{(I)}\Theta^+_{NoI,II} - {}^{(I)}\Theta_{NoI,II}\right]\sin\psi_o - {}^{(I)}\psi_o\,\Theta_{EoI,II}\sin\psi_o\,. \qquad (8.15)\end{aligned}$$

Denoting with δ the difference of corresponding values of the two gyropendulums, for instance

$$\delta\Delta\Theta^*_{xo} = \Delta\Theta^*_{xoI} - \Delta\Theta^*_{xoII}, \qquad (8.16)$$

we obtain for matched self alignment condition:

$$\delta\Delta\Theta^{*}_{xo} \overset{!}{=} 0 \approx$$

$$\delta(I)\Theta_x - \left[\delta(I)\Theta^{+}_{No} - \delta(I)\Theta_{No}\right]\cos\psi_o$$

$$- \left[\delta(I)\Theta^{+}_{Eo} - \delta(I)\Theta_{Eo}\right]\sin\psi_o$$

$$+ (I)\psi_o\,\delta\Theta_{Eo}\cos\psi_o \qquad (8.17)$$

and

$$\delta\Delta\Theta^{*}_{yo} \overset{!}{=} 0 \approx$$

$$\delta(I)\Theta_y - \left[\delta(I)\Theta^{+}_{Eo} - \delta(I)\Theta_{Eo}\right]\cos\psi_o$$

$$+ \left[\delta(I)\Theta^{+}_{No} - \delta(I)\Theta_{No}\right]\sin\psi_o$$

$$- (I)\psi_o\,\delta\Theta_{Eo}\sin\psi_o \qquad (8.18)$$

where in connection with the supposedly small error $(I)\psi_o$ we may approximate

$$\delta\Theta_{Eo} \approx -\frac{2\omega^{ie}\cos L_o}{\omega^{s}_{o}} \qquad (8.19)$$

(s. eq. (8.2)). Multiplying eq. (8.17) with $\cos\psi_o$ and (8.18) with $\sin\psi_o$ and subtracting both results gives for the azimuth error

$$(I)\psi_o \approx$$

$$\frac{\omega^{s}_{o}}{2\omega^{ie}\cos L_o}\left[\delta(I)\Theta_x\cos\psi_o - \delta(I)\Theta_y\sin\psi_o - \delta(I)\Theta^{+}_{No} + \delta(I)\Theta_{No}\right]. \qquad (8.20)$$

According to eq. (8.1), $\delta(I)\Theta_{No}$ is made up of the difference of the disturbance torque inaccuracies for the north axis of the two gyropendulums

$$\delta(I)\Theta_{No} \approx \frac{1}{H'_o\,\omega^{s}_{o}}\left[(I)M^{d}_{NoI} - (I)M^{d}_{NoII}\right], \qquad (8.21)$$

where again

$$(I)M^{d}_{No} = M^{d*}_{No} - M^{d}_{No} \qquad (8.22)$$

is the difference between our knowledge of the disturbance torque and the actual disturbance torque. So we find finally

$$(I)\psi_o \approx \frac{(I)M^d_{NoI} - (I)M^d_{NoII}}{2H'_o\,\omega^{ie}\cos L_o} + \frac{\omega^s_o}{2\omega^{ie}\cos L_o}\left[\delta(I)\Theta_x \cos\psi_o - \delta(I)\Theta_y \sin\psi_o - \delta(I)\Theta^+_{No}\right]. \qquad (8.23)$$

In a nonpendulous gyro, M^d/H corresponds to a gyro drift, and the first term on the right hand side is well known among experts. It is inherent in all self-aligning inertial platform systems (s. [13], eq. (2.45)). The terms within the bracket are firstly the readout errors $\delta(I)\Theta_x$ and $\delta(I)\Theta_y$ of the signal generators which may also include errors due to vehicle vibration, and secondly the error $\delta(I)\Theta^+_{No}$, indicating that the gyropendulums may not have settled to their static equilibrium about the north axis (s. eq. (C3)).

Assuming the worst case for the alignment procedure, that all the inaccuracies of the sensors are of equal magnitude but of opposite sign, we find for the azimuth alignment error per 1 MERU

$$(I)\psi_o \approx 4.9\ \widehat{\text{min}}\ \text{per MERU}\ \frac{(I)M_{No}}{H'_o} \qquad (8.24)$$

which corresponds to the result in eq. (8.13). As might be remembered this result read: the azimuth error $(I)\psi_o$ of the gyrocompass must be less than $4.9\ \widehat{\text{min}}$ if one wants to define the disturbance torque with an accuracy corresponding to 1 MERU.

In Chapter 7, eq. (7.16) we have found that the signal generators and the initial settling of the gyropendulums to their equilibrium must meet the requirement $(I)\Theta \leq 7.24\ \widehat{\text{sec}}$ in order to keep the corresponding computed velocity error smaller than 1 km/h. Assuming the same inaccuracy during initial alignment, each term in eq. (8.23) may contribute an additional azimuth error of:

$$(I)\psi = 2.9\ \widehat{\text{min}}\ \text{per}\ 7.24\ \widehat{\text{sec}}\ \text{readout and spin vector alignment error.} \qquad (8.25)$$

Once the azimuth is adjusted in the way described above, the attitude angles φ^*_o and ϑ^*_o are indicated in Fig. 4.3 by the sums: $(\Delta\Theta_{xoI} + \Delta\Theta_{xoII})/2$ and $(\Delta\Theta_{yoI} + \Delta\Theta_{yoII})/2$. Again φ^*_o and ϑ^*_o contain the inaccuracy terms, which if

in connection with $(I)\psi$ we neglect the mean angle $\bar{\Theta}_{Eo}$ of both sensors we obtain from eqs. (8.14) and (8.15)

$$(I)\varphi_o \approx (I)\bar{\Theta}_x - \left[(I)\bar{\Theta}^+_{No} - (I)\bar{\Theta}_{No}\right]\cos\psi_o - \left[(I)\bar{\Theta}^+_{Eo} - (I)\bar{\Theta}_{Eo}\right]\sin\psi_o \qquad (8.26)$$

$$(I)\vartheta_o \approx (I)\bar{\Theta}_y - \left[(I)\bar{\Theta}^+_{Eo} - (I)\bar{\Theta}_{Eo}\right]\cos\psi_o + \left[(I)\bar{\Theta}^+_{No} - (I)\bar{\Theta}_{No}\right]\sin\psi_o \,. \qquad (8.27)$$

Again, if the readout inaccuracy and initial spin vector misalignment $(I)\bar{\Theta}_x$ and $(I)\bar{\Theta}_y$ meet the requirement of eq. (7.16), the corresponding attitude error is of the same magnitude:

$$(I)\varphi_o = (I)\vartheta_o = 7.24 \widehat{\text{sec}} \text{ per } 7.24 \widehat{\text{sec}} \text{ readout and spin vector alignment error.} \qquad (8.28)$$

Finally an inaccuracy in our knowledge of the stationary disturbance torque corresponding to 1 MERU causes via $(I)\Theta_{No}$ and $(I)\Theta_{Eo}$ an additional attitude error of

$$(I)\varphi_o = (I)\vartheta_o = 12.2 \widehat{\text{sec}} \text{ per MERU } \frac{(I)M^d}{H'_o} \qquad (8.29)$$

which could have been derived directly from eq. (4.9).

These results show us that it is much more difficult to achieve good accuracy with the self-alignment procedure compared to the alignment based on external measurements.

9. SUMMARY

An inertial navigation system is described and analyzed based on three two-degree-of-freedom gyroscopic sensors mounted on a common base which is strapped down to the vehicle. Two of the sensors are Schuler-gyropendulums with their spin vectors pointing up and down. The third sensor is an azimuth gyro with its spin vector pointing northerly parallel to the earth axis.

The two gyropendulums are each base motion isolated about their two input axes by means of two gimbals (one of which being the gyro case) and a gimbal follow-up control (s. Chapter 3, Fig. 3.2).

When moving over the surface of the earth, the spin vector of each properly tuned gyropendulum will tilt with respect to the vertical in the plane normal to the motion with an angle proportional to their velocity with respect to inertial space assuming that no error oscillations are superposed on the useful signal. Looking into the direction of the motion, the arrowheads of the upward and downward pointing spin vectors will both tilt to the left, indicating a negative and positive angle of 7.24 $\widehat{sec}$/(km/h) from the vertical (s. eqs. (3.9) to (3.11) for principles and eqs. (4.35) to (4.39) for more details).

Since the velocity of any point on the surface of the earth is known, the difference of corresponding readouts of the two gyropendulums can be used for ground speed and position computation. The sum of corresponding readouts can be used for tracking the vertical. The signal flow of this computation is shown in Fig. 3.5 for principles and Fig. 4.3 for more details. It is based on small angles for pitch and roll, but a large yaw angle which is measured by the azimuth gyro.

The azimuth gyro may have a gimbal follow-up control similar to the gyropendulums (s. Fig. 3.3). It is then base-motion isolated about its two input axes. Unfortunately, for high latitudes the maneuverability of the vehicle is limited for a gimballed gyro. If latitude plus pitch angle or roll angle amount to 90°, gimbal-lock may occur. This is prevented by an electrostatically supported azimuth gyro where direction cosine pattern readout is used. Chapter 5 treats this subject.

Error oscillations of the gyropendulums, inaccuracies of the signal generators and the computational process and errors in the measurement of the azimuth cause computational velocity errors. A simplified error analysis for the navigational system moving over a spherical earth was carried out in Chapter 7

where the accuracy requirements for the major sensitive items in the operation of the system were defined.

It was assumed that each item may contribute a computational velocity error of 1 km/h, when the system is mounted on three types of aircraft, a private plane or helicopter (V = 250 km/h), a subsonic jet (V = 900 km/h) and a supersonic transport (SST, V = 2,500 km/h). The major sensitive items in the operation of the system are:

a) The gyropendulum must be properly tuned in order to prevent horizontal and vertical accelerations from starting oscillations with approximately the Schuler period of 84 minutes (s. Chapter 4). The tuning condition (s. eqs. (4.10) and (4.3)) is a function of easterly velocity, latitude and vertical Coriolis and centrifugal accelerations and must be matched by a proper control of the angular momentum (s. Fig. 6.1). The change in angular momentum is approximately 6 % for an easterly flying SST at 40° to 50° latitude (s. eq. (6.9) and Table 6.1). An inaccuracy of 0.014 % in this angular momentum control causes a velocity error of 1 km/h on the SST (s. Table 7.1a).

b) The Coriolis and centrifugal accelerations due to horizontal velocity must be properly compensated by means of command torques, applied to the gyropendulum (s. eqs. (4.12), (4.13) and Fig. 6.1). Expressing the command torque as M^{cmd}/H, an inaccuracy of 0.009 deg/h causes a computational velocity error of 1 km/h (s. Table 7.1a). This means that the Coriolis and centrifugal acceleration must be compensated to an accuracy of 0.24 % on the SST.

c) The gyropendulums must have settled initially to their static equilibrium, which in the absence of disturbance torques is 0° from the vertical about the north axis and approximately $\mp 2.4^{\circ}$ ($\mp$, because spin vectors are pointing up and down) about the east axis. The latter value is due to the equilibrium of the gyroscopic torque caused by the horizontal component of earth rate and the pendulous torque (s. eqs. (4.4) to (4.9)). An initial offset angle of 7.24 $\widehat{\text{sec}}$. between the spin vectors of the gyropendulums and their equilibrium causes a computational velocity error of 1 km/h (s. eq. (7.16) and Table 7.1a). Constant disturbance torques, causing constant gyro drift in a non-pendulous gyro, cause a constant bias from this equilibrium in the gyropendulum. This may be compensated if known beforehand or measured during initial alignment (s. Chapter 8).

The compensation error of the disturbance torque M^{d}/H must be smaller than 0.009 deg/h in order to keep the resulting computational error below 1 km/h (s. eq. (7.20) and Table 7.1a). The same figure applies to the change of the dusturbance torques during flight, be it deterministic or random in nature.

d) The velocity computation is based upon the output signals of the four signal generators in the two TDF gyropendulums. A readout inaccuracy of 7.24 $\widehat{\text{sec}}$ corresponds to a velocity inaccuracy of 1 km/h (s. eq. (7.16) and Table 7.1a)

e) For the computational process to obtain ground speed from the output signals of the gyropendulums, the azimuth with respect to north must be known. On an easterly flying vehicle, for instance, any azimuth error will be interpreted by the system as a northerly component. The azimuth accuracy is effected by initial alignment accuracy and gyro drift, both causing the gyro on a stationary vehicle to oscillate with a 24 h mode with respect to the earth. It is effected furthermore by the readout accuracy and compensation for the vehicle's attitude. In order to keep the computational velocity error smaller than 1 km/h, the accuracy requirement for the azimuth (alignment, readout, attitude compensation) must be known within 0.94 $\widehat{\text{min}}$ on an SST (s. eq. (7.26) and Table 7.1c). The corresponding requirement for gyro drift is 0.009 deg/h.

f) Since, in the computational process for ground speed, the earth's velocity has to be subtracted, latitude and altitude of the vehicle must be known. The former is an output signal of the system itself (s. Fig. 4.3), the latter must be measured externally. For a computational velocity error of 1 km/h latitude and altitude, i.e. position and altitude must be known within 0.54 km (s. eqs. (7.18), (7.19) and Table 7.1a).

This study includes some design considerations in Chapter 6 and initial alignment considerations in Chapter 8.

Dr.-Ing. Bernhard STIELER, Institut für Flugführung der DFVLR, 33 Braunschweig-Flughafen

Appendix A

Derivation of the Performance Equations for a Gyropendulum with Vertical Spin Axis in a Dynamic Environment

A1 Readout Angles in the Navigational Frame

The model of a pendulous two-degree-of-freedom gyro with vertical spin axis, used by Schuler in [1] is shown in Fig. A1. We will assume that the gimbal

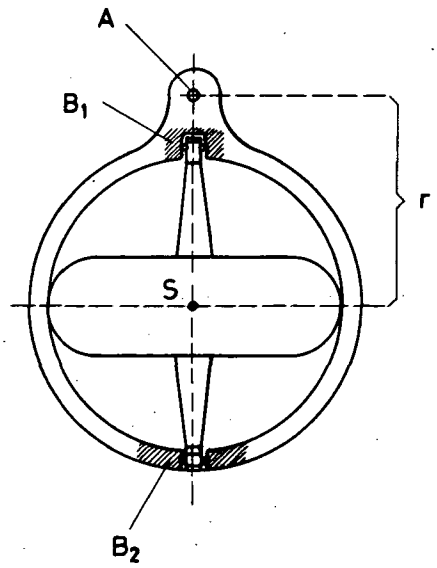

Fig. A1 **Model of the Pendulous Two-Degree-of-Freedom Gyroscope with Vertical Spin Axis**

A spherical gimbal bearing

B_1, B_2 rotor bearings

S center of gravity

r lever arm of pendulosity

bearing A in this model is nearly frictionless, so that the rotational motion of the base on which this bearing is mounted, exerts only a small disturbance torque M^d on the gyro. The attitude of the gyro's spin vector with respect to the vertical is affected mainly by the pendulous torques due to linear accelerations. Let us assume for the present that we may read this attitude in the navigational frame (subscript "n") about the north and east axis as shown in Fig. A2.

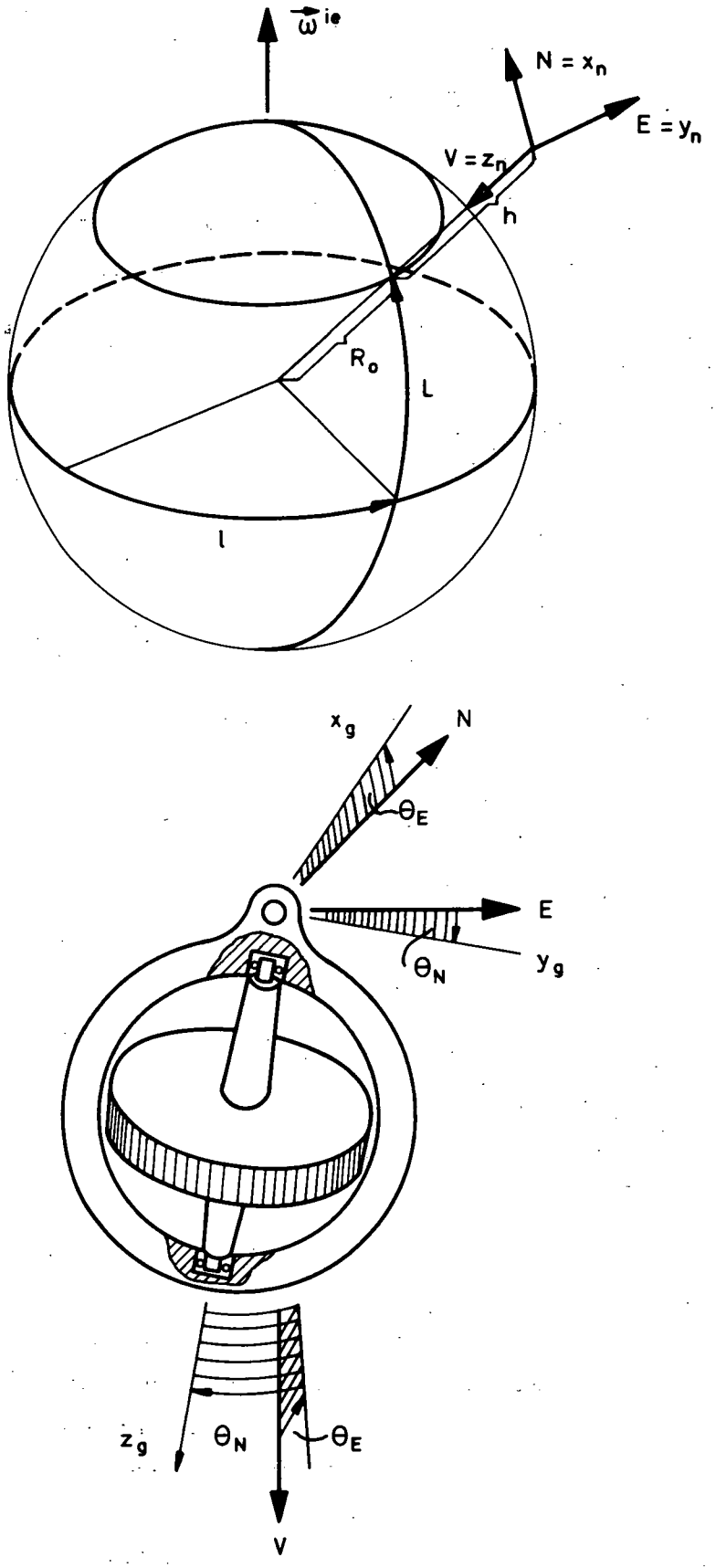

Fig. A2 The Navigational Frame and the Gyro Frame

In the following we will derive the performance equation of the gyropendulum in terms of these readout angles Θ_N and Θ_E.

Applying Newton's Law

$$\vec{M} = \left.\frac{d\vec{H}^t}{dt}\right|_i = \left.\frac{d\vec{H}^t}{dt}\right|_g + \vec{\omega}^{ig} \times \vec{H}^t \tag{A1}$$

to the gyropendulum, we assume that in the total angular momentum H^t, the spin angular momentum H is the dominant part and constant

$$H^t \approx H = \text{const.} \tag{A2}$$

So we may rewrite eq. (A1) in the gyro frame (subscript "g") as

$$\vec{M}_g \approx \vec{\omega}^{ig}_g \times \vec{H}\,, \tag{A3}$$

where according to Fig. A2

$$\vec{H}_g = H \begin{pmatrix} 0 \\ 0 \\ 1 \end{pmatrix}. \tag{A4}$$

The angular velocity $\vec{\omega}^{ig}_g$ may be split up into two components

$$\vec{\omega}^{ig} = \vec{\omega}^{in} + \vec{\omega}^{ng}\,, \tag{A5}$$

where the latter component is the angular velocity vector of the gyro with respect to the navigational frame (s. Fig. A2, Θ_N and Θ_E are small angles)

$$\omega^{ng} = \begin{pmatrix} p\Theta_N \\ p\Theta_E \\ 0 \end{pmatrix} \tag{A6}$$

and the former one is the angular velocity vector of the navigational frame with respect to inertial space. In the navigational frame, this vector is

$$\vec{\omega}^{in}_n = \begin{pmatrix} \omega_N \\ \omega_E \\ \omega_v \end{pmatrix} = \begin{pmatrix} (\omega^{ie} + pl)\cos L \\ -pL \\ -(\omega^{ie} + pl)\sin L \end{pmatrix}. \tag{A7}$$

By means of the transformation matrix

$$C_{gn} = \begin{pmatrix} 1 & 0 & -\Theta_E \\ 0 & 1 & \Theta_N \\ \Theta_E & -\Theta_N & 1 \end{pmatrix} \tag{A8}$$

$\vec{\omega}_n^{in}$ may be transformed into the gyro frame

$$\vec{\omega}_g^{in} = C_{gn} \vec{\omega}_n^{in} \quad . \tag{A9}$$

Let us now introduce eqs. (A4) to (A9) into eq. (A3) and assume that we have two gyropendulums, the spin vector of the first one (upper sign) pointing up and that of the second one (lower sign) pointing down. The basic performance equation for these sensors is

$$\begin{pmatrix} \mp H\omega_v^{in} & \mp Hp \\ \pm Hp & \mp H\omega_v^{in} \end{pmatrix} \begin{pmatrix} \Theta_N \\ \Theta_E \end{pmatrix} = \vec{M}_g \mp H \begin{pmatrix} -\omega_E^{in} \\ \omega_N^{in} \end{pmatrix}. \tag{A10}$$

In eq. (A7) let us write the rate of change of latitude and longitude in terms of the northerly and easterly ground speed on an earth assumed to be spherical

$$pL = V_N/R \tag{A11}$$

$$pl = V_E/(R \cos L), \tag{A12}$$

where

$$R = R_o + h \tag{A13}$$

is the magnitude of the radius vector from the center of the earth to the gyropendulum. The easterly velocity with respect to inertial space is:

$$V_{iE} = R\omega^{ie} \cos L + V_E \quad . \tag{A14}$$

The rate of change of celestial longitude is defined as

$$p\lambda = \omega^{ie} + pl = V_{iE}/(R \cos L). \tag{A15}$$

We introduce this and eqs. (A11) and (A14) into eq. (A7) and obtain

$$\omega_n^{in} = \begin{pmatrix} \omega_N^{in} \\ \omega_E^{in} \\ \omega_v^{in} \end{pmatrix} = \begin{pmatrix} p\lambda \cos L \\ -pL \\ -p\lambda \sin L \end{pmatrix} = \begin{pmatrix} V_{iE}/R \\ -V_N/R \\ -(V_{iE}/R) \tan L \end{pmatrix}. \tag{A16}$$

Let us now draw our attention to the torque $\vec{M}_g$ acting on the gyropendulum. We may write

$$\vec{M}_g = m\vec{r}_g \times \vec{f}_g + \vec{M}_g^{cmd} + \vec{M}_g^{d} \tag{A17}$$

where $\vec{M}^d$ is the disturbance torque which generates the gyro drift in a non-pendulous gyro, $\vec{M}^{cmd}$ is the command torque generated by special torquers (s. Fig. 3.2), m is the mass of the pendulosity,

$$\vec{r}_g = \begin{pmatrix} 0 \\ 0 \\ r \end{pmatrix} \tag{A18}$$

is the radius vector from the gyropendulum's center of support to the center of gravity and $\vec{f}$ is the nongravitational specific force which the gyropendulum exerts on the gimbal bearing A in Fig. A1. This specific force vector is

$$\vec{f} = \vec{G} - \vec{a}^{ig} \tag{A19a}$$

where $\vec{G}$ is the gravitational field intensity vector (mass attraction) and $\vec{a}^{ig}$ is the acceleration vector of the gyropendulum with respect to inertial space.

Since it is more convenient to calculate in terms of the gravity vector $\vec{g}$, defined as

$$\vec{g} = \vec{G} - \vec{\omega}^{ie} \times (\vec{\omega}^{ie} \times \vec{R}),$$

we obtain for eq. (A19a) after a few additional calculations

$$\vec{f} = \vec{g} - 2\vec{\omega}^{ie} \times \vec{V} - \vec{a} \tag{A19b}$$

where $\vec{a}$ is the acceleration vector with respect to an earth-fixed point and $\vec{V}$ is the ground speed vector. In [13], eq. 12.3 we find an expression for the specific force $\vec{f}_n$ in the navigational frame. According to [13], eq. (2.1), this is the negative of the force defined in eq. (A19). Assuming a spherical earth (in [13]: $e = 0$, $r_l = r_L \hat{=} R$) and zero deflection of the vertical (in [13]: $\xi = \eta = 0$) [13], eq. (2.3) reads with $\dot{R} = ph$

$$\vec{f}_n = \begin{pmatrix} -R\,p^2L - \frac{1}{2}R\left[(p\lambda)^2 - \omega^{ie\,2}\right]\sin 2L - 2ph\,pL \\ -R\,\cos L\,p^2\lambda + 2R\,\sin L\,pL\,p\lambda - 2ph\,p\lambda\,\cos L \\ g + p^2h - R\left[(p\lambda)^2 - \omega^{ie\,2}\right]\cos^2 L - R(pL)^2 \end{pmatrix}. \tag{A20a}$$

Collecting terms, we may derive the following equation

$$\vec{f}_n = \begin{pmatrix} -pV_N - phV_N/R - \left[V_{iE}^2/R - R(\omega^{ie}\cos L)^2\right]\tan L \\ -pV_{iE} - (ph - V_N \tan L)V_{iE}/R \\ g + p^2h - V_N^2/R - V_{iE}^2/R + R(\omega^{ie}\cos L)^2 \end{pmatrix} \qquad \text{(A20b)}$$

which may be transformed into the gyro frame as was eq. (A9).

The Coriolis and centrifugal acceleration shall comprise two different terms $\vec{b}$ and $\vec{c}$, where $\vec{b}$ refers to a horizontally flying vehicle

$$b_N = \left[V_{iE}^2/R - R(\omega^{ie}\cos L)^2\right]\tan L \qquad \text{(A21a)}$$

$$b_E = -V_N V_{iE}/R \tan L \qquad \text{(A22a)}$$

$$b_v = V_N^2/R + V_{iE}^2/R - R(\omega^{ie}\cos L)^2 \qquad \text{(A23a)}$$

and $\vec{c}$ is the additional Coriolis acceleration caused by the vertical velocity ph

$$c_N = ph\, V_N/R \qquad \text{(A21b)}$$

$$c_E = ph\, V_{iE}/R \qquad \text{(A22b)}$$

$$c_v = 0. \qquad \text{(A23b)}$$

So we can rewrite eq. (A20b) in the following form

$$\vec{f}_n = \begin{pmatrix} f_N \\ f_E \\ g + \Delta f_v \end{pmatrix} = \begin{pmatrix} -pV_N - b_N - c_N \\ -pV_{iE} - b_E - c_E \\ g + p^2h - b_v \end{pmatrix} . \qquad \text{(A24)}$$

We transform this into the gyro frame similarly to eq. (A9) and put the result into eq. (A17) in order to find the torque acting on the gyropendulum

$$\vec{M}_g = mr \begin{pmatrix} pV_{iE} + b_E + c_E - \Theta_N(g + p^2h - b_v) \\ -pV_N - b_N - c_N - \Theta_E(g + p^2h - b_v) \\ 0 \end{pmatrix} + \begin{pmatrix} M_N^{cmd} + M_N^d \\ M_E^{cmd} + M_E^d \\ 0 \end{pmatrix} . \qquad \text{(A25)}$$

Inserting this expression and eq. (A16) into (A10), we obtain

$$\begin{pmatrix} mr(g + p^2h - b_v) \pm H\, V_{iE}/R \tan L & \mp Hp \\ \pm Hp & mr(g + p^2h - b_v) \pm H\, V_{iE}/R \tan L \end{pmatrix} \begin{pmatrix} \Theta_N \\ \Theta_E \end{pmatrix} =$$

$$\begin{pmatrix} mr\,(pV_{iE} + b_E + c_E) \mp HV_N/R + M_N^{cmd} + M_N^d \\ -mr\,(pV_N + b_N + c_N) \mp HV_{iE}/R + M_E^{cmd} + M_E^d \end{pmatrix}. \qquad (A26)$$

Before taking the Laplace transform of eq. (A26), we have to specify the coefficients which are time-dependent in general, especially those of the matrix on the left-hand side. The frequency Ω, found by the evaluation of its determinant and describing the undamped coning motion of the gyropendulum

$$\Omega = \frac{mrg}{H}\left(1 + \frac{p^2h}{g} - \frac{b_v}{g}\right) \pm \left(\omega^{ie} \cos L + \frac{V_E}{R}\right) \tan L \qquad (A27)$$

depends on the vertical acceleration p^2h which has zero mean indeed for a horizontally flying vehicle, but may have short time peaks of up to 1 g or more. In order to estimate its effect upon the motion of the gyropendulum we assume that this vertical acceleration is an impulse function which occurs at the time τ

$$p^2h = ph\,\delta(t - \tau) \qquad (A28)$$

whose product with the current angle $\Theta_N(t)$ and $\Theta_E(t)$ becomes

$$mr\,p^2h\,\Theta_{N,E}(t) = mr\,ph\,\delta(t - \tau)\,\Theta_{N,E}(\tau). \qquad (A29)$$

Since $\Theta(\tau)$ is a constant angle, this enters the right hand side of eq. (A26), leaving the slowly varying frequency on the left hand side

$$\Omega^c = \frac{mgr}{H}\left(1 - \frac{b_v}{g}\right) \pm \left(\omega^{ie} \cos L + \frac{V_E}{R}\right) \tan L\,. \qquad (A30)$$

For the angles Θ_N and Θ_E we will introduce a quasi static equilibrium Θ_{N1}, Θ_{E1}, and a time dependent dynamic part $\Delta\Theta_N$ and $\Delta\Theta_E$:

$$\Theta_N = \Theta_{N1} + \Delta\Theta_N \qquad (A31)$$

$$\Theta_E = \Theta_{E1} + \Delta\Theta_E\,. \qquad (A32)$$

For all the other variables on the right hand side of eq. (A26), we introduce a steady state term (Subscript "0") referring to the initial value and a

displacement term like, for instance:

$$V = V_o + \Delta V \ . \tag{A33}$$

So we obtain for the quasi static equilibrium of eq. (A26) for zero command torque

$$\Theta_{N1} = \frac{M^d_{No}}{H\Omega^c} \tag{A34}$$

$$\Theta_{E1} = \frac{M^d_{Eo}/H \mp \omega^{ie} \cos L_o}{\Omega^c} \ , \tag{A35}$$

leaving as equation for the displacement angle from this quasi static equilibrium

$$\begin{pmatrix} \Omega^c & \mp p \\ \pm p & \Omega^c \end{pmatrix} \begin{pmatrix} \Delta\Theta_N \\ \Delta\Theta_E \end{pmatrix} = \mp \frac{mr}{H} ph\, \delta(t-\tau) \begin{pmatrix} \Theta_N(\tau) \\ \Theta_E(\tau) \end{pmatrix}$$

$$+ \begin{pmatrix} \frac{mr}{H}(p\,\Delta V_{iE} + b_E + c_E) \mp \Delta V_N/R + (M^{cmd}_N + \Delta M^d_N)/H \\ -\frac{mr}{H}(p\,\Delta V_N + b_N + c_N) \mp \Delta V_{iE}/R + (M^{cmd}_E + \Delta M^d_E)/H \end{pmatrix}. \tag{A36}$$

Let us now specify the coefficients and independent variables. We assume that R, cos L and sin L are constant. The time dependence of ΔV_N and ΔV_{iE} is specified only insofar as we assume that for t = o the velocity does not change discontinuously ($\Delta V^+_{No} = \Delta V^+_{iEo} = 0$). For such small terms as the Coriolis and centrifugal acceleration b in horizontal flight, the additional disturbance torque ΔM^d and the command torque, we simply assume step functions. With the Laplace transform of the additional Coriolis acceleration c_N and c_E due to the vertical velocity (s. eqs. (A21b) and (A22b)), one has to keep in mind that with the assumption in eq. (A28), the Laplace transform of the vertical velocity is $\mathcal{L}\{ph\} = phe^{-s\tau}/s$. Since in eqs. (A21b) and (A22b) V_N/R and V_{iE}/R will be assumed to be constant at the time $t \geq \tau$, the Laplace transform of c_N, say is $\mathcal{L}\{c_N\} = c_N e^{-s\tau}/s$.

Denoting with Δ the determinant of the left-hand matrix of eq. (A36)

$$\Delta = s^2 + (\Omega^c)^2 \ . \tag{A37}$$

we obtain the following equations for the displacement angles from the quasi static equilibrium in eqs. (A34) and (A35)

$$\Delta\tilde{\Theta}_N = \frac{1}{\Delta}\left\{ \mp \frac{mr}{H}\left(s^2 + \Omega^c \frac{H}{mr\,R}\right)\tilde{\Delta V}_N + \left(\frac{mr}{H}\Omega^c - \frac{1}{R}\right) s\,\tilde{\Delta V}_{iE} \right.$$

$$+ \frac{\Omega^c}{sH}\left[mr\left(b_E + \frac{V_{iE}}{R}\,ph\,e^{-s\tau}\right) + M_N^{cmd} + \Delta M_N^d \right]$$

$$\mp \frac{1}{H}\left[mr\left(b_N + \frac{V_N}{R}\,ph\,e^{-s\tau}\right) - M_E^{cmd} - \Delta M_E^d \right]$$

$$\mp \Omega^c\left[\Delta\Theta_{Eo}^+ \pm \Theta_N(\tau)\,e^{-s\tau}\,\frac{mr}{H}\,ph \right]$$

$$\left. + s\left[\Delta\Theta_{No}^+ \mp \Theta_E(\tau)\,e^{-s\tau}\,\frac{mr}{H}\,ph \right] \right\} \qquad \text{(A38)}$$

$$\Delta\tilde{\Theta}_E = \frac{1}{\Delta}\left\{ \mp \frac{mr}{H}\left(s^2 + \Omega^c \frac{H}{mr\,R}\right)\tilde{\Delta V}_{iE} - \left(\frac{mr}{H}\Omega^c - \frac{1}{R}\right) s\,\tilde{\Delta V}_N \right.$$

$$- \frac{\Omega^c}{sH}\left[mr\left(b_N + \frac{V_N}{R}\,ph\,e^{-s\tau}\right) - M_E^{cmd} - \Delta M_E^d \right]$$

$$\mp \frac{1}{H}\left[mr\left(b_E + \frac{V_{iE}}{R}\,ph\,e^{-s\tau}\right) + M_N^{cmd} + \Delta M_N^d \right]$$

$$\pm \Omega^c\left[\Delta\Theta_{No}^+ \mp \Theta_E(\tau)\,e^{-s}\,\frac{mr}{H}\,ph \right]$$

$$\left. + s\left[\Delta\Theta_{Eo}^+ \pm \Theta_N(\tau)\,e^{-s\tau}\,\frac{mr}{H}\,ph \right] \right\}. \qquad \text{(A39)}$$

A2 Readout Angles in the Body Frame

The eqs. (A38) and (A39) transformed into the time domain and added to eqs. (A34) and (A35) describe the attitude Θ_N and Θ_E of the gyropendulum's spin vector with respect to the vertical about the north and east axis of the navigational frame. If, as proposed in Fig. 3.2, the actual gyro readout takes place in the body frame, we have to derive the corresponding equations for Θ_x and Θ_y, the readout angles along the vehicle's longitudinal axis and pitch axis. They may be obtained in the following way:

The unit-spin vector $\vec{1}^s = \frac{\vec{H}}{H}$, given in the navigational frame, may be transformed into the body frame via the rotation ψ about the vertical or yaw axis ($\psi = 0$ for northerly flying vehicle), the rotation ϑ about the pitch axis ($\vartheta > 0$ for tail down), and the rotation φ about the longitudinal axis ($\varphi > 0$ for right wing down). So we obtain

$$\vec{1}_b^s = C_{bn}\,\vec{1}_n^s = C_{ng}\,\vec{1}_g^s\,, \qquad \text{(A40)}$$

where

$$C_{bn} \approx \begin{pmatrix} \cos\psi & \sin\psi & -\vartheta \\ -\sin\psi & \cos\psi & \varphi \\ \vartheta\cos\psi + \varphi\sin\psi & -\varphi\cos\psi + \vartheta\sin\psi & 1 \end{pmatrix} \tag{A41}$$

(the attitude angles ϑ and φ are assumed to be small). C_{ng} can be taken from eq. (A8), and

$$\vec{1}_g^s = \begin{pmatrix} 0 \\ 0 \\ 1 \end{pmatrix}. \tag{A42}$$

So we find

$$\vec{1}_b^s \approx \begin{pmatrix} -\vartheta + \Theta_E\cos\psi - \Theta_N\sin\psi \\ \varphi - \Theta_N\cos\psi - \Theta_E\sin\psi \\ 1 \end{pmatrix}. \tag{A43}$$

The unit-spin vector in the body frame may also be described in terms of the readout angles Θ_x and Θ_y, i.e. the angles between the gyro frame and the body frame (positive when the body moves positively around the x and y axes). Since the attitude angles ϑ and φ of the vehicle with respect to the navigational frame are small, as well as the attitude of the spin vector with respect to the navigational frame, also Θ_x and Θ_y are small, which are composed of both kinds of angles. From comparison with Fig. A2 and eq. (A8) (replace Θ_N by Θ_x, Θ_E by Θ_y, the n-frame by the g-frame and the g-frame by the b-frame), we obtain

$$\vec{1}_b^s \approx \begin{pmatrix} 1 & 0 & -\Theta_y \\ 0 & 1 & \Theta_x \\ \Theta_y & -\Theta_x & 1 \end{pmatrix} \begin{pmatrix} 0 \\ 0 \\ 1 \end{pmatrix} = \begin{pmatrix} -\Theta_y \\ \Theta_x \\ 1 \end{pmatrix}. \tag{A44}$$

Eqs. (A43) and (A44) describe the same spin vector, so we may deduce:

$$\Theta_x = \varphi - \Theta_N\cos\psi - \Theta_E\sin\psi \tag{A45}$$

$$\Theta_y = \vartheta - \Theta_E\cos\psi + \Theta_N\sin\psi \tag{A46}$$

A3 Application of the Command Torques in the Free Azimuth Frame

Command torques which have to be applied to the gyropendulum were denoted in the previous sections as M_N^{cmd} and M_E^{cmd}, as torques about the north and

east axis of the navigational frame. The magnitude of these torques is defined in Chapter 4, eq. (4.12) and (4.13).

In the proposed design for the gyropendulum, the gyro case including the gyro torquer is base-motion isolated about the input axes but not about the spin axis of the gyro. So the reference frame in which the torque is applied to the gyropendulum coincides approximately with the free azimuth frame which is rotated relative to the navigational frame through the azimuth angle ψ. In reality there is a small difference caused by the angles Θ_N and Θ_E which we will neglect, since for the small angles Θ_N or Θ_E ($< 5^\circ$) horizontal command torques are only affected by cos Θ_N or cos Θ_E, which can be assumed to be unity, especially since the command torques for compensating Coriolis and centrifugal accelerations are small. So we write:

$$\vec{M}_a^{cmd} = C_{an}\, \vec{M}_n^{cmd} \tag{A47}$$

where

$$C_{an} = \begin{pmatrix} \cos\psi & \sin\psi & 0 \\ -\sin\psi & \cos\psi & 0 \\ 0 & 0 & 1 \end{pmatrix} \tag{A48}$$

(s. eq. (A41) for $\vartheta = \varphi = 0$).

For the components of the gyro torquer we obtain

$$M_x^{cmd} = M_N^{cmd} \cos\psi + M_E^{cmd} \sin\psi \tag{A49}$$

$$M_y^{cmd} = M_E^{cmd} \cos\psi - M_N^{cmd} \sin\psi\,. \tag{A50}$$

Appendix B

Derivation of the Performance Equations of a Two-Degree-of-Freedom Azimuth Gyro with its Spin Axis Pointing Northerly, Parallel to the Earth Axis

B1 Readout Angles in the Equatorial Tangent Frame

We define the equatorial tangent coordinate frame (subscript "t") as a frame with the x or N'-axis pointing northerly parallel to the earth axis, the y or E-axis pointing horizontal to the east and the z or D-axis pointing downward tilted from the vertical by an angle equal to the latitude angle (s. Fig. B1).

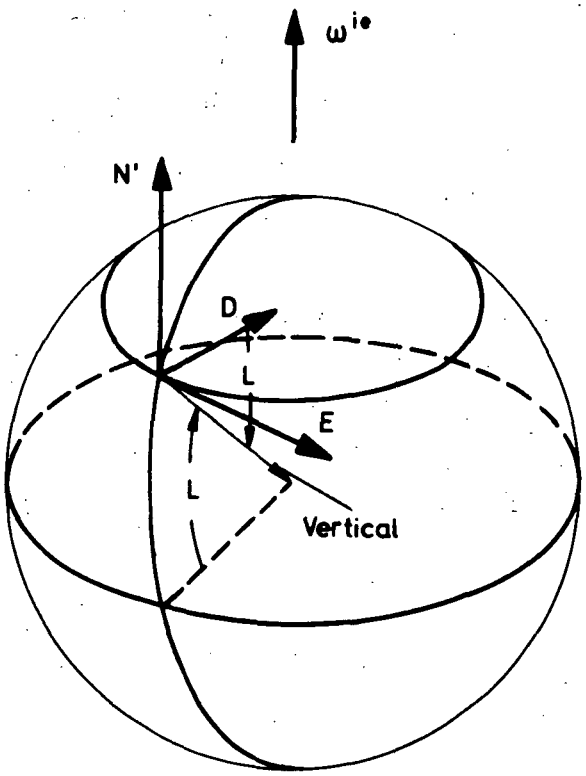

Fig. B1 The Equatorial Tangent Coordinate Frame

The basic equation for the performance of a TDF azimuth gyro with its spin axis pointing northerly parallel to the earth axis may be obtained from eq. (A10), the corresponding equations for a TDF gyro with vertical spin axis, by a cyclic permutation of the subscripts as follows:

V → N'

N → E

E → D.

Keeping in mind that the azimuth gyro is non-pendulous (r = 0), we obtain

$$\begin{pmatrix} H\omega^{it} & Hp \\ -Hp & H\omega^{it} \end{pmatrix} \begin{pmatrix} \Theta_E \\ \Theta_D \end{pmatrix} = \vec{M}_g \qquad \text{(B1)}$$

where the only input angular rate ω^{it} is

$$\omega^{it} = \omega^{ie} + V_E/(R \cos L). \qquad \text{(B2)}$$

Assuming first that the only torque acting on the gyro is the constant disturbance torque generating the gyro drift

$$\vec{M}_g = \vec{M}_g^d = H \begin{pmatrix} \omega_D^d \\ -\omega_E^d \end{pmatrix}, \qquad \text{(B3)}$$

second that the gyro has an initial misalignment about the east and down axes Θ_{Eo}^+ and Θ_{Do}^+ and finally that the easterly velocity V_E is constant, we obtain in the Laplace domain:

$$\tilde{\Theta}_E = \frac{1}{\Delta} \left(\frac{\omega^{it}}{s} \omega_D^d + \omega^{it} \Theta_{Do}^+ + \omega_E^d + s \Theta_{Eo}^+ \right) \qquad \text{(B4)}$$

$$\tilde{\Theta}_D = \frac{1}{\Delta} \left(- \frac{\omega^{it}}{s} \omega_E^d - \omega^{it} \Theta_{Eo}^+ + \omega_D^d + s \Theta_{Do}^+ \right) \qquad \text{(B5)}$$

where

$$\Delta = s^2 + (\omega^{it})^2. \qquad \text{(B6)}$$

The signal flow diagram for this gyro is very similar to the one for the gyropendulum in Fig. 4.1 except the gyro is nonpendulous (r = 0) and the subscripts are different (as mentioned above).

B2 Readout Angles in the Body Frame for a Gimballed Gyro

As mentioned in Chapter 3, the azimuth gyro is base-motion isolated about its input axis by means of one gimbal between the gyro case and the vehicle (s. Fig. 3.3), the gyro case serving as second gimbal. In order to derive the readout equations of the two signal generators for Θ_y and Θ_z in the body frame, we proceed as in Appendix A, Section A2, i.e., we first describe the unit spin vector $\vec{1^s}$ in the body frame in terms of the angles Θ_E, Θ_D, L (latitude) and ψ, ϑ, φ

$$\vec{1^s}_b = C_{bn} C_{nt} C_{tg} \vec{1^s}_g \qquad \text{(B7)}$$

where C_{tg} is the transformation matrix between the gyro frame and the equatorial tangent frame (rotation through Θ_E, Θ_D)

$$C_{tg} = \begin{pmatrix} 1 & -\Theta_D & \Theta_E \\ \Theta_D & 1 & 0 \\ -\Theta_E & 0 & 1 \end{pmatrix}, \tag{B8}$$

C_{nt} is the transformation matrix between the equatorial tangent frame and the navigational frame (rotation through L about east axis)

$$C_{nt} = \begin{pmatrix} \cos L & 0 & \sin L \\ 0 & 1 & 0 \\ -\sin L & 0 & \cos L \end{pmatrix} \tag{B9}$$

and C_{bn} from eq. (A41).

So we obtain

$$\vec{1}_b^s = \begin{pmatrix} \cos\psi \cos L + (\vartheta - \Theta_E \cos\psi) \sin L + \Theta_D \sin\psi \\ -\sin\psi \cos L - (\varphi - \Theta_E \sin\psi) \sin L + \Theta_D \cos\psi \\ -\sin L + (\vartheta \cos\psi + \varphi \sin\psi - \Theta_E) \cos L \end{pmatrix}. \tag{B10}$$

We now derive the same unit spin vector in terms of the readout angles Θ_y and Θ_z which are positive when the gimbal rotates with respect to the gyro about the y-axis and the vehicle rotates with respect to the gimbal about the z-axis. This results in

$$C_{bg} = \begin{pmatrix} \cos\Theta_y \cos\Theta_z & \sin\Theta_z & -\sin\Theta_y \cos\Theta_z \\ -\cos\Theta_y \sin\Theta_z & \cos\Theta_z & \sin\Theta_y \sin\Theta_z \\ \sin\Theta_y & 0 & \cos\Theta_y \end{pmatrix} \tag{B11}$$

and

$$1_b^s = \begin{pmatrix} \cos\Theta_y \cos\Theta_z \\ -\cos\Theta_y \sin\Theta_z \\ \sin\Theta_y \end{pmatrix}. \tag{B12}$$

By equating eqs. (B10) and (B12) we find

$$\cos\Theta_y \sin\Theta_z = \sin\psi \cos L + \varphi \sin L - \Theta_E \sin\psi \sin L - \Theta_D \cos\psi \tag{B13}$$

and

$$\sin \Theta_y = - \sin L + (\vartheta \cos \psi + \varphi \sin \psi - \Theta_E) \cos L. \qquad (B14)$$

Using the formula

$$\arcsin (u\sqrt{1 - v^2} \pm v \sqrt{1 - u^2}) = \arcsin u \pm \arcsin v \qquad (B15)$$

and putting

$$u = - \sin L \qquad (B16)$$

$$v = \vartheta \cos \psi + \varphi \sin \psi - \Theta_E , \qquad (B17)$$

we may approximate eq. (B14) with v considered small as

$$\Theta_y \approx - L + \vartheta \cos \psi + \varphi \sin \psi - \Theta_E. \qquad (B18)$$

This angle might very well become 90° at high latitudes for which eq. (B13) deteriorates, indicating that "gimbal lock" occurs. For situations when this is not the case, we may put eq. (B18) into (B13) and solve for $\sin \psi$. In connection with small quantities, we approximate $\sin \Theta_z \approx \sin \psi$ and find in a way similar to eqs. (B15) to (B18)

$$\Theta_z \approx \psi - (\vartheta \sin \psi - \varphi \cos \psi) \tan L + \frac{\Theta_D}{\cos L} . \qquad (B19)$$

The next section deals with the readout equations of a gyroscope, where "gimbal lock" does not occur.

B3 Readout Angles in the Body Frame for an Electrostatic Gyro (ESG) with Direction Cosine Pattern Readout

No gimbals are required for the operation of an electrostatic gyro with direction cosine pattern readout (as described in [12]) which removes the danger of gimbal lock.

The performance equations in section B1 might be very well applied to the ESG, also eq. (B10) for describing the attitude of the unit vector of the angular momentum with respect to the body frame in terms of the displacement angles Θ_E and Θ_D, the latitude L, the attitude ϑ and φ and the azimuth ψ. Only the readout angles which we denote with Θ'_y and Θ'_z are different; they are shown in Fig. B2. Instead of eq. (B12) we may write now

$$\vec{1}_b^s = \begin{pmatrix} \cos\Theta_{xx} \\ \cos\Theta_{yx} \\ \cos\Theta_{zx} \end{pmatrix} = \begin{pmatrix} \cos\Theta_{xx} \\ \cos\Theta'_z \\ \cos\Theta_y \end{pmatrix} \qquad \text{(B20)}$$

which may be equated with eq. (B10). Similar to eq. (B18) we find from the z-component

$$\Theta'_y \approx 90^\circ + L - \vartheta \cos\psi - \varphi \sin\psi + \Theta_E \; ; \qquad \text{(B21)}$$

from the y-component we obtain

$$\Theta'_z = \arccos\left[- \sin\psi \cos L - (\varphi - \Theta_E \sin\psi) \sin L + \Theta_D \cos\psi \right], \qquad \text{(B22)}$$

which shows that at the north pole only ψ cannot be measured by Θ'_z .

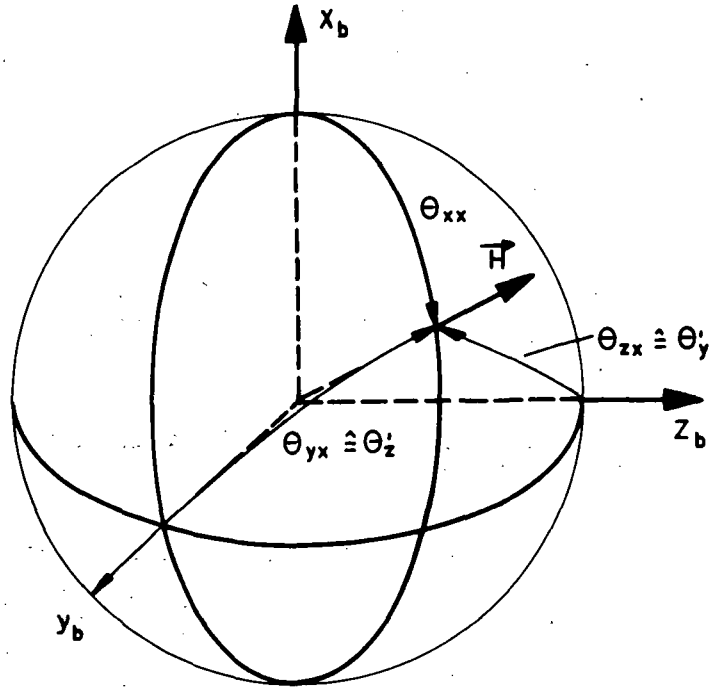

Fig. B2 Readout Angles of an Electrostatic Gyro

Appendix C

Derivation of the Error Equation of the Gyropendulum Within the Navigational Frame

In the following we will denote all computed values by an asterisk. They differ from the accurate ones by the inaccuracy, e.g., (s. eqs. (4.12) and (4.13))

$$(I)M_N^{cmd} = M_N^{cmd*} + mr\, b_E \tag{C1}$$

$$(I)M_E^{cmd} = M_E^{cmd*} - mr\, b_N. \tag{C2}$$

The initial alignment inaccuracy of the spin vector from the equilibrium in eqs. (4.4) and (4.5) is

$$(I)\Theta_{No}^{+} = \Theta_{No}^{+} - \Theta_{No} = \Theta_{No}^{+} - M_{No}^{d}/(H\Omega_o^c) \tag{C3}$$

$$(I)\Theta_{Eo}^{+} = \Theta_{Eo}^{+} - \Theta_{Eo} = \Theta_{Eo}^{+} - (M_{Eo}^{d}/H \mp \omega^{ie} \cos L_o)/\Omega_o^c\ . \tag{C4}$$

These inaccuracy terms may be put directly into eqs. (A38) and (A39). It is a little more difficult to derive the equation for the inaccuracy of the tuning condition. The computed tuning condition is derived from the equations

$$\frac{H^*}{mr\, R^*} = \Omega^{c*}, \tag{C5}$$

which, when evaluated similarly to eqs. (6.1) to (6.9), gives for the computed angular momentum H^*

$$H^* = H_o + \Delta H^* = H_o \left(1 + \frac{\Delta\Omega^{c*}\big|_{H_o}}{2\omega_o^s} + \frac{h^*}{2R_o}\right), \tag{C6}$$

where we assume the zero-values to be accurately known. The term $\Delta\Omega^{c*}\big|_{H_o}$ and h^* are known quantities; $\Delta\Omega^{c*}\big|_{H_o}$ is computed from eq. (6.7)

$$\frac{\Delta\Omega^{c*}\big|_{H_o}}{\omega_o^s} \approx -\frac{2h^*}{R_o} - \frac{b_v^*}{g} \pm \frac{1}{\omega_o^s}\left[\left(\omega^{ie}\cos L_o + \frac{V_E^*}{R\cos^2 L_o}\right) L^* + \frac{V_E^*}{R^*}\tan L_o\right]. \tag{C7}$$

This computed frequency change for constant angular momentum, which in our analysis is the basis for the computation of the angular momentum H^*, differs from the exact value by the inaccuracy

$$\Delta\Omega^{c*}\big|_{H_o} = \Delta\Omega^{c}\big|_{H_o} + (I)\Omega^{c}\big|_{H_o}, \tag{C8}$$

where in similar fashion to eq. (C7),

$$\frac{(I)\Omega^c\big|_{H_o}}{\omega_o^s} \approx \frac{-2(I)h}{R_o} - \frac{(I)b_v}{g} \pm \frac{1}{\omega_o^s}\left[(\omega^{ie}\cos L_o + \frac{V_E}{R\cos^2 L_o})\,(I)L + \frac{(I)V_E}{R}\tan L_o\right]. \quad (C9)$$

With the known computed angular momentum H^*, we may tackle the computation of the tuning condition in the first parenthetical expression on the right hand side of eqs. (A38) and (A39)

$$\Omega^c(H^*)\,\frac{H^*}{mrR} = \Omega^c(H^*)\,\frac{H^*}{mr\,R^*(1 - (I)h/R^*)} \approx \Omega^c(H^*)\,\Omega^{c*}\,(1 + (I)h/R_o). \quad (C10)$$

The relationship between the computed coning frequency Ω^{c*} and the actual frequency $\Omega^c(H^*)$ which is based on the erroneous angular momentum is still unknown. In order to compute $\Omega^c(H^*)$ in terms of Ω^{c*} we write for H^*

$$H^* = H + (I)H, \quad (C11)$$

where similarly to eq. (6.9),

$$\frac{(I)H}{H} \approx \frac{(I)H}{H_o} = \frac{(I)\Omega^c\big|_{H_o}}{2\,\omega_o^s} + \frac{(I)h}{2\,R_o}\,. \quad (C12)$$

So we obtain, with eq. (A30), the actual frequency

$$\Omega^c(H^*) \approx \Omega^c - \frac{mgr}{H}\,\frac{(I)H}{H} \approx \Omega^c - \omega_o^s\,\frac{(I)H}{H_o}\,. \quad (C13)$$

The accurate frequency, written in terms of the computed one and the inaccuracy term is

$$\Omega^c = \Omega^{c*} - (I)\Omega^c, \quad (C14)$$

where $(I)\Omega^c$ is similar to eq. (6.11)

$$(I)\Omega^c = \Omega_o^c\left(\frac{(I)H}{H_o} - \frac{(I)h}{R_o}\right). \quad (C15)$$

So we find finally

$$\Omega^{c*} = \Omega^c(H^*) + \Omega_o^c\left(\frac{2(I)H}{H_o} - \frac{(I)h}{R_o}\right) \quad (C16)$$

and using eq. (C10) for the tuning term in the first parenthesis of eqs. (A38) and (A39), this becomes

$$\Omega^c(H^*)\,\frac{H^*}{mrR} \approx \Omega^c(H^*)^2\left(1 + \frac{2(I)H}{H_o}\right). \qquad (C17)$$

Similarly, the second parenthesis on the right hand side of eqs. (A38) and (A39) becomes

$$\frac{mr}{H^*}\,\Omega^c(H^*) - \frac{1}{R} \approx -\,2\,\frac{mr}{H^*}\,\Omega^c(H^*)\,\frac{(I)H}{H_o}\,. \qquad (C18)$$

Before we solve eqs. (A38) and (A39) in the time domain, including the error equation from eqs. (C1) to (C4) and (C17) and (C18), we have to specify the transient of ΔV_N and ΔV_{iE}. For the derivation in Chapter 4 these transients did not have to be specified, except for continuity ($\Delta V^+_{No} = \Delta V^+_{iEo} = 0$) because for accurate tuning, the first parenthesis of the right hand side of eqs. (A38) and (A39) cancels with the determinant Δ and the second parenthesis becomes zero. This meant that the accurately tuned gyropendulum follows any transient of ΔV without time lag or oscillation. That does not hold any longer for inaccurate tuning and the transients have to be specified for evaluating these equations in the time domain. We will assume that ΔV_N and ΔV_{iE} are step functions but with no discontinuity at t = 0. Mathematically this is verified by writing for instance

$$\Delta\tilde{V}_N = \frac{\Delta V_N}{s(1 + Ts)} \qquad (C19)$$

which in the time domain is

$$\Delta V_N\,(t) = V_N\,(1 - e^{-t/T}). \qquad (C20)$$

We assume that T is so small that for the time of observation $e^{-t/T}$ is negligible. This matches the physical world much better than the accurate step functions.

So we find from eqs. (A38) and (A39) for the indicated displacement angles about the north and east axis with respect to the equilibrium in eqs. (A34) and (A35)

$$\Delta\Theta_N = \mp \frac{mr}{H^*}\left(1 + \frac{2(I)H}{H_o}\right)\Delta V_N + \frac{1}{H^*\Omega^c(H^*)}\left((I)M_N^{cmd} + \Delta M_N^d\right)$$

$$+ \frac{mr}{H^*}\frac{V_{iE}}{R\Omega^c(H^*)}\,\mathrm{ph}\; f(t-\tau)$$

$$+ \left[\pm\frac{mr}{H^*}\frac{2(I)H}{H_o}\Delta V_N - \frac{1}{H\Omega^c(H^*)}\left((I)M_N^{cmd} + \Delta M_N^d\right) + (I)\Theta_{No}^+\right]\cos\left(\Omega^c(H^*)\,t\right)$$

$$- \left[\frac{mr}{H^*}\frac{2(I)H}{H_o}\Delta V_{iE} \mp \frac{1}{H\Omega^c(H^*)}\left((I)M_E^{cmd} + \Delta M_E^d\right) \pm (I)\Theta_{Eo}^+\right]\sin\left(\Omega^c(H^*)\,t\right)$$

$$- \frac{mr}{H^*}\,\mathrm{ph}\; f(t-\tau)\left[\left(\frac{V_{iE}}{R\Omega^c(H^*)} \pm \Theta_E(\tau)\right)\cos\left(\Omega^c(H^*)\,(t-\tau)\right)\right.$$

$$\left. \pm \left(\frac{V_N}{R\Omega^c(H^*)} \pm \Theta_N(\tau)\right)\sin\left(\Omega^c(H^*)\,(t-\tau)\right)\right] \qquad (C21)$$

$$\Delta\Theta_E = \mp \frac{mr}{H^*}\left(1 + \frac{2(I)H}{H_o}\right)\Delta V_{iE} + \frac{1}{H^*\Omega^c(H^*)}\left((I)M_E^{cmd} + \Delta M_E^d\right)$$

$$- \frac{mr}{H^*}\frac{V_N}{R\Omega^c(H^*)}\,\mathrm{ph}\; f(t-\tau)$$

$$+ \left[\pm\frac{mr}{H^*}\frac{2(I)H}{H_o}\Delta V_{iE} - \frac{1}{H^*\Omega^c(H^*)}\left((I)M_E^{cmd} + \Delta M_E^d\right) + (I)\Theta_{Eo}^+\right]\cos\left(\Omega^c(H^*)\,t\right)$$

$$+ \left[\frac{mr}{H^*}\frac{2(I)H}{H_o}\Delta V_N \mp \frac{1}{H^*\Omega^c(H^*)}\left((I)M_N^{cmd} + \Delta M_N^d\right) \pm (I)\Theta_{No}^+\right]\sin\left(\Omega^c(H^*)\,t\right)$$

$$+ \frac{mr}{H^*}\,\mathrm{ph}\; f(t-\tau)\left[\left(\frac{V_N}{R\Omega^c(H^*)} \pm \Theta_N(\tau)\right)\cos\left(\Omega^c(H^*)\,(t-\tau)\right)\right.$$

$$\left. \pm \left(\frac{V_{iE}}{R\Omega^c(H^*)} \pm \Theta_E(\tau)\right)\sin\left(\Omega^c(H^*)\,(t-\tau)\right)\right]. \qquad (C22)$$

As to the last bracket on the right hand side of eqs. (C21) and (C22), it can be shown to be negligible even if $\Theta_N(\tau)$ and $\Theta_E(\tau)$ are not exactly proportional to $\mp\, V_N/(R\Omega^c(H^*))$ and $\pm\, V_{iE}/(R\Omega^c(H^*))$, respectively, as had been found in eqs. (4.18) and (4.19) for an accurately working gyropendulum. Assuming that from either amplitude within the bracket, an inaccuracy angle $(I)\Theta$ remained, the vertical acceleration would cause the gyropendulum to oscillate with an amplitude of $\frac{mr}{H^*}\,\mathrm{ph}\,(I)\Theta$. In terms of indicated velocity error this would be

$$(I)V(\mathrm{ph}) = \mathrm{ph} \cdot (I)\Theta. \qquad (C23)$$

Since ph is in the order of meters per second and (I)Θ in the order of arc seconds, this can really be neglected.

In Chapter 4 we have also found that the third term on the right hand side of eqs. (C21) and (C22), i.e., the bias due to vertical velocity, can be left out. It drops out in any case in the computation of the difference of corresponding readouts of the two gyropendulums, i.e., it does not directly affect the velocity computation. Its effect on the attitude computation, which is based on the sum of corresponding readouts, is negligible (s. eq. (4.23)).

The total indicated angle of the gyropendulum about the north and east axes (s. eqs. (A31) and (A32)) comprises firstly the quasi static equilibrium (s. eqs. (A34) and (A35)) where the denominator is now $H^*\Omega^c(H^*)$

$$\Theta_{N1} = \frac{M^d_{No}}{H^*\Omega^c(H^*)} \approx \frac{M^d_{No}}{H_o\,\omega^s_o} \tag{C24}$$

$$\Theta_{E1} = \frac{M^d_{Eo}/H^* \mp \omega^{ie}\cos L_o}{\Omega^c(H^*)} \approx \frac{M^d_{Eo}}{H_o\,\omega^s_o} \mp \frac{\omega^{ie}\cos L_o}{\Omega^c(H^*)}\,. \tag{C25}$$

It comprises secondly the dynamic angles $\Delta\Theta_N$ and $\Delta\Theta_E$ from eqs. (C21) and (C22) and thirdly the readout inaccuracies $(I)\Theta_N$ and $(I)\Theta_E$. So we find for the total indicated angles about the north and east axes

$$\Theta^*_N = \Theta_N + (I)\Theta_N = \Theta_{N1} + \Delta\Theta_N + (I)\Theta_N \tag{C26}$$

$$\Theta^*_E = \Theta_E + (I)\Theta_E = \Theta_{E1} + \Delta\Theta_E + (I)\Theta_E\,. \tag{C27}$$

In Fig. 4.3 it is shown that the biases of the readout angles, which according to eqs. (4.4) and (4.5) are the angles due to initial horizontal earth rate and disturbance torques, are subtracted from the readout angles. This may cause an additional error for slightly erroneous biases which we denote as

$$(I)\Theta_{N1} = \frac{M^{d*}_{No}}{H^*\Omega^{c*}} - \frac{M^d_{No}}{H^*\Omega^c(H^*)} \approx \frac{(I)M^d_{No}}{H_o\,\omega^s_o} \tag{C28}$$

$$(I)\Theta_{E1} = \frac{M_{Eo}^{d*}/H^* \mp \omega^{ie}\cos L_o}{\Omega^{c*}} - \frac{M_{Eo}^{d}/H^* \mp \omega^{ie}\cos L_o}{\Omega^{c}(H^*)}$$

$$\approx \frac{(I)M_{Eo}^{d}}{H_o\,\omega_o^s} \pm \frac{\omega^{ie}\cos L_o}{\Omega^{c*}} \left(\frac{2(I)H}{H_o} - \frac{(I)h}{R_o}\right). \qquad (C29)$$

Multiplying the readout angles of one gyropendulum by $\frac{H^*}{mr}$ gives the computed velocity. In connection with small quantities, we may approximate in eqs. (C21) and (C22)

$$\frac{H^*}{mr\,\Omega^c(H^*)} \approx R_o \qquad (C30)$$

(s. eq. (C18)) and

$$\Omega^c(H^*) \approx \omega_o^s \qquad (C31a)$$

$$H^* \approx H_o. \qquad (C31b)$$

Before we write down the computational velocity errors, let us introduce some abbreviations into eqs. (C21) and (C22) multiplied with $\mp \frac{H^*}{mr}$. First we split up ΔV_{iE} into its two components $\Delta V_E + \Delta V^{ie}$ with

$$\Delta V^{ie} = R\omega^{ie}(\cos L - \cos L_o) \qquad (C32)$$

(s. eq. (A14)). Then we define as "dynamic velocity errors for perfect initial alignment"

$$(I)\Delta V_N' = \frac{2(I)H}{H_o}\Delta V_N \mp \frac{R_o}{H_o}\left((I)M_N^{cmd} + \Delta M_N^{d}\right) \qquad (C33)$$

$$(I)\Delta V_E' = \frac{2(I)H}{H_o}\Delta V_E \mp \frac{R_o}{H_o}\left((I)M_E^{cmd} + \Delta M_E^{d}\right) \qquad (C34)$$

$$(I)\Delta V^{ie'} = \frac{2(I)H}{H_o}\Delta V^{ie}. \qquad (C35)$$

So we finally find an expression for the computational error of the velocity with respect to inertial space. (The formal steps for the north component say are as follows: take eq. (C22), add the readout inaccuracy $(I)\Theta_N$, subtract eq. (C28), multiply by $\mp \frac{H^*}{mr}$ and take into account eq. (C30) to (C35))

$$(I)\Delta V_N = (I)V_N \approx$$

$$(I)\Delta V'_N \mp R_o\omega^s_o\,(I)\Theta_N \pm R_o\,\frac{(I)M^d_{No}}{H_o}$$

$$-\left[(I)\Delta V'_N \pm R_o\omega^s_o\,(I)\Theta^+_{No}\right]\cos\left(\Omega^c(H^*)\,t\right)$$

$$\mp\left[(I)\Delta V'_E + (I)\Delta V^{ie'} \pm R_o\omega^s_o\,(I)\Theta^+_{Eo}\right]\sin\left(\Omega^c(H^*)\,t\right) \qquad (C36)$$

and

$$(I)\Delta V_{iE} \approx$$

$$(I)\Delta V'_E + (I)\Delta V^{ie'} + R^*\omega^{ie}\cos L_o\left(\frac{2(I)H}{H_o} - \frac{(I)h}{R_o}\right)$$

$$\mp R_o\omega^s_o\,(I)\Theta_E \pm R_o\,\frac{(I)M^d_{Eo}}{H_o}$$

$$-\left[(I)\Delta V'_E + (I)\Delta V^{ie'} \pm R_o\omega^s_o\,(I)\Theta^+_{Eo}\right]\cos\left(\Omega^c(H^*)\,t\right)$$

$$\mp\left[(I)\Delta V'_N \pm R_o\omega^s_o\,(I)\Theta^+_{No}\right]\sin\left(\Omega^c(H^*)\,t\right). \qquad (C37)$$

In this latter equation, another error source has to be included, the error occuring in the computation of the easterly ground speed from the easterly velocity ΔV^*_{iE} with respect to inertial space. Fig. 4.3 shows us how this is accomplished. First the total easterly velocity V_{iE} with respect to inertial space is computed by adding to ΔV_{iE} the computed velocity $V^{ie*}_o = R^*\omega^{ie}\cos L_o$ of a point above the starting point with the same radius as the vehicle:

$$V^*_{iE} = V^{ie*}_o + \Delta V^*_{iE} = R^*\omega^{ie}\cos L_o + \Delta V^*_{iE}. \qquad (C38)$$

From this equation we may derive the error

$$(I)V_{iE} = (I)h\omega^{ie}\cos L_o + (I)\Delta V_{iE}. \qquad (C39)$$

Then in Fig. 4.3, the computed velocity $R^*\omega^{ie}\cos L$ is subtracted in order to obtain the easterly ground speed V^*_E. Since

$$L^* = L + (I)L, \qquad (C40)$$

we obtain

$$V_E^* = \Delta V_{iE}^* + R^* \omega^{ie} (\cos L_o - \cos L^*)$$

$$= \Delta V_{iE} + (I)\Delta V_{iE} + R^* \omega^{ie} (\cos L_o - \cos L^*)$$

$$\approx V_E + (I)\Delta V_{iE} + (I)h\ \omega^{ie} (\cos L_o - \cos L^*) + R^* \omega^{ie} \sin L^* \cdot (I)L. \qquad (C41)$$

So we find the computational error of the easterly ground speed to be

$$(I)V_E \approx (I)\Delta V_E' + R^* \omega^{ie} \left[\cos L^* \left(\frac{2(I)H}{H_o} - \frac{(I)h}{R_o}\right) + (I)L \cdot \sin L^*\right]$$

$$\mp R_o \omega_o^s\ (I)\theta_E \pm R_o \frac{(I)M_{Eo}^d}{H_o}$$

$$- \left[(I)\Delta V_E' + (I)\Delta V^{ie'} \pm R_o \omega_o^s\ (I)\theta_{Eo}^+\right] \cos\left(\Omega^c(H^*)\ t\right)$$

$$\mp \left[(I)\Delta V_N' \pm R_o \omega_o^s\ (I)\theta_{No}^+\right] \sin\left(\Omega^c(H^*)\ t\right). \qquad (C42)$$

References

[1] Dr. Maximilian Schuler "Die Störung eines Pendels und eines Kreiselgerätes infolge Beschleunigung des Fahrzeugs", Physikalische Zeitschrift, Vol. 24, pp. 334-350, July 1923, Kiel, Germany. (An English translation can be found in [5], Appendix A, to which reference is made in this study).

[2] Walter Wrigley, "Schuler Tuning Characteristics in Navigational Instruments", MIT-Instrumentation Laboratory, Report 6398-S-14, April 1951.

[3] Siegfried Reisch, "Zur Physik und Technik des 84-Minuten Pendels als Hauptelement der Trägheitsortungsanlage", Jahrbuch 1960 der Wissenschaftlichen Gesellschaft für Luftfahrt, pp. 249-257.

[4] Charles S. Draper, Walter Wrigley, John Hovorka, "Inertial Guidance", Pergamon Press, Oxford, London, New York, Paris, 1960.

[5] George R. Pitman, Jr. Editor, "Inertial Guidance", John Wiley & Sons, Inc., New York, London, 1962.

[6] Charles S. Draper, "Mechanization of Inertial Guidance Systems", in [7], pp. 92-118.

[7] Hans Ziegler, Editor, "Kreiselprobleme, Gyrodynamics", Springer Verlag, Berlin, Goettingen, Heidelberg, 1963.

[8] Eduard Fischel, "Das Kreisellot und seine Technik", Luftfahrttechnik, Raumfahrttechnik 10, (1964) No. 4, April.

[9] Karl-Johan Åström, Folke Hektor, "Vertical Indication with a Physical Pendulum Based on Electromechanical Synthesis of a High Moment of Inertia", Elteknik 8 (1965), No. 4 (April).

[10] Edmund J. Koenke, "Analysis and Evaluation of a Novel Inertial Navigation System", Master Thesis, MIT, Department for Aeronautics and Astronautics, June, 1969.

[11] J. N. Schmidt, "The Autonetics G10B Gyro for Strapdown Applications", Autonetics, a Division of North American Aviation, INC., No. T6-358/201, February, 1966.

[12] "Research in Electrically Supported Vacuum Gyroscope",
R.K. Phelps, "Volume I-Summary",
G.A. Matchett, "Volume II-Electric Torque on an ESVG",
K.W. Exworthy, "Volume III-ESVG Suspension Research",
J.C. Wacker, "Volume IV-ESVG Readout Accuracy Improvement Research",
Prepared under Contract NAS-12-542 by Honeywell, Inc., Systems & Research Div., Minneapolis, Minn. for NASA.

[13] Kenneth R. Britting, "Error Analysis of Strapdown and Local Level Inertial Systems which Compute in Geographic Coordinates" MIT-Measurement Systems Laboratory, Rep. No. RE-52, November, 1969.

[14] Egmar Lübeck, "Erprobung und Vergleich von Testverfahren für hochgenaue Lagekreisel", Deutsche Forschungs- und Versuchsanstalt für Luft- und Raumfahrt e.V., Institut für Flugführung, Braunschweig, Germany, April, 1969, DLR FB 69-77.

[15] A. Stratton, "The Schuler Pendulum and Inertial Navigation", Institute of Navigation, Journal, Vol. 21, Oct. 1968, pp. 507-510.